NOVEL MICROSTRIP ANTENNAS FOR MULTIBAND AND WIDEBAND APPLICATIONS

A Thesis Submitted to
The Graduate School of Engineering and Sciences of
İzmir Institute of Technology
In Partial Fulfillment of the Requirements for the Degree of

MASTER OF SCIENCE

in Electronics and Communication Engineering

by
Göksenin BOZDAĞ

July 2014
İZMİR

We approve the thesis of **Göksenin BOZDAĞ**

Assoc. Prof. Dr. Alp KUŞTEPELİ
Department of Electrical and Electronics Engineering/Izmir Institute of Technology

Assoc. Prof. Dr. Mustafa SEÇMEN
Department of Electrical and Electronics Engineering/Yasar University

Assit. Prof. Dr. Fatih YAMAN
Department of Electrical and Electronics Engineering/Izmir Institute of Technology

14 July 2014

Assoc. Prof. Dr. Alp KUŞTEPELİ
Supervisor
Department of Electrical and Electronics Engineering/ Izmir Institute of Technology

Prof. Dr. M. Salih DİNLEYİCİ
Head of the Department of
Electrical and Electronics Engineering

Prof. Dr. R. Tuğrul SENGER
Dean of the Graduate School of
Engineering and Sciences

ACKNOWLEDGMENTS

I would firstly like to express my sincere gratitude to my supervisor Assoc. Prof. Dr. Alp KUŞTEPELİ not only for his guidance but also for his support, trust and encouragement during this study. I am very proud that I had the chance to work with him.

I also appreciate to Assoc. Prof. Dr. Mustafa SEÇMEN for his useful comments and valuable advices throughout this study.

I would like to thank to the member of my thesis committee Assist. Prof. Dr. Fatih YAMAN for his contribution.

I would like to express my special gratitude to Asst. Prof. Dr. A. Sevinç AYDINLIK BECHTELER for encouraging me to have graduate education, valuable information given by her during her lessons and leading to improve my laboratory skills.

I wish also express my thanks to Assoc. Prof. Dr. Thomas F. BECHTELER for sharing his invaluable experiences especially in microwave measurement techniques.

I would like to thank Izmir Institute of Technology, where I work as a research assistant, for the financial support.

I am also grateful to İsmail Yıldız for his cooperation in building up measurement systems, unfailing encouragement and never-ending friendship.

I would also like to thank my father Özcan BOZDAĞ and my mother Perihan BOZDAĞ for their endless support and sympathy. They really deserve every good intention.

I thank specially to my girlfriend Bahar ÖZEN for her understanding, trust and encouragement throughout this study.

Lastly, I would like to thank my colleagues, Deniz PALA, Burçin GÜZEL, Dr. Osman Akın, Dr. İlhan BAŞTÜRK, Basri MUMCU, Bilal Orkan OLCAY, Başak Esin KÖKTÜRK, Tufan BAKIRCIGİL, Şükrü DURBAŞ, Ufuk YÜCEL, Esra AYCAN, Oktay KARAKUŞ and the others for their great support and friendship.

ABSTRACT

NOVEL MICROSTRIP ANTENNAS FOR MULTIBAND AND WIDEBAND APPLICATIONS

In this study, four novel microstrip antennas are designed for various wireless systems in two different types which are log periodic dipole array and planar monopole. In the first design, multiband behavior of standard printed log periodic dipole array antenna is converted to wideband by employing sub-sectional tapered feeding and the operating bandwidth is increased by using a feed point patch. By the way, the proposed antenna becomes capable of GPS (L1 and L2), PCS, IMT-2000, WLAN, WiMAX, UWB and X Band systems. The other designs are printed planar monopole antennas which have small size and low group delay. Microstrip inset feeding, sectional design and slot loading methods are basically used for these antennas. First printed planar monopole antenna is designed for WLAN, WiMAX, UWB and X Band applications by employing inset feeding and sectional design. In the second and the third printed monopole designs, slot loading technique is also employed. It provides both exciting extra resonance frequencies and keeping S_{11} performance below -10 dB level. In the second design, a novel slot geometry is implemented on the first printed monopole design for PCS band. Then, desired frequency resonance with required bandwidth is reached and the antenna becomes capable of PCS in addition to UWB and X Band. In the third design, another novel slot geometry is also implemented on the first printed monopole design for GPS band. Consequently, the antenna becomes capable of GPS in addition to WLAN, WiMAX, UWB and X Band.

ÖZET

ÇOK BANTLI VE GENİŞ BANTLI UYGULAMALAR İÇİN ÖZGÜN MİKROŞERİT ANTENLER

Bu çalışmada, çeşitli kablosuz sistemler için log periyodik dipol dizi ve düzlemsel monopol olmak üzere iki farklı tipte dört adet özgün mikroşerit anten tasarlanmıştır. İlk tasarımda, standart basılı log periyodik dipol dizi antenin çok bantlı davranışı, alt-bölümlü konik besleme kullanılarak geniş bantlı hale dönüştürmüş ve antenin çalışma bantgenişliği bir besleme noktası yaması kullanılarak arttırılmıştır. Böylece, önerilen anten GPS (L1 ve L2), PCS, IMT-2000, WLAN, WiMAX, UWB ve X Bant sistemleri için uygun hale gelmiştir. Diğer tasarımlar küçük boyutlara ve düşük grup gecikmesine sahip basılı düzlemsel monopol antenlerdir. Mikroşerit içe doğru besleme, bölümlü tasarlama ve yarık yükleme yöntemleri geniş bant ve çok bantlı basılı düzlemsel tek kutuplu anten tasarımlarında temel olarak kullanılmıştır. İlk basılı düzlemsel tek kutuplu anten WLAN, WiMAX, UWB ve X Bant sistemleri için miktoşerit içe doğru besleme ve bölümlü tasarlama methotları kullanılarak tasarlanmıştır. İkinci ve üçüncü tek kutuplu tasarımlarında ise yarık yükleme tekniği de kullanılmıştır. Bu teknik hem fazladan rezonans frekanslarının uyarılmasında hem de S_{11} perferomansının -10 dB seviyesinin altında tutulmasını sağlamıştır. İkinci tek kutuplu tasarımında, PCS bandı için özgün bir yarık geometrisi ilk tek kutuplu anten tasarımı üzerine uygulanmıştır. Ardından, istenilen rezonans frekansı gerekli bantgenişliği ile birlikte elde edilmiş ve anten UWB ve X Banda ek olarak PCS bandına da uygun bir hale gelmiştir. Üçüncü tek kutuplu tasarımında ise başka bir özgün yarık geometrisi yine ilk tek kutuplu anten tasarımı üzerine GPS bandı için uygulanmıştır. Sonuç olarak anten WLAN,WiMAX,UWB ve X Bantlarına ek olarak GPS bandı için de uygun hale gelmiştir.

TABLE OF CONTENTS

LIST OF FIGURES

LIST OF TABLES

Table **Page**

LIST OF ABBREVIATIONS

AUT	Antenna Under Test
AWR	Advancing The Wireless Revolution
CST	Computer Simulation Technology
DSCS	Defense Satellite Communication System
DTH	Direct to Home
EIRP	Emitted Isotropic Radiated Power
EMC	Electromagnetic Compatibility
EMI	Electromagnetic Immunity
FCC	Federal Communication Committee
FDTD	Finite Difference Time Domain
FEM	Finite Element Method
FEMM	Finite Element Method Magnetics
FIT	Finite Integration Technique
GPIB	General Purpose Interface Bus
GPS	Global Positioning System
GSM	Global System for Mobile Communication
HFSS	High Frequency Structure Simulator
IEEE	Institute of Electrical and Electronics Engineers
IMT	International Mobile Communication
ISAR	Inverse Synthetic Aperture Radars
ITU-R	International Telecommunication Union for Radio Communication
LPDA	Log Periodic Dipole Array
MILSTAR	Military Strategic and Tactic Relay
MMIC	Monolithic Microwave Integrated Circuit
MoM	Methods of Moment
PAN	Personal Area Network
PCS	Public Communication System
PML	Perfectly Matched Layer
PR	Photo Resist
RFID	Radio Frequency Identification

SAR	Synthetic Aperture Radar
SDARS	Satellite Digital Audio Radio Services
SsTF	Sub-Sectional Tapered Fed
TLM	Transmission Line Model
UV	Ultraviolet
UWB	Ultra Wideband
VNA	Vector Network Analyzer
VSAT	Very Small Aperture Terminal
VSWR	Voltage Standing Wave Ratio
WBAN	Wireless Body Area Network
Wi-Fi	Wireless Fidelity
WiMAX	Worldwide Interoperability for Microwave Access
WLAN	Wireless Local Area Network

CHAPTER 1

INTRODUCTION

Wireless communication has being important role in society since the proving of the existence of electromagnetic waves by Hertz and the demonstration of wireless telegraph by Marconi. Today, wireless communication systems such as Wi-Fi, GSM, 3G, Bluetooth, whether transmitting or receiving large amount of data or making home entertainment systems more convenient, are one the key measures to our modern day quality of life. On the other hand, wireless systems are not only used for conventional communication but also used for many different applications such as medical purposes, remote sensing, wall imaging, radar applications and geographical positioning.

An antenna that resonates at the operating frequency of the system and converts guided energy to radiated energy or vice versa, is one of the crucial part of any wireless communication system. It helps to improve overall radio frequency link budget, allows multiple users to utilize the single interface and thereby increases the capacity of the wireless systems (Waterhouse and Novak, 2007). Moreover, an antenna must satisfy the many critical specifications such as return loss, necessary bandwidth and gain, desired radiation pattern with acceptable physical size in modern wireless systems.

Presently, even a cheap commercial mobile phone or a high cost military missile, the devices need to be integrated with more than one wireless communication systems operating different frequency bands. Using more than one antenna in a device can be thought as a solution to overcome the problem. However, this solution is not appropriate in the sense of engineering due to physical constraints of devices such as structural situation or dimensions and the complexity increase. At this point, the solution is designing an antenna capable with different operating frequency bands. By the way, the antenna occupies less place, complexity of the device and the cost decrease.

In this study, four novel wideband microstrip antennas are designed in different geometries for multipurpose wireless devices. One of them is sub-sectional tapered fed log periodic dipole array antenna with feed point patch operating from 1 GHz to 13.8 GHz. Its' design procedure bases on standard log periodic array antenna design but

applied modifications on the feed part makes the antenna more appropriate for wideband applications. The others are designed printed planar monopole antenna form. One of them operates between 2.37 GHz and 12 GHz which is capable of WLAN, WiMAX, UWB and X Band. The second and third printed monopole antennas have slot loadings and their operating frequencies include one or more bands of GPS, PCS, WLAN and WiMAX bands in addition to UWB and X Band. Although, monopole antennas and log-periodic antenna address the same bandwidth, dimensions of monopoles are less than log-periodic antenna. Moreover, log-periodic dipole array antenna have more directional radiation patterns while monopoles have omni-directional like radiation patterns.

In the next sections of this chapter, microstrip antennas are introduced briefly and then motivation of the study is explained extensively. Chapter 2 gives information about numerical method and used simulation program. Design, fabrication processes, measurement processes and results of proposed antennas are presented in Chapter 3 and conclusion is given in Chapter 4.

1.1. Overview of Microstrip Antennas

Low profile antennas are generally required when the size, weight, cost, performance, ease of installation and aerodynamic profile are constraints. Presently, these constraints not only for high performance aircraft, spacecraft, satellite and missile applications but also for many other government and commercial applications, such as mobile radio and wireless communications. Microstrip antennas can be an excellent candidate to meet these requirements (Balanis, 2005).

Low-profile antenna structure, conformability to planar and non-planar surfaces, low manufacturing cost, allowing simultaneously fabrication of matching networks and feeding lines with antenna structure, mechanically robust when mounted on rigid surfaces, compatible with MMIC designs. In addition to these physical advantages, they are very versatile in terms of resonant frequency or frequencies, polarization, pattern and impedance when the particular patch shape and mode are selected (Balanis, 2005).

On the other hand, there are some limitations and disadvantages for microstrip antennas. The majors are low efficiency, low power handling capacity, poor polarization purity, poor scan performance, spurious feed radiation and very narrow

frequency bandwidth which is typically a few percent. However, some methods have been studied to overcome these disadvantages. While using proper substrate and feeding with impedance matching help to broad frequency bandwidth, many different array configurations can be used for increase of gain and power handling capacity (Balanis, 2005; Garg et al., 2001).

The concept of microstrip radiator was first introduced by Deschamps in 1953 and patented by Gutton and Baissnot in 1955. However, microstrip antennas received considerable attention in the beginning of 1970s by availability of good dielectric substrates and development of fabrication process. The first practical antennas were developed by Howell in 1972 and Munson in 1974. Since then, but mainly last three descends, antenna community has devoted much effort to theoretical and experimental research on this kind of antennas (Garg et al., 2001; Lee and Chen, 1997).

Today, there are many microstrip antenna types are designed for different purposes with different structures as a result of the growing number of studies. All these printed antenna types can be divided into four basic categories according to their geometrical shapes and dimensions: Patch antennas, dipole antennas, slot antennas and traveling-wave antennas (Garg et al., 2001).

Basic configuration of a microstrip or printed antenna shown in Figure 1.1 consists of three main elements: Radiating patch (strip), dielectric substrate and ground plane. Radiating patch and ground plane are separated each other by a dielectric substrate. The radiating patch, copper or gold in general, can be any shape but regular shapes such as rectangular, circle, annular-ring and equilateral triangle are commonly preferred for prediction of performance and simplification of analysis. There are numerous substrates that can be used for microstrip antenna designs. Their dielectric constants (ε_r) and thickness (h) have significant effect on antenna radiation performance in conjunction with radiator patch. Dielectric constants of substrates usually vary between 2.2 and 12. Thick substrates with lower dielectric constants, ideally below 2.55, are more desirable because of providing better efficiency, larger bandwidth and loosely bounding fields for radiation (fringe effect). However, this condition makes the antenna size larger. On the other hand, thin substrates with higher dielectric constants tightly bound the fields and lead to smaller antenna sizes but they are less efficient due to greater losses and have relatively smaller bandwidths. Additionally, tangent loss of the dielectric substrate which is a frequency dependent factor must be considered in

terms of antenna efficiency because higher tangent loss causes more dielectric loss (Grag et. al., 2001; Balanis, 2005).

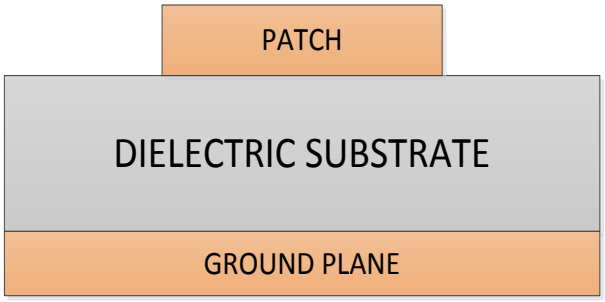

Figure 1.1. Basic configuration of Microstrip Patch Antenna

In spite of the wire dipoles had been one of the well-known and examined antennas; printed dipoles became popular after successful applications of rectangular patch antennas. The difference between printed patches and dipole antennas is width-to-length ratio. The radiator width must be less than 0.05 of free space wavelength for printed dipole antennas. Radiation patterns and gain characteristics of dipole antennas are similar with patch antennas and their bandwidth is lower. However, printed dipoles have found widespread usage especially in array antennas because of occupying less area compared to other microstrip antennas. (Garg et. al, 2001; Pozar, 1983)

Printed slot antennas are generated by subtracting any number and any shape of straplines from ground planes of microstrip antennas. These antennas are able to provide bidirectional radiation patterns, dualband or multiband resonant characteristics and circular polarization.

Microstrip travelling wave antennas are generally periodic structures and analyze in two sections. One of them is terminated with matched resistive load and named as travelling wave microstrip antenna, the other one is terminated with open circuit or short circuit and named as standing wave microstrip antennas. Radiation pattern of travelling wave antennas can be adjusted to desired direction but standing wave antennas generally radiate in the direction of wide part of the antenna (Çakır, 2004). In Figure 1.2, microstrip antenna types are represented.

Feeding is another important parameter for microstrip antennas because antenna parameters, especially radiation pattern, bandwidth and polarization, are highly effected by feeding points and techniques. There are varieties of methods for excitations of

microstrip antennas. They can be classified into two categories: Conducting feeding and non-conducting feeding. The most commons are coaxial probe, microstrip line, coplanar waveguide as conducting excitation and aperture coupling as non-conducting excitation.

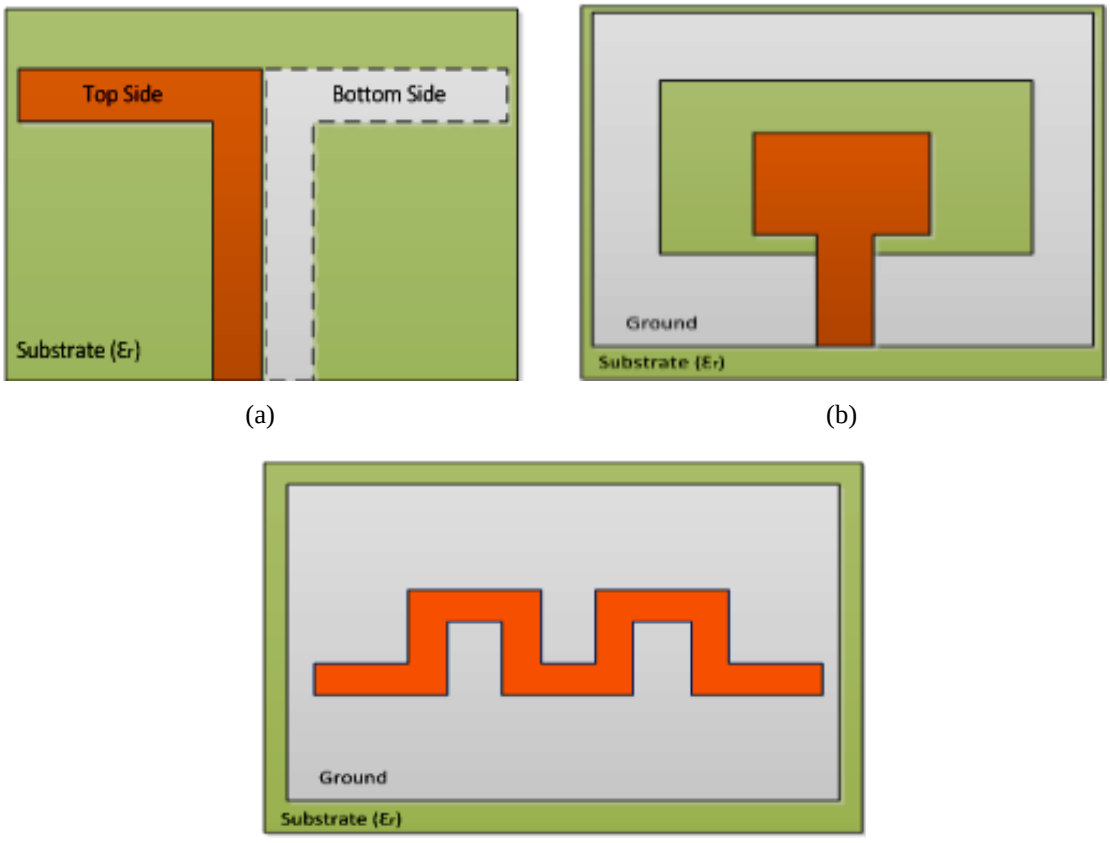

(a) (b)

(c)

Figure 1.2. Model Printed Antennas (a) Dipole Antenna (b) Slot Antenna (c) Traveling Wave Antenna

The advantages of microstrip antennas make them suitable not only for conventional wireless systems such as cellular systems but also for many applications in various fields such as aerospace, satellite, military and medicine. Some of these applications are missile and satellite communication, RFID Systems, Ground Positioning System, WLAN/WiMAX applications, Telemedicine (WBAN) applications and wearable antennas, radar applications, aircrafts and remote sensing (James & Hall, 1989; Kumar and Ray, 2003). In Figure 1.3, some example for commercial applications of microstrip antennas are given.

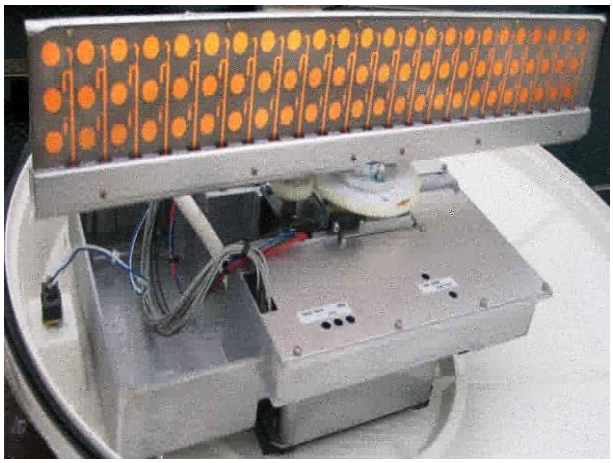

(a)

(b)

(c)

(d)

Figure 1.3. Microstrip Antenna Applications (a) JRC 3000 Radar Antenna without radome (b) MFS-P Receiving Satellite Antenna (c) ESA SMOS Satellite Antenna (d) Cisco ANT5195-P WiMAX Antenna

1.2. Motivation and Thesis Objective

Today, many electronic devices especially mobile handsets are designed and produced with the capability of various wireless systems to improve functionality and satisfy market demands. According to globally accepted foresight, today's popular multifunctional devices will be developed to be more multifunctional devices in the near future and it is claimed that they would need twenty antennas. However, almost all of the wireless systems have their own operating frequency bands. Thus, the multifunctional devices have to satisfy frequency band requirements of involved wireless systems. Available spaces for antennas generally very limited in that devices so

instead of employing individual one or more antenna just for each wireless system, compact and wideband printed antennas can be employed.

Design and fabrication of compact printed antennas completely or partially capable with GPS, PCS, IMT-2000, WLAN, UWB and X-Band are aimed in this study. Frequency allocations of interested wireless systems are shown in Table 1.1. Among the interested wireless systems, GPS, PCS, IMT-2000, WLAN and WiMAX are more conventional, commercial and end-user oriented than UWB and X Band. However, recently, many academic researches and industrial projects have being carried out to develop devices employing UWB and X-Band.

Table 1.1. Frequency Allocations of Interested Wireless Systems

Wireless System	Operating Frequency (GHz)	Band Name or Protocol
Global Positioning System	1.227	(L2)
	1.575	(L1)
Public Communication System	1.710 - 1.784	(uplink)
	1.805 - 1.879	(downlink)
Wireless Local Area Network	2.412 - 2. 472	(802.11a/b/d/e/g/h/i/j/n)
	3.657 - 3.690	(802.11y)
	4.942 - 4.948	(802.11a/b/d/e/g/h/i/j)
	5.180 - 5.825	(802.11a/g/n)
IMT-2000	2.110 - 2.200	
Bluetooth	2.400 - 2.485	(802.15.1)
WiMAX	2.5, 3.5, 10.5	(licensed)
	2.4, 5.8	(unlicensed)
Ultrawideband	3.1 - 10.6	(802.15.3)
X Band	8.0 -12.0	

Global Positioning System is a space based satellite navigation system. It is successfully integrated to the many different systems and used for both military applications such as target tracking, missile guidance and civil applications in many areas such as astronomy, cellular telephony, mining and robotics. Although, it is constructed and organized by US government, it is a freely accessible system to users having GPS capable devices. Civil GPS receivers generally listen 1.575 GHz called L1 band and 1.227 GHz called L2 band. Listening both L1 and L2 bands increases positioning accuracy but only L1 band can be listened to get positioning data.

Public Communications System also called Digital Cellular System or GSM 1800 is digital telephony system which is used widely in Europe, America, Asia and the rest of the world. PCS uses 1710 - 1785 MHz band as uplink to send information from the mobile station to the base station and 1805 - 1880 MHz as downlink to send information base station to the mobile station (Rappaport, 2002).

The third generation of mobile telecommunications technology bases on a set of standards called International Mobile Telecommunications-2000. 3G provides higher capacity and network functionalities which allow advanced services and applications such as voice telephony, mobile internet access, mobile television and video calling. IMT-2000 frequency allocation is not standard for all around the world. Different frequency bands from 450 MHz to 3600 MHz are used. (ITU-R M.1036-2, 2003) However, 2100 MHz band is used for 3G by the whole service providers in Turkey.

As a result of the popularization of the electronic devices such as desktops, laptops, printers, switches, modems, tablet computers, video game consoles and so on at homes and offices, interconnection of these devices has become a need. At this point, Wireless Local Area Network is a proper solution because it does not require wires and gives real mobility to devices. WLAN or commercially Wi-Fi uses IEEE 802.11 protocols and locates at 2.4 GHz, 3.6 GHz, 4.9 GHz and 5 GHz band in the radio frequency spectrum. Today, WLAN is a widespread and IEEE 802.11b/g/n protocols are standard for all of the laptops, smart phones and the other Wi-Fi capable devices. However, the interconnection providing by WLAN is range and data rate limited. Typically, data rate is up to 54 Mbps and the range is about 30 meters for indoor and about 100 meters for outdoor (Korowajczuk, 2011; IEEE 802.11, 2002)

WiMAX is an another wide-spread wireless communication technology which bases on IEEE 802.16 standards and supports typically 20 Mbps to 30 Mbps data rate. WiMAX has much more range than WLAN. It has up to 50 km range at line-of-sight and typically 6 km to 10 km range at non line-of-sight. It has been designed to be a cost effective way to deliver broadband data over a large area by improving spectrum efficiency. It is intended to handle high-quality voice, data and video services with offering a high quality of service. WiMAX systems are allocated on both licensed frequencies as 2.5 GHz, 3.5 GHz, 10.5 GHz and unlicensed frequencies as 2.4 GHz and 5.8 GHz (Banerji and Chowdhury, 2013).

In today’s information era, necessity of wideband wireless communications technology is increasing rapidly due to the need to support more users to provide

information with higher data rates. UWB is a new term to describe a technology which had been known as carrier-free, baseband or impulse technology since the early 1960's. UWB technology was started to use in military radar systems and the first US patent was awarded for UWB communications in 1973. However, UWB devices and systems were not commercialized for end user consumers until late 1990s (Ghavami, Michael and Kohno, 2005). In 2002, the Federal Communications Commission adopted the First Report and Order that permitted the commercial operation of UWB technology. 7.5 GHz bandwidth is allocated between 3.1 GHz and 10.6 GHz and Equivalent Isotropic Radiated Power (EIRP) emission level is limited to -41.3 dBm/MHz or 75 nW/MHz (FCC 02-48, 2002). The standardization efforts of UWB technology are still in progress under the name of IEEE 802.15.3.

The fundamental concept of UWB is transmitting and receiving an extremely short duration pulses typically having of a few tens of picoseconds to a few nanoseconds duration. The shorter duration pulses in time domain corresponds to wider bandwidth in frequency domain. The Shannon-Nyquist criterion for the maximum channel capacity or data rate is given in 1.1 where C is channel capacity, BW is bandwidth and SNR is signal to noise ratio (Proakis, 2004).

$$C = BW\ log_2\ (1 + SNR) \qquad (1.1)$$

Increasing bandwidth is more effective to reach maximum channel capacity rapidly than increasing SNR. Since the UWB have much more bandwidth than the other narrowband systems, UWB has significantly higher data rates which are between 110 Mbps and 480 Mbps. On the other hand, such higher data rates can be provided only short ranges maximum about 10 meters because of the power restriction in the UWB band. However, these limitations satisfies FCC Part 15 rules and makes UWB technology license-free and enable to coexist with current radio services with minimal interference. In Figure 1.4, spectrum of narrowband and ultra wideband are shown (Tanyer-Tiğrek, 2009; Matin, 2010).

Bluetooth, Wi-Fi and UWB are different technologies can be used for Personal Area Networks (PANs). Bluetooth operates in the frequencies between 2.4 GHz and 2.485 GHz. Its' data rates reaches to 12 Mbps which is only a fraction of UWB data rates. Bluetooth technology is widely used for voice transfer but not sufficient for big and fast data transfer. UWB and Wi-Fi are generally seen as complementary

technologies due to their ranges. However, wireless video streaming is the only area where two technologies overlap. Although, Wi-Fi is used currently in most of the devices, it is not effective way because of its' low and insufficient data rates for wireless video applications. UWB is superior technology than Wi-Fi and the other wireless technologies in this area (Matin, 2010).

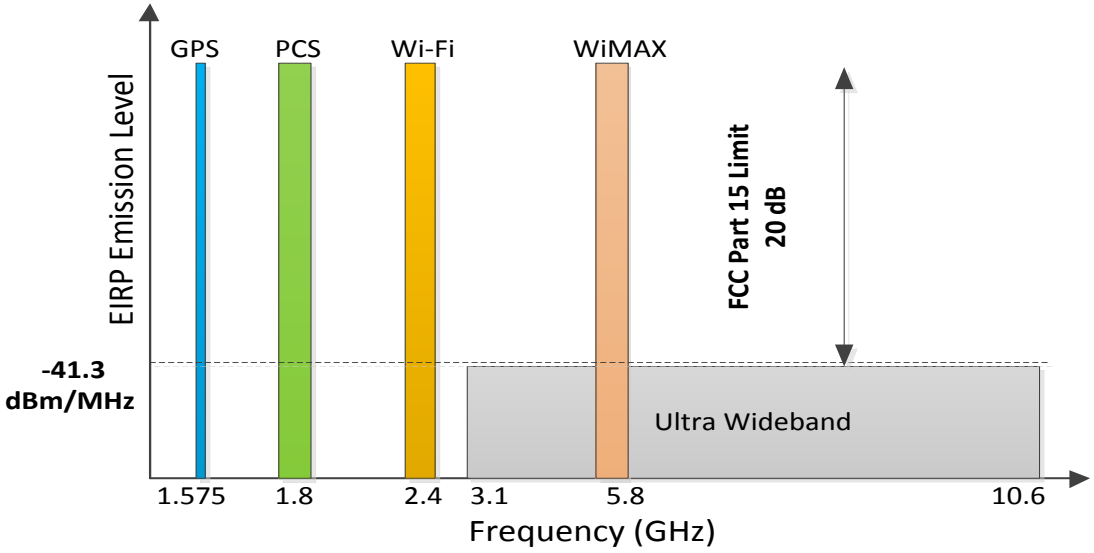

Figure 1.4. Spectrum of Ultra Wideband and Narrow Band Systems

Besides high data rates, UWB technology offers several advantages such as better multipath immunity, high resistance for jamming and low equipment cost (Ghavami, Michael and Kohno, 2005). In parallel with the development of UWB antennas and UWB capable integrated circuits, many academic and commercial researches based on UWB technology have been carried out especially in sensor networks, ground penetrating radars, wall imaging systems, positioning and medical applications (Engin et al., 2007; Javashvili, 2009; Ralston et. al., 2010; Vaddagiri, 2012; Wang et. al., 2014; Bernardi et. al., 2014). In Figure 1.5 UWB based commercial devices using for high definition television and surgical video streaming are showed. Recently developed and commercialized UWB based radar applications are represented in Figure 1.6.

(a) (b)

Figure 1.5. UWB Based Commercial Devices (a) NDS ZeroWire UWB based wireless high definition surgical video streaming device (b) Iogear GWAV8200K UWB based wireless high definition television streaming device

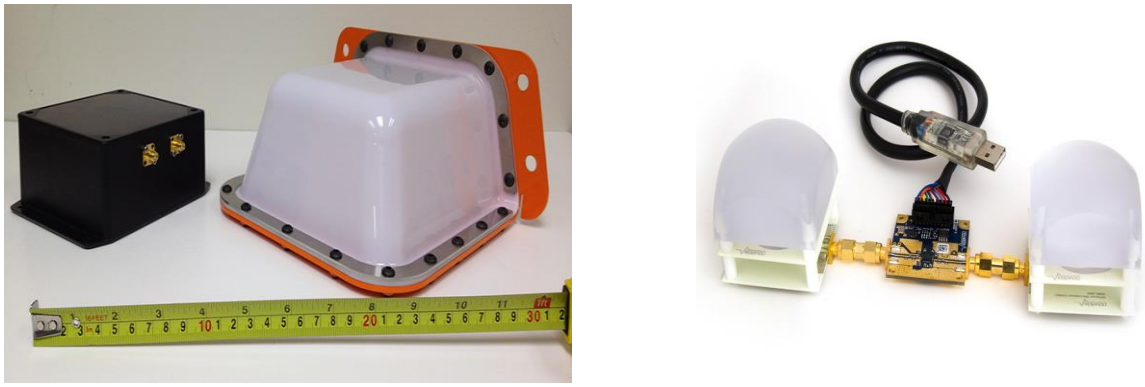

(a) (b)

Figure 1.6. UWB Based Radar Applications (a) Snow Depth Sensor (b) Radar Development Kit (Source: a) www.flatearthinc.com b) www.novelda.no)

X Band is a popular radar and satellite communication band for both military and civil applications. It is allocated between 8 GHz and 12 GHz in electromagnetic spectrum. X Band systems provide more service quality and these systems generally have convenient sizes. Therefore, they are very suitable for the applications where mobility and light weight are important and very long range is not a major requirement. X Band systems are also good with high resolution systems thanks to its' relatively wide frequency range. In military applications, X Band systems are generally employed in airborne radars servicing as interceptor, fighter or attacker and imaging radars based on Synthetic Aperture Radar (SAR) and Inverse Synthetic Aperture Radar (ISAR). Additionally, many military satellite systems such as Defense Satellite Communication

System (DSCS) and Military Strategic and Tactical Relay (MILSTAR) use X Band frequencies. In civil area, X Band is also used effectually all over the world. Its' operation band is suitable for marine radars, weather avoidance radars and Doppler navigation radars. Commercial satellite communication systems such as Satellite Digital Audio Radio Service (SDARS) for digital radio broadcasting, Direct to Home (DTH) signals providing satellite television broadcasts for home reception and Very Small Aperture Terminal (VSAT) networks generally utilizing for maritime communication over satellite use X Band. Moreover, X Band systems can be used as sensor such as motion detection sensor for traffic lights crossing. In Figure 1.7, military and civil applications of X Band applications are represented. However, the performance of X Band systems can be affected from rain because of the high operating frequency (Skolink, 2008; Elbert, 2004).

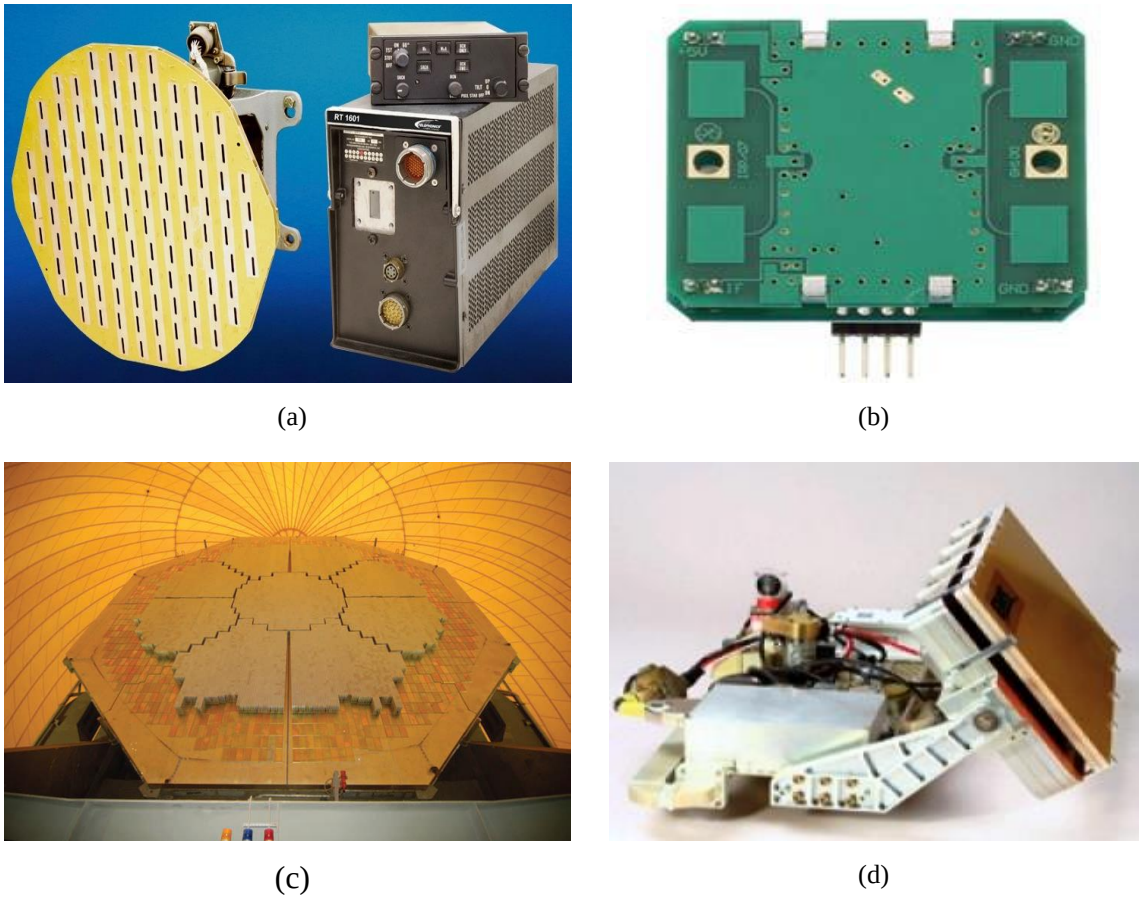

(a) (b)

(c) (d)

Figure 1.7. X-Band Applications (a) Telephonics RDR 1600 X-Band Radar (b) Parallax Motion Detector (c) Sea-Based Radar (d) Wavestrom Satcom Antenna (Source: a) www.telephonics.com b) www.parallax.com c) www.mda.mil d) www.militaryaerospace.com)

CHAPTER 2

NUMERICAL METHOD

There are different methods developed to analyze microstrip antennas. These methods are broadly generalized into two sections: Analytical and Numerical methods. Analytical methods such as transmission line and cavity methods are based on equivalent magnetic current distribution around the patch edges similar to analysis of slot antennas. Numerical or full-wave methods that are based on electric current distribution on the patch conductor and ground plane similar to analysis of dipole antennas (Kumar, 2003).

Transmission line model (TLM) can be only applied for microstrip antennas having rectangular or square geometries. Besides, TLM does not give reliable results especially in high frequencies because desired antenna parameters are derived by several empirical formulas. One of the other methods to analyze microstrip antennas is Cavity model developed by Lo. Differently from TLM, this model can be applied for much geometry in addition to rectangular geometries. Although, the results driven from cavity model are more reliable than TLM, the sensitivity is less when the used dielectric thickness is greater relatively to wavelength (Çakır, 2004).

In the beginning of 1970s, full wave analysis of microstrip antennas were developed as a result of the unreliable results of TLM and cavity models in some conditions. Moreover, the numerical methods are used to analyze any complex antenna geometry even if includes irregular shape, finite dielectric or ground plane size and anisotropic dielectric radome etc. The most common numerical techniques for antenna analysis are method of moments (MoM), finite difference time domain (FDTD) and finite element method (FEM) (Guha and Antar, 2011).

FDTD and MoM are conceptually simpler and easier to program but FEM is more powerful and versatile numerical technique for handling problems involving complex geometries and inhomogeneous media. In addition, systematic generality of the method provides constructing general purpose computer programs to solve wide range of problems and these constructed programs developed for a particular discipline

can be easily applied to solve problems in a different field with little or no modification. (Sadiku, 2000).

Today, many commercial and free electromagnetic simulator programs that are based on different numerical solving techniques have been developed. For instance, FIT based CST Microwave Studio, FFTD based XFDTD, MoM based AWR Axiem and SONNET, and FEM based FEMM. In this thesis, one of the commercial FEM based computer program High Frequency Structure Simulator (HFSS) is used for simulations. FEM method and HFSS program are briefly introduced in the next parts of this chapter.

2.1. Finite Element Method

The finite element method is a numerical technique that is used for obtaining approximate solutions to boundary-value problems of mathematical physics. It was first proposed by Cournat in 1943 and began to use in the 1950s for structural analysis such as aircraft designs. Since then the method was applied to electromagnetic problems in 1968, it has been employed in diverse areas from electromagnetic radiation and absorption problems to electrical machines and semiconductor applications (Sadiku, 2000), (Jin, 2002).

In this method, the structure is represented by an assemblage of sub-regions called finite elements. Nodes are the joints where the considered interconnections of the finite elements. Displacement functions are the simple functions that are chosen in order to approximate of the distribution or variation of the actual displacements over each finite element. Displacements are the unknown magnitudes or amplitudes of the displacement functions at the nodes. Therefore, the method aims to approximate displacements at the nodes as a solution (Desai and Abel, 1972). To sum up, the solving procedure of the FEM can be generalized in four steps: Discretization of the solution region into a finite number of sub-regions (finite elements), selection of interpolation function, formulation of the system of equations and solution of the system of equations (Jin, 2002).

Discretization, the first and perhaps the most important step in any FEM analysis, can be simply described as the process of subdivision of the structure into an equivalent system of finite elements. The typical finite elements which are shown in Figure 2.1 may be triangle, group of triangles, tetrahedra or hexahedra according to the

dimension of the structure. Discretization effects the computer storage requirements, the computation time and the accuracy of the numerical results as a pre-processing task. Presently, many well developed FEM based electromagnetic simulators are capable with subdividing of any arbitrary structure (Jin, 2002). In Figure 2.2, discretization process of FEM is presented. In this example, an arbitrary shaped solution region is divided into sub regions by finite elements.

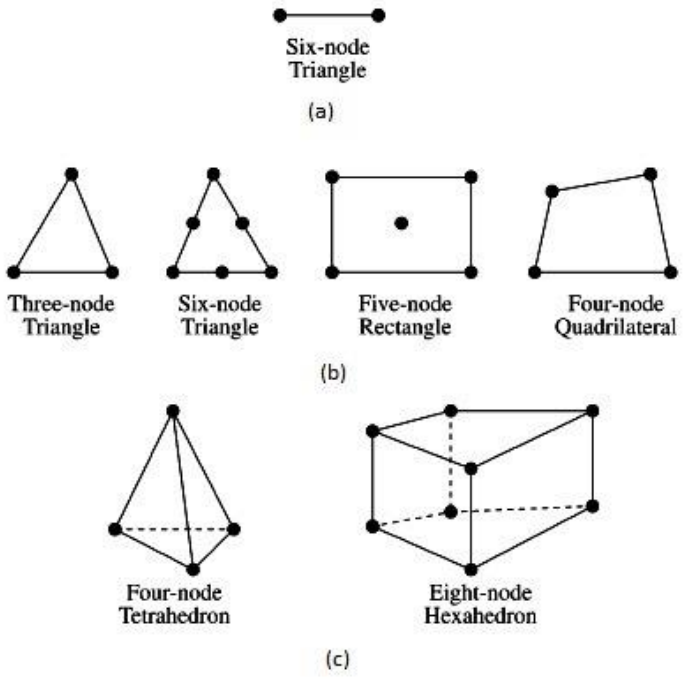

Figure 2.1. Typical Finite Elements (a) One-dimensional (b) Two-dimensional (c) Three-dimensional (Source: Sadiku, 2000)

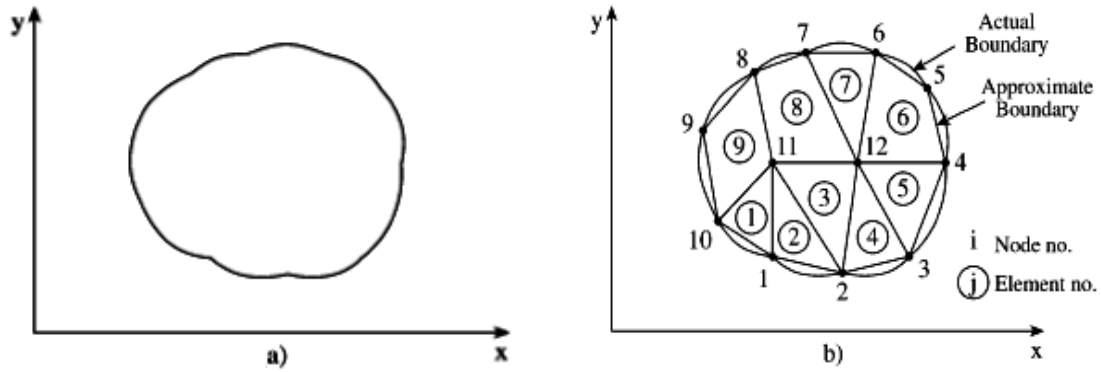

Figure 2.2. Discretization Process of FEM (a) The Solution Region (b) Finite Element Discretization (Source: Sadiku, 2000)

The second step is the selection of an interpolation function or displacement model that provides an approximation of the unknown solution with an element. The interpolation function can be expressed in various simple forms, such as polynomials and trigonometric functions. Since polynomials offer ease in mathematical manipulations, first (linear), second (quadratic) or higher order polynomials are usually employed in finite element applications. Although employing higher order polynomials improves accuracy, usually it causes more complicated formulation than employing lower order polynomials. Hence, the simple linear interpolation is still widely used. Once the order of the polynomial is selected, an expression for the unknown solution in an element can be derived (Jin, 2002).

The third step is formulation of the system of equations and it includes three substeps. Firstly, the elemental equation is generally formulated by using Ritz's or Galerkin's methods. Then, all of the elemental equations are formed the system of equations, a process called assembling. Lastly, the boundary conditions such as Neumann and Dirichlet conditions are imposed to obtain the final form of the system of equations. In computer applications, instead of separating these substeps, they are intertwined. During the assembling process, generation of elemental equation and imposition of boundary conditions are done. (Jin, 2002)

The last step is solving of the system of equations. The resultant system has the form shown in 2.1.

$$[K][\phi] = [b] \tag{2.1}$$

Equation 2.1 is of the deterministic type, resulting from either an inhomogeneous differential equation or inhomogeneous boundary conditions or both. In electromagnetics, deterministic systems are usually associated with scattering, radiation and other problems where there exists a source or excitation

Once the system of equations are solved for $[\phi]$, then desired parameters such as input impedances, scattering or radiation parameters are computed and the results are displayed in the forms of curves, plots or etc. This final stage called postprocessing is separated completely from the other steps (Jin, 2002).

2.2. High Frequency Structure Simulator

HFSS is a high-performance FEM based electromagnetic field simulator for modeling to arbitrary three dimensional volumetric passive devices. Its' standard accuracy, advanced solver and computation technology make it useful and preferable tool for engineers designing high frequency and high speed electronic components. HFSS integrates simulation, visualization, solid modeling and automation in an easy-to learn environment, besides solving three dimensional electromagnetic problems in acceptable solution time and accuracy. In HFSS, any structure is defined by adaptive meshing to get more accurate results. S parameters, resonant frequencies, radiation patterns and fields can be calculated by the software (User's Guide, 2005). In this thesis, HFSS v13 is used for antenna simulations and numerical results.

Antenna simulation with HFSS can be separated roughly into six steps: Solution type decision, modeling antenna structure, excitation of ports, creating boundary, setting up solution parameters and getting postprocessing results.

In HFSS, there are many solution types such as driven modal, driven terminal, and transient. However, driven modal and driven terminal solutions are interested in this thesis. For calculations of the mode based S parameters of the structure which are driven by a source and computing incident plane wave scattering, driven modal solution type is used. When multi conductor transmission line ports such as coaxial cable is employed as source, driven terminal solution type is used for calculation of terminal based S parameters of structures.

The structure of the antenna can be modeled in two dimensional, three dimensional or combination of them according to your design. HFSS allows one, two or three dimensional drawings. Objects can be drawn either directly or equation based. One dimensional objects called polylines such as straight line, arc line etc. are open objects. They have length, but no surface or volume. These objects are generally used to create two dimensional objects. Any surfaces such as rectangles, circles, connected polylines or etc. are two dimensional and closed sheet objects enclosing a region without a volume. Three dimensional objects such as boxes, cylinders, cones etc. can be either drawn directly or created by manipulating of two dimensional objects. They have boundaries that enclose a region with volume. After drawing the structure of the antenna, material assignments such as air, copper and FR4 for three dimensional objects

and boundary assignments such as perfect electric and perfect magnetic boundaries for two dimensional objects are done. In this thesis, radiators, feedings and ground planes of the designed antennas are modeled as two dimensional objects that are assigned as perfect electric boundary and substrates are modeled as three dimensional FR4 plate.

Excitations in HFSS such as wave port, lumped port, terminal, floquet port are used to specify the sources of electromagnetic fields, charges, currents or voltages on objects or surfaces. Wave ports and lumped ports are used in this thesis. Wave ports represent places where excitation signals enter and leave in the antenna geometry. They are used for modeling strip lines and waveguide structures such as coaxial cables. Differently from the wave ports, lumped ports can be located internally of the structure. They have complex user-defined impedance and compute S parameters directly at the port.

Boundary conditions specify the field behavior on the boundaries of the problem region and object interfaces. In HFSS, there are many boundary conditions such as perfect electric boundary, radiation boundary, perfectly matches layer (PML), lumped RLC having different purposes. Even if radiation and perfect electric boundaries have been basically used, perfectly match layer has been also used for comparison and verification of some simulation results in this thesis. Perfect electric boundary represents perfectly conducting surfaces. Radiation boundary is an open boundary that absorbs outgoing waves. It is used to simulate an open problem, such as antenna problem, allowing to radiate infinitely far into space. The location of the radiation boundary is very important to get accurate results and it must be located away from the structure part at least quarter wavelength of minimum operating frequency. Another open boundary condition in the program is PML. Although, setting up a PML boundary is similar to setting up radiation boundary, PML is not only covers surfaces of the boundary but also covers the volume so it is used to fully absorb the electromagnetic field. PML boundary must be located away from radiator part at least one-eighth wavelength of the minimum operating frequency. Using PML boundary provides absorbing wider range of waves in terms of frequency and direction. However, it increases significantly solving time and memory usage.

Setting up solution parameters that are solution frequency, maximum number of passes and maximum delta S parameters specifies how the program will compute a solution. In HFSS, solution frequency is usually set to center frequency or about center frequency of the operating frequency band. If a range of frequencies are used for

solving the structure, a frequency sweep (operating frequency band) is defined. Then, an adaptive analysis is performed at the solution frequency and all of the calculations for frequencies in the sweep are performed basing on the solution frequency. In adaptive analysis, HFSS refines the mesh or finite element sizes. Maximum number of mesh refinement cycles called maximum number of passes value is one of limiting criteria for stopping adaptive solution. When maximum number of passes is completed, the adaptive solution stops. If the maximum number of passes is not completed, the adaptive solution continue until reaching the convergence criteria. The amount of the required memory to generate a solution increases with each adaptive refinement cycle. Too high number of passes causes requesting more memory than is available or taking excessive time to compute solutions. Another limiting criterion of adaptive solving is maximum delta S parameter. The delta S is the magnitude of the change of the S parameters between two consecutive passes. If the delta S is less the entered maximum delta S value between adjacent two iterations, the adaptive analysis stops. Otherwise, adaptive solution continues until reaching the maximum number of passes. Almost the whole antenna simulations in this thesis, solution frequency is chosen between 5 GHz and 7 GHz, frequency sweep is adjusted between 1 GHz and 15 GHz, maximum number of passes parameter is set to 20 and maximum delta S parameter is set to 0.01. Moreover, an extra meshing refinement is defined on radiation boundary to improve the accuracy of directivity, gain and radiation pattern parameters. Maximum length of meshing element is adjusted to approximately 10% of the maximum wavelength.

Final step of modeling with HFSS is getting postprocessing results. While the program is generating a solution or when it is completed, convergence information, computing resources, mesh statistics, S parameters, impedances and radiation parameters can be viewed, plotted and exported.

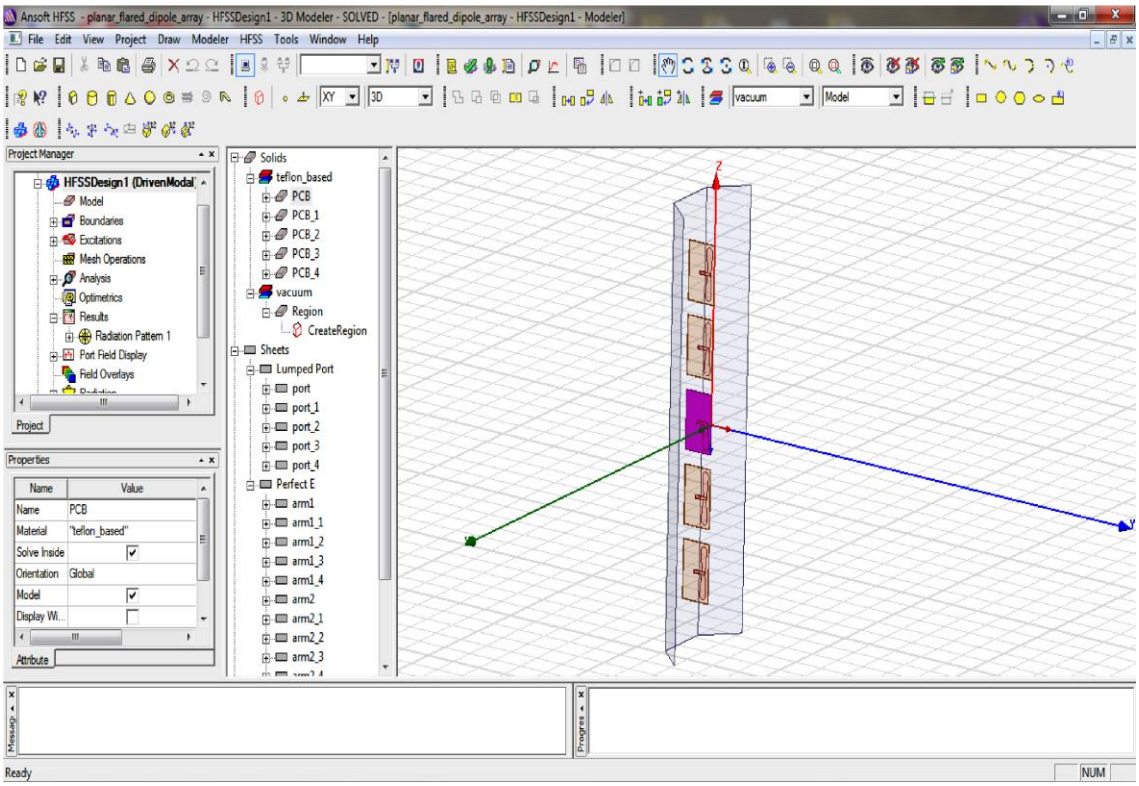

Figure 2.3. HFSS User Interface

CHAPTER 3

ANTENNA DESIGNS

Today, employing antennas structurally simple, easy fabricated, small sized and lightweight, having constant group delay, higher gain and operating at the whole frequency bands of interested wireless systems are naturally aimed and demanded. However, all of those cannot be derived practically from a single radiator; most of them can be provided. In this study, two different antenna types, printed log periodic dipole array antennas and printed planar monopole antennas, are investigated to satisfy most of these antenna features.

3.1. Log Periodic Dipole Array Antenna

In wideband antenna technology, a breakthrough was made in 1950s and the bandwidths of the antennas extended from one octave to several octaves. These antennas have been referred to as frequency independent antennas (Balanis, 2005). Impedance and pattern properties of an antenna will be frequency independent, if the antenna shape is specified only in terms of angles (Rumsey, 1957).

Many studies have been carried on frequency independent antennas since the late 1950s and many experiments with several geometries such as spiral, biconical and fractal have been developed (Stutzman, 1981). Log Periodic Dipole Array (LPDA) firstly introduced by DuHumel and Isbell in 1957 as one of the frequency independent antenna (DuHumel and Isbell, 1957). It can be simply explained as a series-fed array of parallel linear dipoles whose lengths, spacings and diameters increase logarithmically from the feed point at the apex. This logarithmic increase defining as inverse of geometric ratio (τ) given in 3.1 and spacing factor (σ) given in 3.2 are the main parameters which associated with the characteristics of the antenna. It can be seen from the Figure 3.1 that dipoles are located in the envelope which is formed by an angle 2α. As it has been mentioned, it is the characteristics of frequency independent antennas.

$$\frac{1}{\tau} = \frac{l_2}{l_1} = \frac{l_{n+1}}{l_n} = \frac{R_2}{R_1} = \frac{R_{n+1}}{R_n} = \frac{d_2}{d_1} = \frac{d_{n+1}}{d_n} \tag{3.1}$$

$$\sigma = \frac{R_{n+1} - R_n}{2l_{n+1}} \tag{3.2}$$

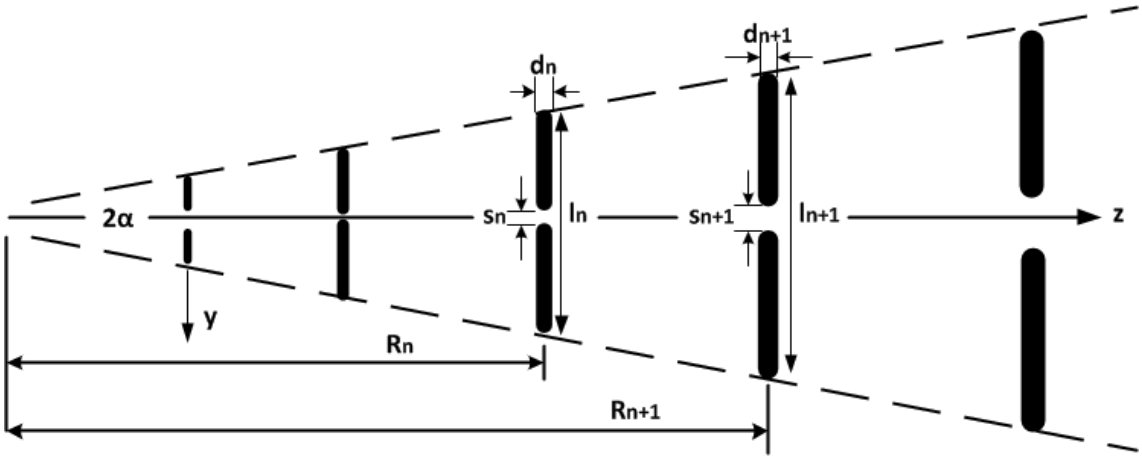

Figure 3.1. Log Periodic Dipole Antenna

Input impedance of a log periodic antenna is repetitive in linearly scaled frequency. However, it is periodic when the frequency is scaled logarithmically. The other antenna parameters such as pattern, directivity and beam width show the same variations (Balanis, 2005; Yang, 2012). On the other hand, log periodic dipole array which is thought as infinite structure should be truncated at both ends to get useful and practical broadband radiator whose operating frequency is limited. The lowest and the highest cutoff frequencies of the antenna are determined by the electrical lengths of the lowest and the highest elements in the array. Lower cutoff frequency occurs when the longest element and higher cutoff frequency occurs when the shortest element is in very narrow active region. An LPDA structure usually categorized as active and passive regions. Active region covers the elements whose lengths are nearly half of the wavelengths of corresponding frequency and passive region covers the elements which are not in active region. Active region passes from the longer to the shorter elements when the frequency increases and a negligible amount of energy reflects from the truncated end thanks to the rapidly decreasing energy from the shorter active elements travelling toward the longer inactive elements (Balanis, 2005).

All elements of a LPDA antenna are directly energized by the feeding. Straight and crisscross feedings shown in Figure 3.2 are the two basic methods using to connect and feed the elements of a LPDA antenna. In both cases, feeding terminal is generally located at the small end of the array. The main difference of feeding methods is current phases between terminals and elements. This difference highly affects antenna patterns. In straight method, currents in the elements have the same phase relationship as the terminal phases. The phase progression of the currents occurs from smaller elements to longer elements so an end-fire antenna pattern with interference effects is produced in the direction of the longer elements. In crisscross method, a 180^{o} phase difference is mechanically generated on the terminal of each element and the opposition phases occurs between adjacent elements. The phase reversal between these elements produces a phase progression from longer elements to shorter elements so an end-fire antenna pattern with less interference is produced in the direction of the shorter elements. The most active elements for this feed arrangement are those that are near resonant with a combined radiation pattern toward the vertex of the array. Additionally, crisscross feeding is very convenient because it provides balanced input feeding line like the two conductor transmission line.

Since LPDA antennas have remarkable gain with directional pattern, multiband behavior and linear polarization, they are frequently employed for receiving analog television broadcasts and EMC/EMI measurements (Wakabayashi et. al., 1999; Hagiwara et. al., 2012). However, larger sizes of LPDA antennas make them inconvenient especially for size limited and mobility need applications. At this point, forming LPDA antennas into printed antennas makes them more suitable. Because printed LPDA antennas have many advantages such as low cost, light weight, small size, simple fabrication process and ease of integration in addition to characteristic benefits of LPDAs. Printed LPDA antennas have been successfully participated in many different applications. For examples, direction finding, radio astronomy, digital television broadcasting, radar applications and ultra wideband systems (Guinvarc’h and Ribiere-Tharaud, 2008; Yeo and Lee, 2012; Harrison and Jesup, 2012; Acedo, 2012; Casula et. al., 2013; Elseakh and Abdallah, 2014).

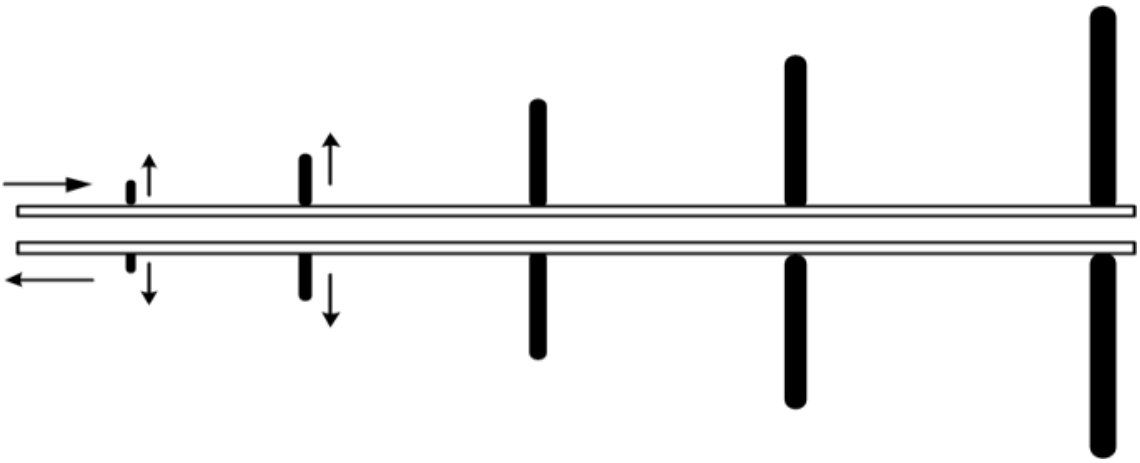

(a)

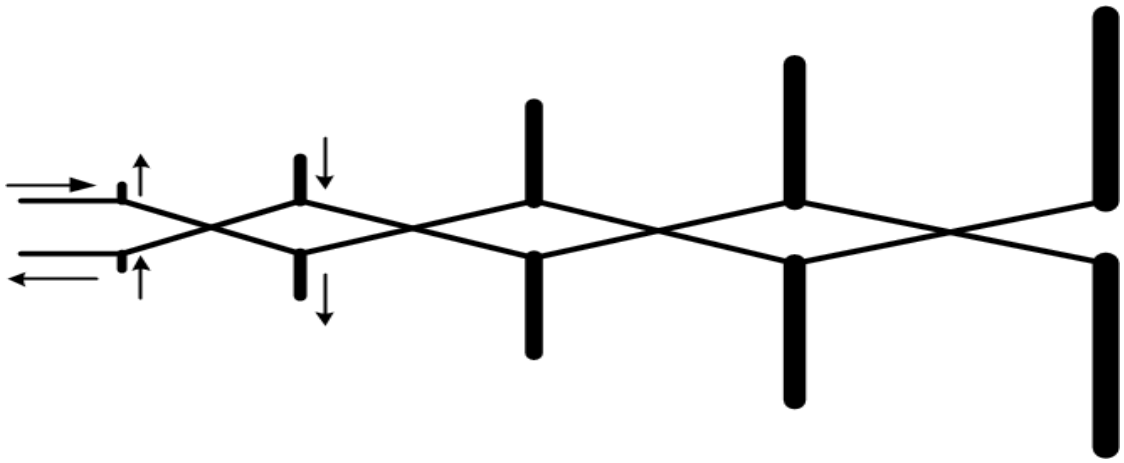

(b)

Figure 3.2. LPDA Antenna Feeding Methods (a) Straight Line (b) Crisscross

3.1.1. Design of Standard Printed LPDA Antenna

Design steps of a standard wire LPDA antenna must be well understood to design a printed LPDA antenna because log periodic antenna structures either wire, planar or printed base on the same conceptual idea. Design parameters of the printed antennas are generally derived from the corresponding wire antennas. Thus, a standard wire LPDA antenna design procedure will be presented firstly. Then, it will be followed to design standard printed LPDA antenna.

Four years later introducing of LPDA antennas by DuHumel and Isbell, Carrel proposed firstly the most informative, useful and practical design procedure which bases on mutual coupling between dipole elements (Carrel, 1961). Carrel describes the general configuration of a LPDA antenna in terms of design parameters τ, α and σ

whose relations are given in 3.3 and he collects a set of curves and contours including these parameters to help in the design.

$$\alpha = tan^{-1}\left[\frac{1-\tau}{4\sigma}\right] \tag{3.3}$$

However, these directivity contours are corrected by Thompson and Butson and Peixeiro who also improved the procedure by demonstrating the influence of feeding impedances (Thompson and Butson, 1976; Peixeiro, 1988). For a certain τ, employing optimum σ through the curves shown in Figure 3.3 provides maximum directivity. On the other hand, one can use σ values which are smaller or greater than optimum σ values. While front to back ratio and directivity decreases in smaller σ cases, side lobes appear in greater σ cases.

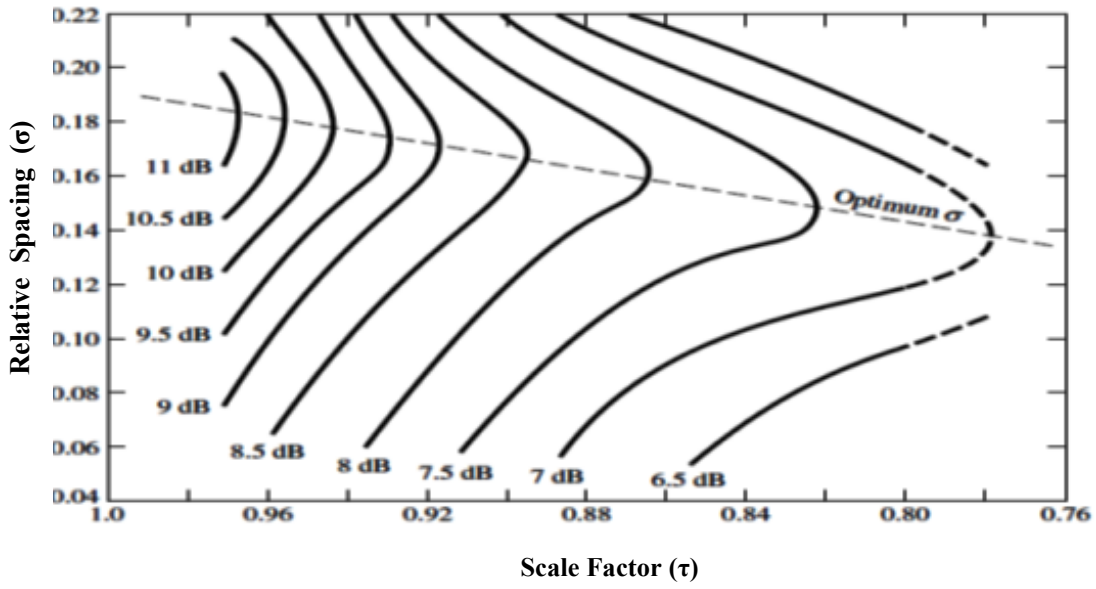

Figure 3.3. Contours of Constant Directivity including corrections
(Source: Balanis, 2005)

In addition to basic parameters τ, σ, α and directivity curves, there is a number of equations which are used for designing log periodic array antennas. While upper and lower cut off frequencies of the log periodic arrays are determined by the lengths of the shortest and longest elements of the structure, design specifications determine the bandwidth of the active region. Carrel's procedure proposes a semi-empirical equation given in 3.4 for calculation the bandwidth of the active region B_{ar}.

$$B_{ar} = 1.1 + 7.7(1-\tau)^2 cot\alpha \quad (3.4)$$

Practically, designed bandwidth B_s is generally chosen as slightly larger than desired bandwidth B which is the ratio of f_{max} to f_{min}. The relationship between these terms is given in 3.5.

$$B_s = BB_{ar} = B[1.1 + 7.7(1-\tau)^2 cot\alpha] \quad (3.5)$$

Total length of the structure from the longest element to shortest element can be obtained by the formula given in 3.6. Another necessary parameter in log periodic structures is number of elements. It can be determined by the equation in 3.7 derived from the geometry of the structure.

$$L = \frac{\lambda_{max}}{4}\left(1 - \frac{1}{B_s}\right)\cot\alpha \quad (3.6)$$

$$N = 1 + \frac{\ln(B_s)}{\ln(1/\tau)} \quad (3.7)$$

Diameters of the dipoles and input impedance which can be specified by design determine the center to center spacing (s) between the two rods of the feed line conductor. Average characteristic impedance (Z_a) of the elements is first defined to get this parameter. The ratio l_n/d_n in equation 3.8 refers to length to diameter ratio of the n^{th} element of the array. This ratio is supposed to be the same for all the elements of the array for an ideal log periodic design. However, especially in wire LPDA applications practically the elements are usually divided into more than one group with all elements in each group having the same diameter but not the same length. The number of groups is determined by the total number of elements of the array. Three groups for small, middle and large elements should be usually sufficient. Then, the characterization of the effective loading of the dipole elements on the input line is calculated by the equation given in 3.9 and another graph of Carrel shown in Figure 3.4.

$$Z_a = 120\left[\ln\left(\frac{l_n}{d_n}\right) - 2.25\right] \tag{3.8}$$

$$s = d\cosh\left(\frac{Z_0}{120}\right) \tag{3.9}$$

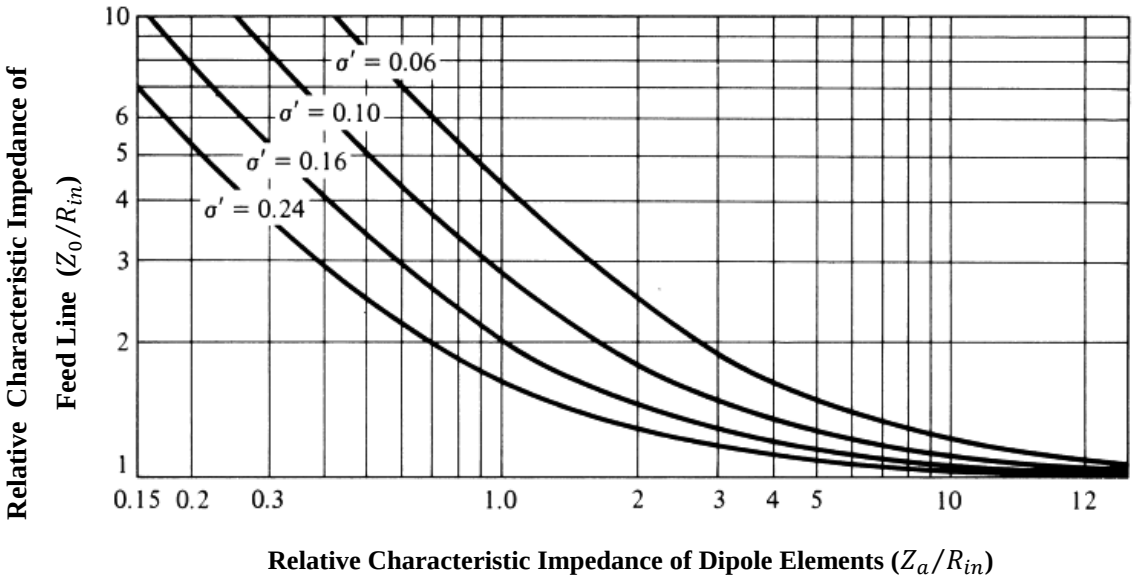

Figure 3.4. Relative characteristic impedance of feed line as a function of relative characteristic impedance of dipole element (Source: Carrel, 1961)

In Figure 3.4, σ' is a ratio called relative mean spacing and equals to $\sigma/\sqrt{\tau}$. R_{in} corresponds to real input impedance while Z_0 corresponds to characteristic impedance of feed line. Z_0 has strong effects on both directivity and bandwidth. Increasing Z_0 causes a decrease in directivity especially in high σ regions and a move towards to antenna apex in active region (Peixeiro, 1988).

Although design procedure of the wire log periodic dipole array antenna includes many equations and graphs, it can be summarized in seven steps. First of all, desired frequency band B and required directivity D are determined. Secondly, scaling factor τ and spacing factor σ parameters are determined with the help of the graph shown in Figure 3.3. Then, α parameter is calculated from equation 3.3. Fourthly, B_s is determined by calculating B_{ar} using equations 3.4 and 3.5. As a fifth step, number of elements and the total length of the structure is determined from equations 3.6 and 3.7. R_{in} is a changeable parameter up to your system but in radio frequency circuits and systems input and termination impedances are generally adjusted to 50 Ω or 75 Ω. The

graph shown in Figure 3.4 helps to determine Z_0 by specifying average characteristic impedance of the feeder line Z_a in the sixth step. Finally, spacing parameter s is calculated from the equation 3.9.

Design of a standard printed LPDA antenna includes more steps in addition to standard wire LPDA antenna because printed antennas have their own specifications and considerations. Once, all of the design parameters obtained from wire antenna design must be revised to get printed structure. Since the other dipoles of the structure are generated from this first dipole according to scaling factor τ, the main element of a log periodic dipole antenna is the first half-wave dipole corresponding to minimum frequency and having maximum length. Cylindrical wire dipoles are represented as rectangular prism whose height is constant. The length is basically related with the effective dielectric constant of the substrate because wavelengths of electromagnetic waves naturally change in different mediums. Maximum length calculations for air and in a medium are given in equation 3.9 and 3.10. The width of the printed dipole is determined as π times greater than the corresponding radius of cylindrical wire dipole as given in 3.11 (Campbell, 1977).

$$l_{max} = \frac{c}{2f_{min}} = \frac{\lambda_{max}}{2} \quad in\ air \tag{3.10}$$

$$l_{max} = \frac{\lambda_g}{2} = \frac{\lambda_{max}}{2\sqrt{\varepsilon_{eff}}} \quad in\ medium \tag{3.11}$$

$$W = \pi.r \tag{3.12}$$

Different methods have been proposed for determination of effective dielectric constant (ε_{eff}) but they are too complex and unsuitable for the designs will be proposed in this study (Campbell, 1977; Bahl and Garg, 1977; Casula et. al., 2011). According to several simulations, ε_{eff} is simply accepted as $\varepsilon_r/2$.

Design and realization of a standard crisscross fed printed log periodic dipole array antenna operating in 1 - 13 GHz and having 7 dBi gain is aimed in this part of the study. Firstly, scaling and spacing parameters are obtained as 0.8 and 0.149 to get desired directivity. Then, α, B_{ar} and B_s parameters are calculated and number of elements is determined. To get wide impedance bandwidth and avoid additional

matching circuitry, input impedance and characteristic impedance of the feed must be properly chosen. When Figure 3.4 showing the relations of impedance parameters and equation 3.7 are analyzed, it is seen that setting R_{in} and Z_o equal to each other causes higher Z_a and higher l_n/d_n ratio. However, producing very thin dipoles generally cannot be possible in realization processes. Thus, Z_a is specified as 350 Ω while input impedance is 50 Ω. Lastly, feed line spacing parameter, which varies with each dipole element as a result of constant length to diameter ratio, is ignored due to constant height of substrate.

In addition to mentioned parameters, there is one more important point must be considered for designing any printed antenna. It is the width of characteristic impedance of feed line. It can be derived from the formula given 3.13. W is width of feed line and d is thickness of substrate (Pozar, 1998). All of the calculated and determined parameters are given in Table 3.1.

$$Z_0 = \begin{cases} \dfrac{60}{\sqrt{\varepsilon_{eff}}} ln\left(\dfrac{8d}{W} + \dfrac{W}{4d}\right) & \text{For } \dfrac{W}{d} < 1 \\ \dfrac{120\pi}{\sqrt{\varepsilon_{eff}}} \dfrac{1}{\left[\dfrac{W}{d} + 1.393 + 0.667\, ln(\dfrac{W}{d} + 1.444)\right]} & \text{For } \dfrac{W}{d} > 1 \end{cases} \quad (3.13)$$

Designed antenna is printed on a low-cost FR4 substrate whose dielectric constant is 4.5, height is 1.55 mm and tangent loss is 0.02. The realization process will be introduced extensively in the next chapters. As a result of several simulation studies and realization constraints, the length of the structure is optimized for 130 mm instead of 143.3 mm and number of elements is optimized for 9 elements instead of 16 elements. Finally, the size of the antenna determined as 130 mm x 100 mm. Corresponding length and width values of the elements are given in Table 3.2. A drawing of the designed structure is given in Figure 3.5. The antenna is printed as double sided. Dark sketch represents to bottom side and transparent sketch represents to top side. It is obviously seen from the Figure 3.5 that halves of the dipoles are printed on top side and the other halves of dipoles are printed on bottom side. This connection type corresponds to crisscross connection in printed log periodic dipole array structure.

Table 3.1. Standard Printed Log Periodic Dipole Array Antenna Design Parameters

Design Parameter	Symbol	Value
Effective Dielectric Constant	ε_{eff}	2.25
Scaling Factor	τ	0.80
Spacing Factor	σ	0.149
α Parameter	α	18.56 ^{o}
Active Region Bandwidth	B_{ar}	2.018
Desired Bandwidth	B	13
Designed Bandwidth	B_s	26.232
Number of Elements	N	16
Total Length of Structure	L	143.3 mm
Relative Mean Spacing	σ'	0.167
Average Characteristic Impedance of Elements	Z_a	350 Ω
Input Impedance	R_{in}	50 Ω
Characteristic Impedance of Feed Line	Z_0	~ 50 Ω
Maximum Dipole Length	l_{max}	100 mm
Feed Line Width	W	4.5 mm

Table 3.2. Length and Width Values of Standard Printed Log Periodic Dipole Array

Element #	**#1**	**#2**	**#3**	**#4**	**#5**	**#6**	**#7**	**#8**	**#9**
Length (mm)	100	80	64	51.2	41	32.8	26.2	21	16.8
Width (mm)	1.8	1.4	1.1	0.92	0.73	0.59	0.47	0.38	0.3

3.1.1.1. Simulation Results of Standard Printed LPDA Antenna

Before realization of designed antennas, their performance is analyzed in case of the any faulty in desired targets. If any undesired result is observed, design is optimized and its performance is analyzed again. The process is continued until reaching the desired results. It is a very helpful and useful process in terms of saving time and cost.

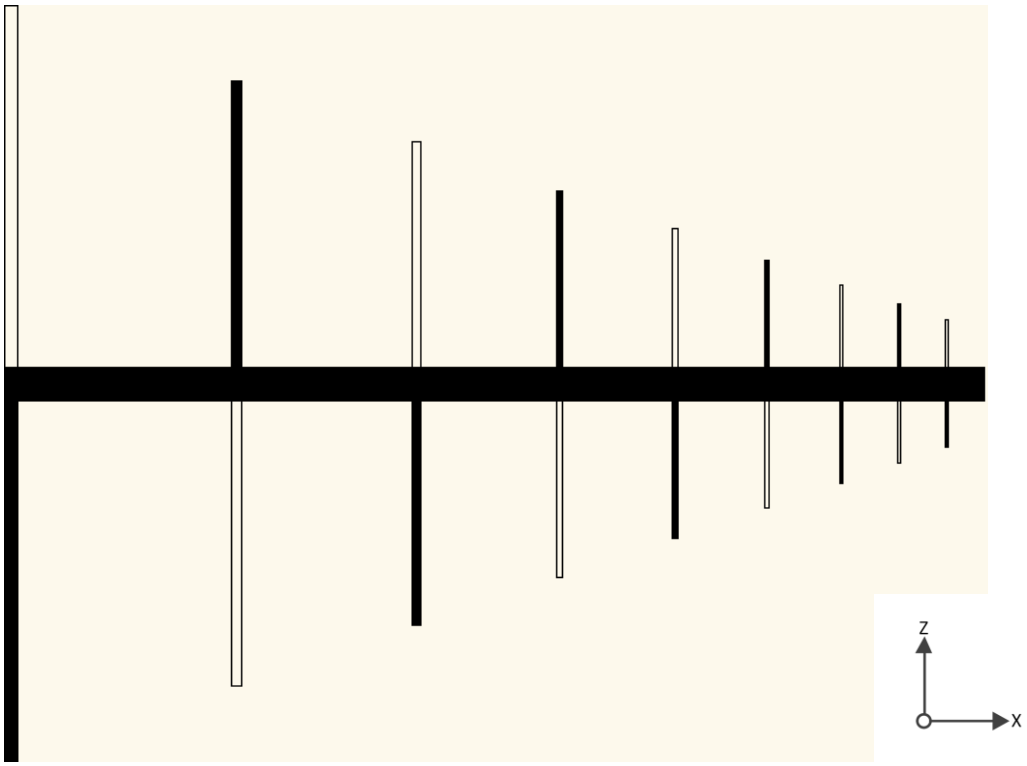

Figure 3.5. Standard Printed Log Periodic Dipole Array Antenna

There are many parameters which are used for determining the performance of an antenna. Five of them which are S_{11}, Voltage Standing Wave Ratio (VSWR), Group Delay, Antenna Pattern and System Gain (G_{sys}), are considered as performance indicators in this study. They can be explained very shortly: S_{11} and VSWR are used to determine frequency bandwidth of antenna. In this study, operating frequency of antenna is accepted as below -10 dB level for S_{11} and below 2 level for VSWR. Figure 3.6 and Figure 3.7 give the simulated S_{11} and VSWR performances. Group delay is a measure of the transit time of a signal through a device versus frequency and it is defined as the negative derivative of the phase response with respect to frequency. The variations in group delay cause signal distortion so it is desired to be constant as far as possible especially in pulse based communication systems, radar and imaging applications (McEvoy et. al., 2008). Usually gain is expressed relative to a reference such as isotropic antenna. In addition to efficiency and directivity, return loss parameter also is taken into account when system gain is determined. G_{sys} is given in Figure 3.8 for the interested frequencies. A radiation pattern is a graphical representation of the far field radiation properties of an antenna. In Figure 3.9, simulated and normalized XZ plane radiation patterns are given for 1.227 GHz, 1.575 GHz, 1.8 GHz, 2.1 GHz, 2.4

GHz, 3.1 GHz, 5.8 GHz, 8 GHz, 10.6 and 12 GHz frequencies. In Figure 3.10, XY plane radiation patters are given for the interested frequencies. When antenna efficiency is 100%, gain corresponds to directivity which can be described as how much it concentrates energy in one direction in preference to radiation in other directions.

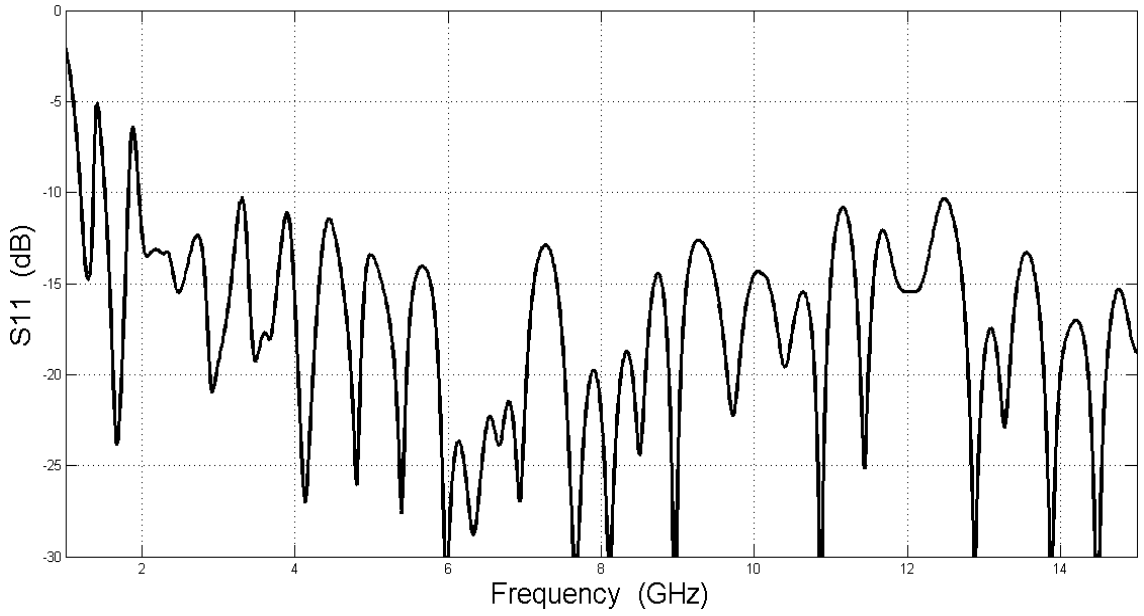

Figure 3.6. Simulated S_{11} of Standard Printed LPDA Antenna

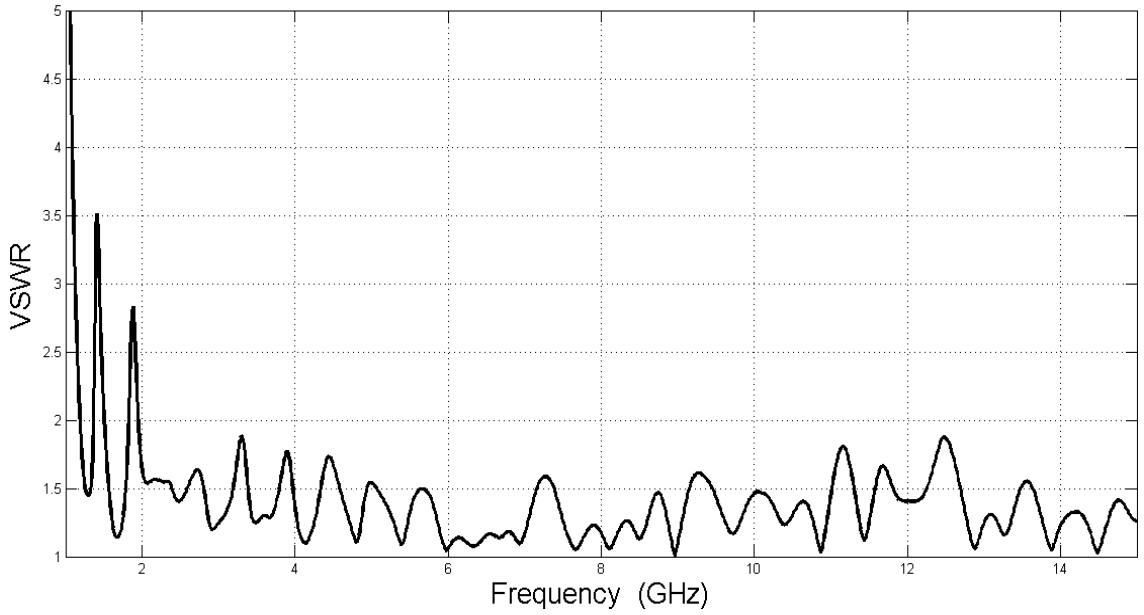

Figure 3.7. Simulated VSWR of Standard Printed LPDA Antenna

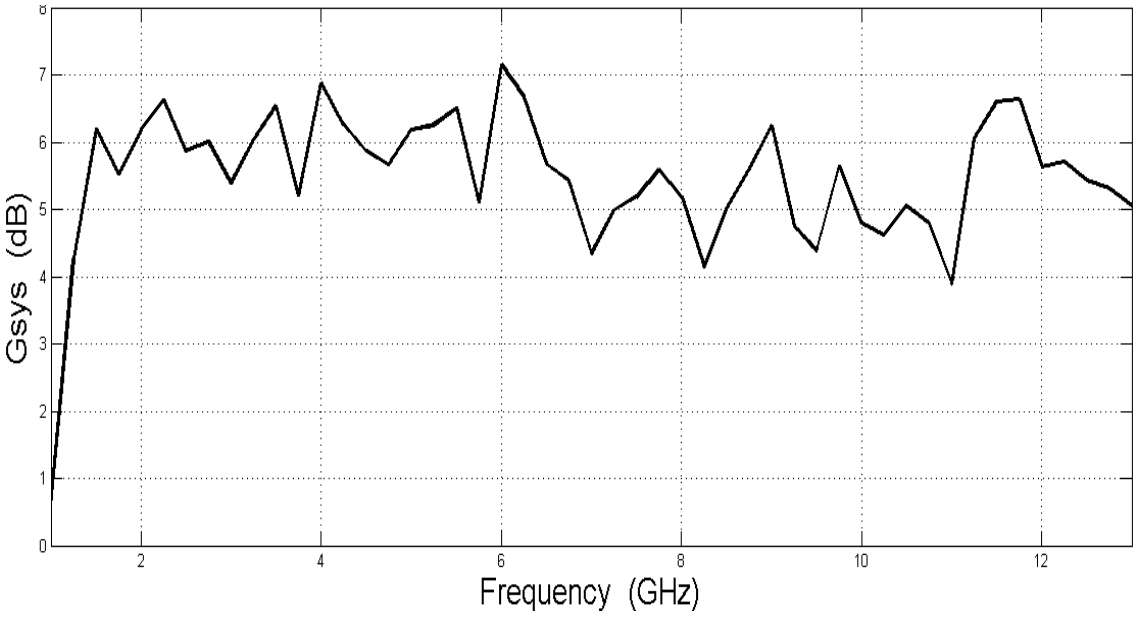

Figure 3.8. Simulated System Gain of Standard Printed LPDA

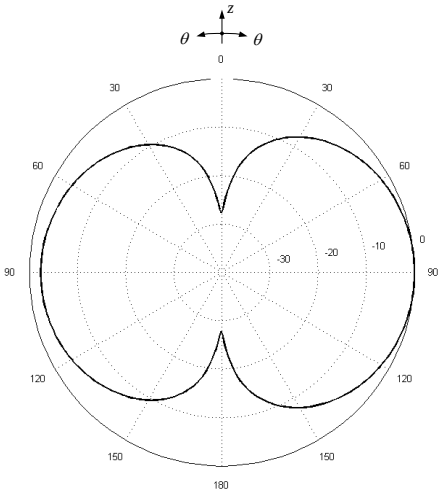

1 GHz

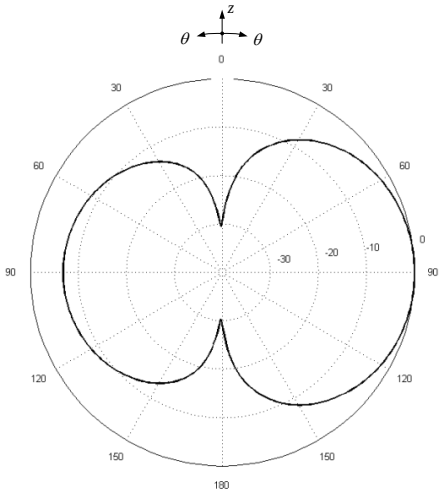

1.227 GHz

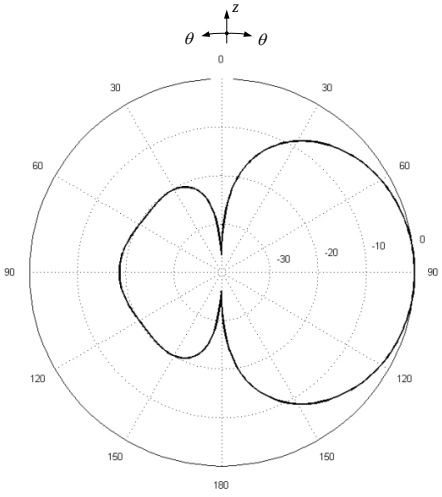

1.575 GHz

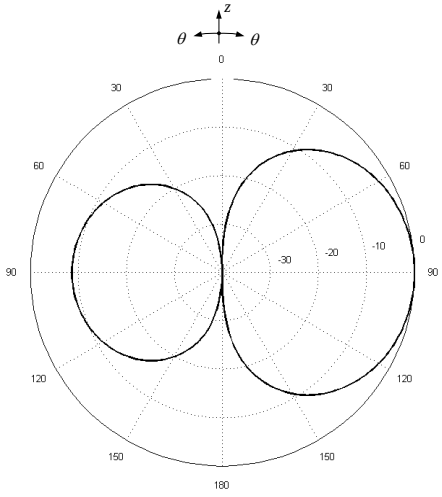

1.8 GHz

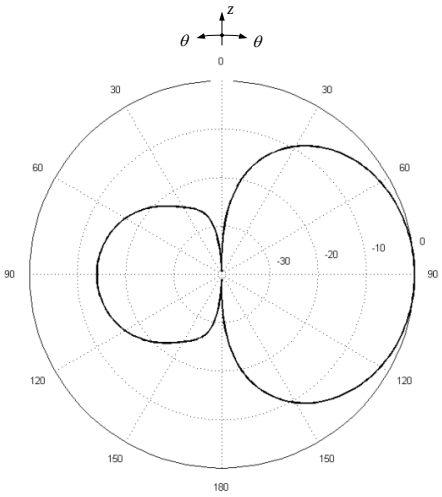

2.1 GHz

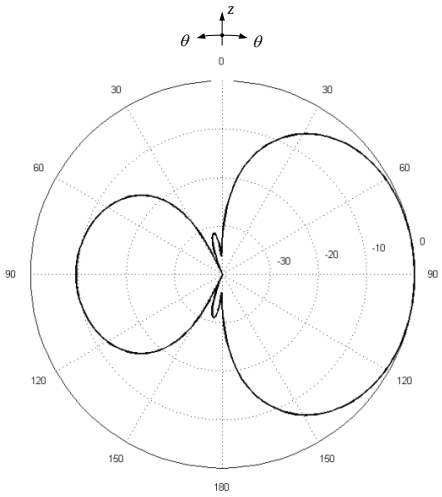

2.45 GHz

Figure 3.9. Simulated XZ Plane of Standard Printed LPDA

(cont. on next page)

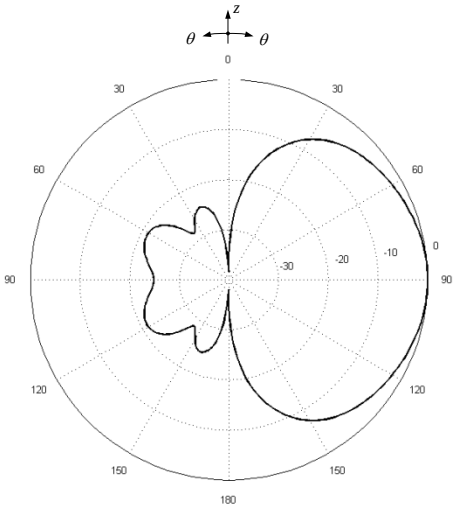

3.1 GHz

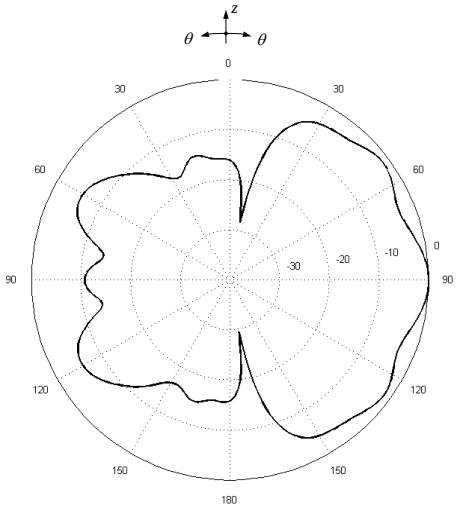

5.8 GHz

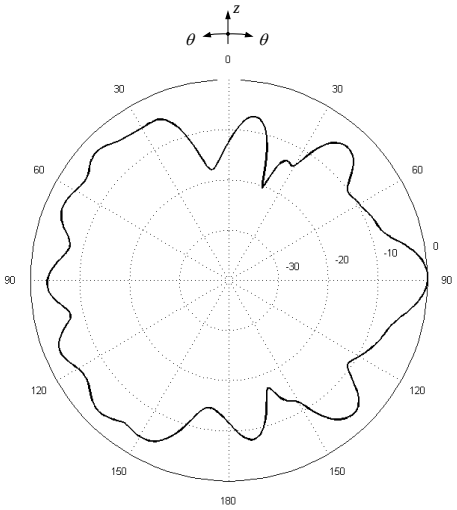

8 GHz

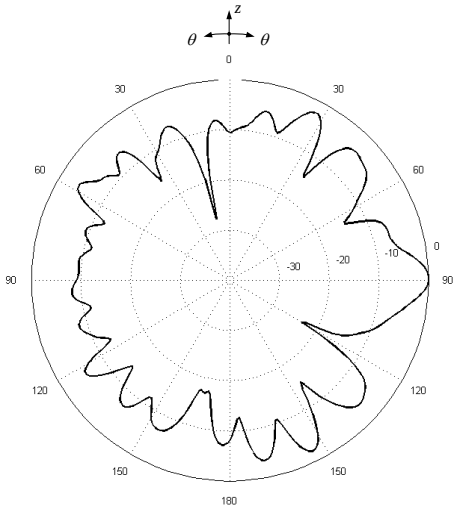

10.6 GHz

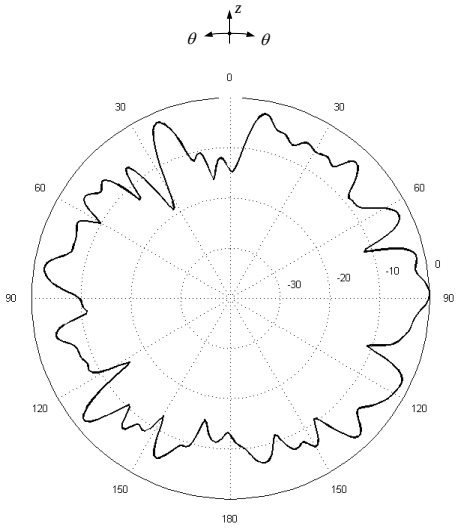

12 GHz

Figure 3.9. **(cont.)**

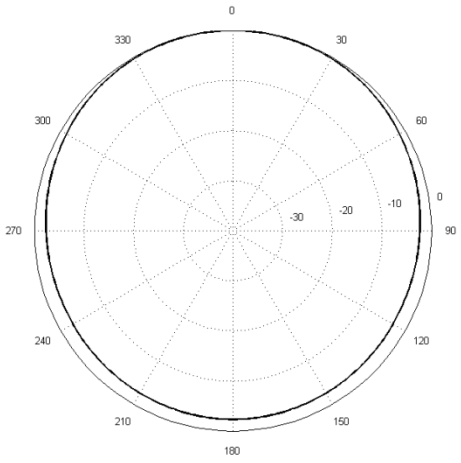

1 GHz

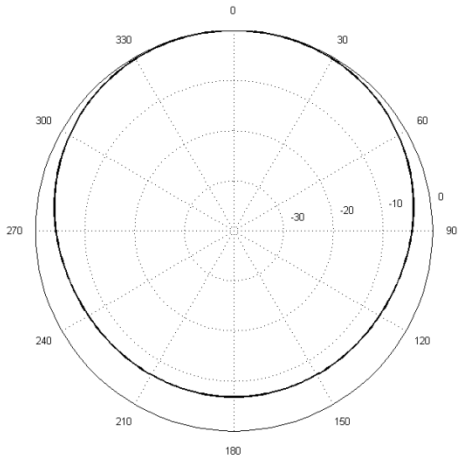

1.227 GHz

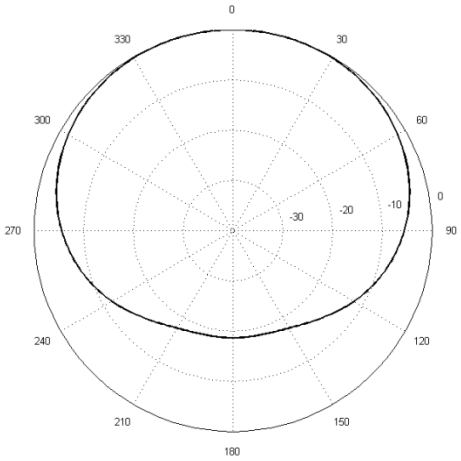

1.575 GHz

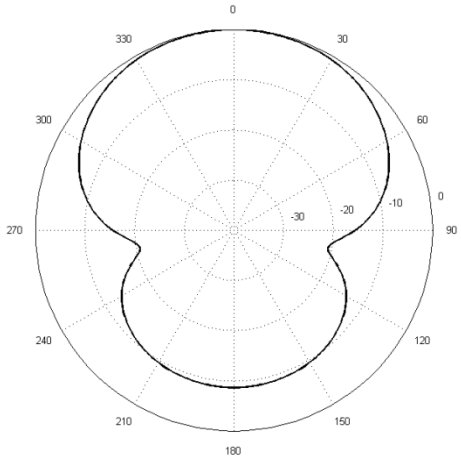

1.8 GHz

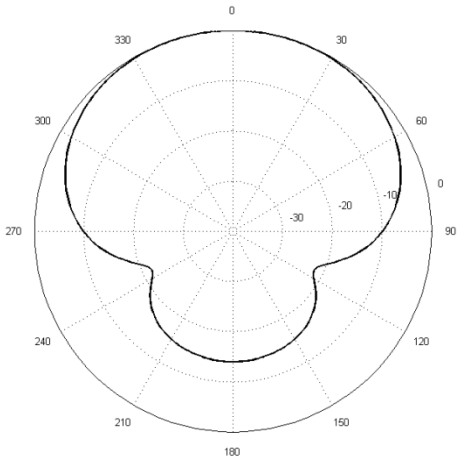

2.1 GHz

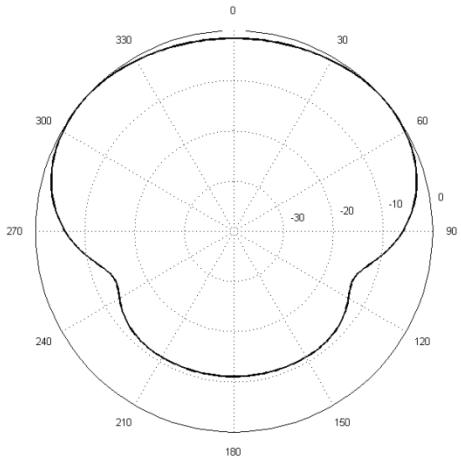

2.45 GHz

Figure 3.10. Simulated XY Plane of Standard Printed LPDA

(cont. on next page)

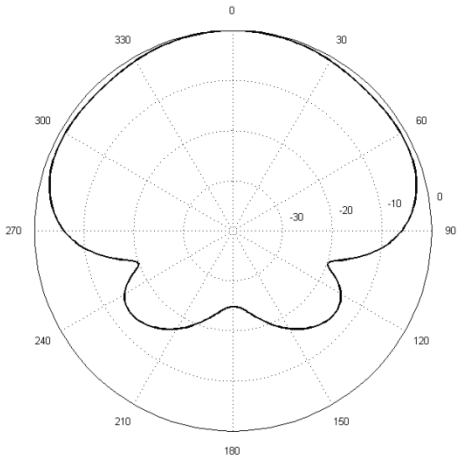

3.1 GHz

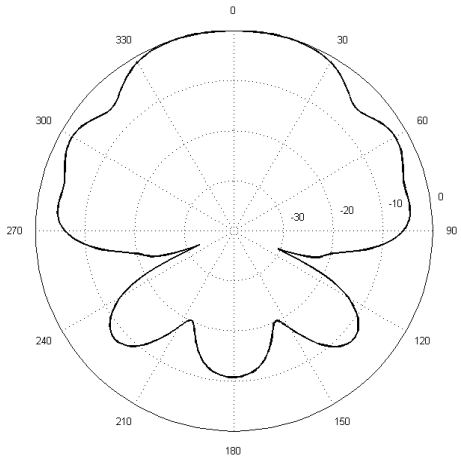

5.8 GHz

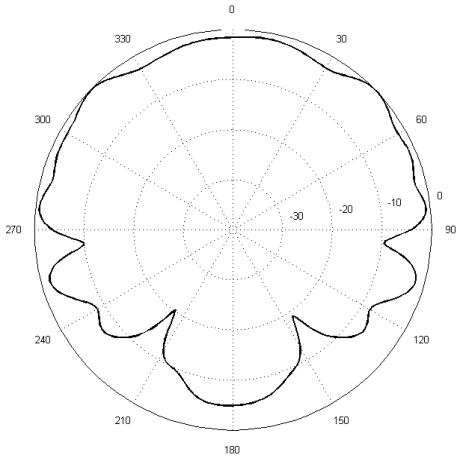

8 GHz

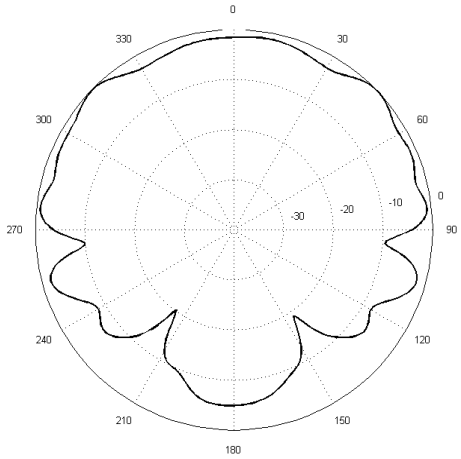

10.6 GHz

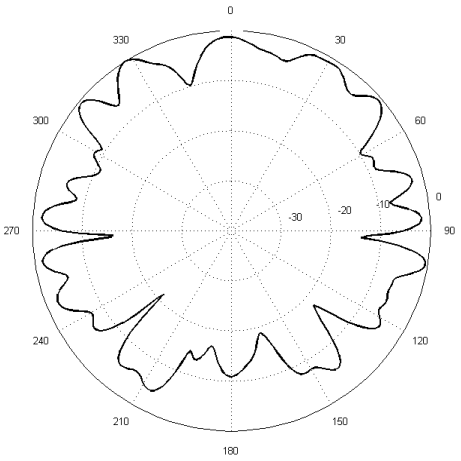

12 GHz

Figure 3.10. **(cont.)**

3.1.2. Design of Sub-Sectional Tapered Fed Printed LPDA Antenna with a Feed Point Patch

Standard Printed LPDA antenna has a highly exciting bandwidth performance at upper frequency bands according to simulation results. However, its' performance is poor at 1.5-2 GHz frequency band that GPS and PCS bands are allocated in. One can see that, it makes the antenna multiband and insufficient for wideband applications and multipurpose devices. On the other hand, standard LPDA antennas generally suffer from these kinds of problems. There are many studies have been carried on to improve performance of printed log periodic antennas. For example, microstrip antennas, helical antennas or fractal antennas are used instead of dipole antennas (Chatterjee and Roy, 1968; Kim et. al., 2000; Filho et. al., 2010; Lin et. al., 2011; Dadel and Srisaytava, 2011). Moreover, different feeding techniques are employed for the same purpose (Smith and Meyes, 1991; Tanyer, 2005; Casula, 2010). Although using different elements instead of dipoles provides size reduction, their frequency bandwidths are not wide enough. On the other hand, the proposed feeding techniques provide a little improvement for bandwidths but they require additional realization efforts and damage the planar form of the printed antennas.

In this study, antenna structure is modified to improve lower frequency performance of the antenna. Firstly, keeping the same dimensions of standard printed LPDA, straight line feeding of the standard printed LPDA is substituted for sub-sectional tapered fed (SsTF) shaped and it is divided into two sections. These sections are designed as tapered to get a smooth impedance matching for each section. Thin strips provide higher impedances as it known from transmission line theory. The first section is optimized as thinner to get better impedance matching between largest three dipoles. The length of the first section feeding is 55.2 mm and the width of the section is 0.5 mm to 0.7 mm from the largest dipole to the third largest dipole. Second section is also a tapered structure but wider than the first section. Length of the second section feeding is 74.8 mm and the width is 0.7 mm to 4.5 mm from the third largest dipole to the port. Drawing of SsTF Printed LPDA antenna is shown in Figure 3.11. This feeding substitution provides good bandwidth performance at lower frequencies and 1.5–2 GHz frequency band is also added to operating frequency of the antenna. However, upper operating frequency decreases to 9 GHz. Lastly, it can be said that multiband behavior

of the standard printed LPDA antenna is converted to wideband antenna which has a 8.27:1 bandwidth ratio.

In addition to feeding line modification, a 10 mm x 3 mm rectangular patch is also added to only one side of SsTF Printed LPDA antenna as a feeding point patch. The ambition of employing this patch is brooding the frequency bandwidth. Drawing of the Sub-Sectional Tapered Fed with a Feed Point Patch is given in Figure 3.12. As a result of this modification higher frequency bandwidth performance of the antenna is improved and 11.36:1 bandwidth ratio is reached. Simulated comparative S_{11} and VSWR results of the antennas are given in the next chapter.

3.1.2.1. Comparative Simulation Results of Designed Printed LPDA Antennas

Three printed LPDA antenna has been designed. First of them is standard printed LPDA antenna and the others are SsTF Printed LPDA and SsTF Printed LPDA with a Feed Point Patch antenna. All of them have them have the same size and the same number of elements. However, their impedance bandwidths are different each other. To observe these differences clearer, simulated bandwidth performances are compared. First of all, SsTF Printed LPDA antenna and Standard Printed LPDA antenna are compared in Figure 3.13 and Figure 3.14. Then, SsTF Printed LPDA antenna and its' feed point patch added version are compared to observe the effect of rectangular patch carefully in Figure 3.15 and Figure 3.16. Bandwidth parameters of the whole designed antennas are shown in Figure 3.17 and Figure 3.18.

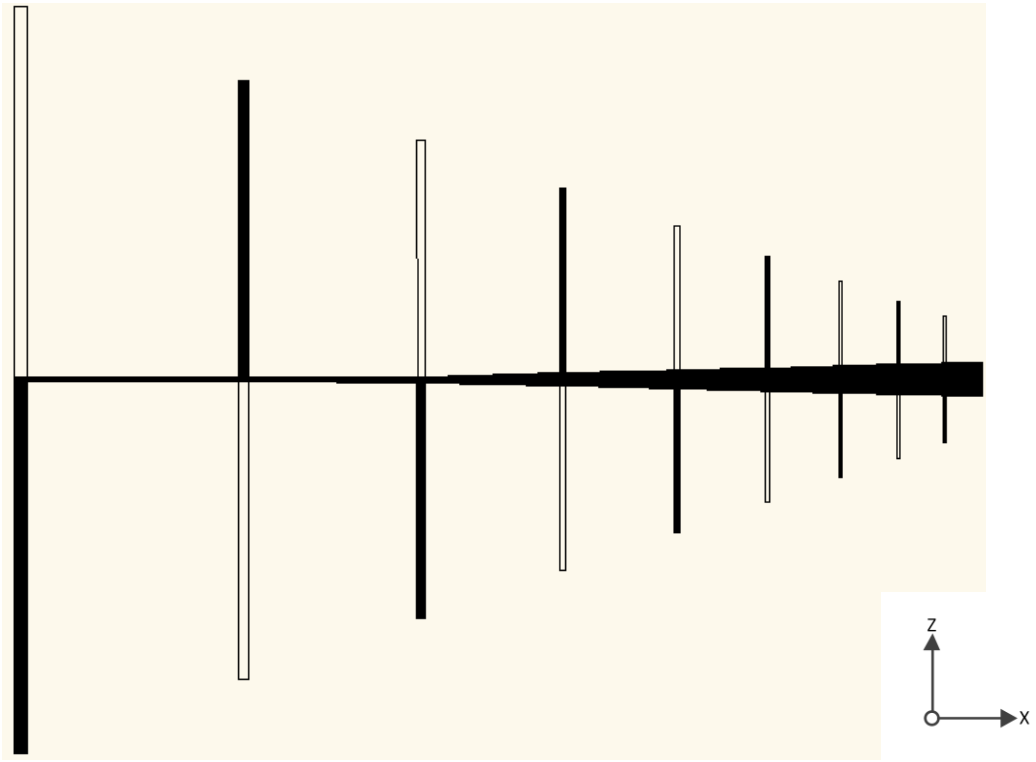

Figure 3.11. Sub-Sectional Tapered Fed Printed LPDA Antenna

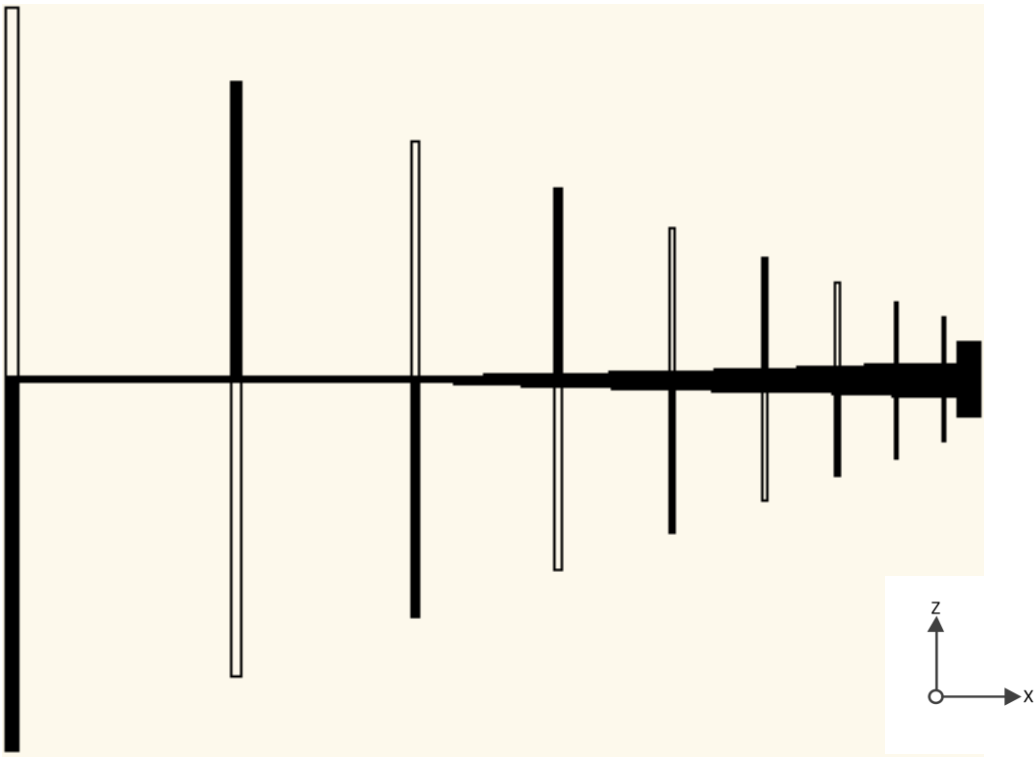

Figure 3.12. Sub-Sectional Tapered Fed Printed LPDA Antenna with a Feed Point Patch

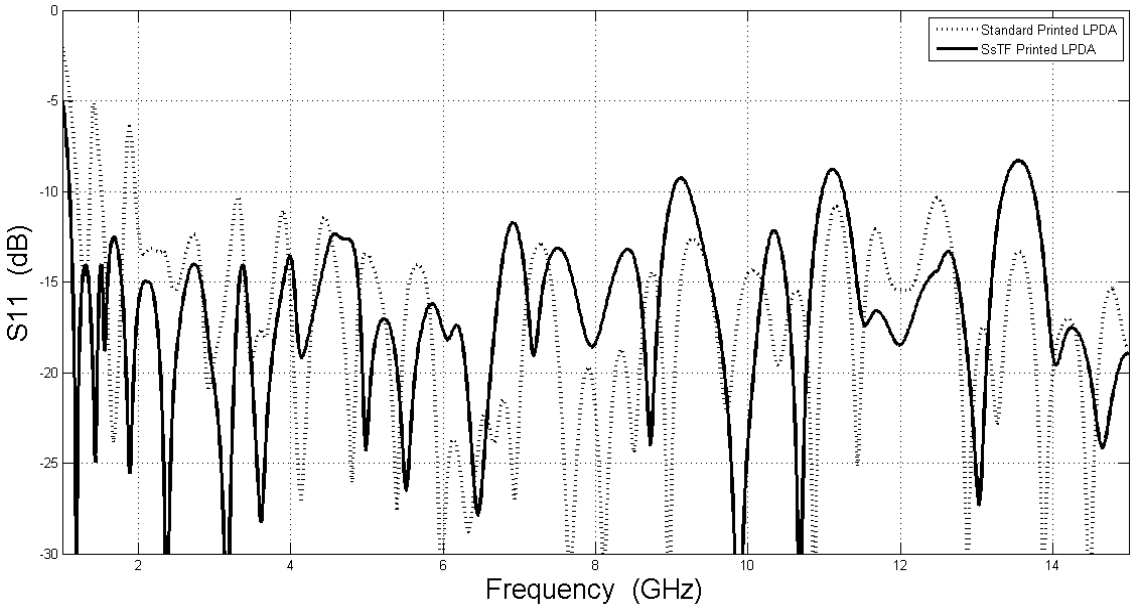

Figure 3.13. Computed S_{11} Comparison of Standard Printed LPDA and SsTF Printed LPDA

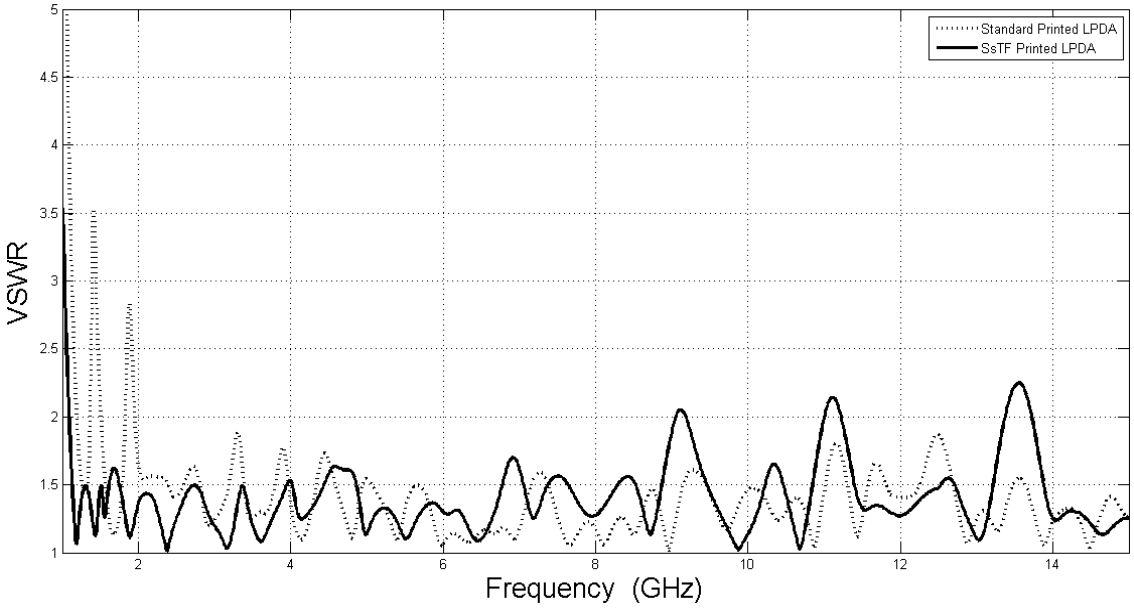

Figure 3.14. Computed VSWR Comparison of Standard Printed LPDA and SsTF Printed LPDA

According to Figure 3.13 and Figure 3.14, standard printed LPDA antenna has a good bandwidth performance at higher frequencies but its' performance is poor at 1.5-2 GHz frequency band that GPS and PCS bands are allocated in. This multiband behavior

of the antenna is converted to wideband by employing sub-sectional tapered feeding. SsTF Printed LPDA antenna operates between 1.1 GHz and 9 GHz. Moreover, its' VSWR is less than 1.5 in the most of the band.

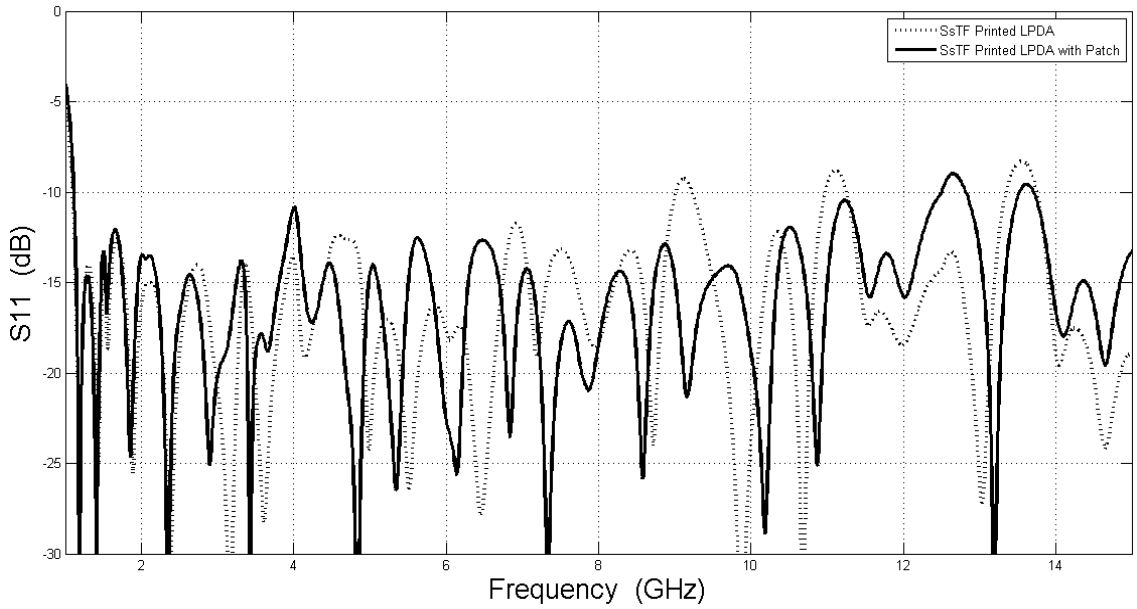

Figure 3.15. Computed S_{11} Comparison of SsTF Printed LPDA and SsTF Printed LPDA with a Feed Point Patch

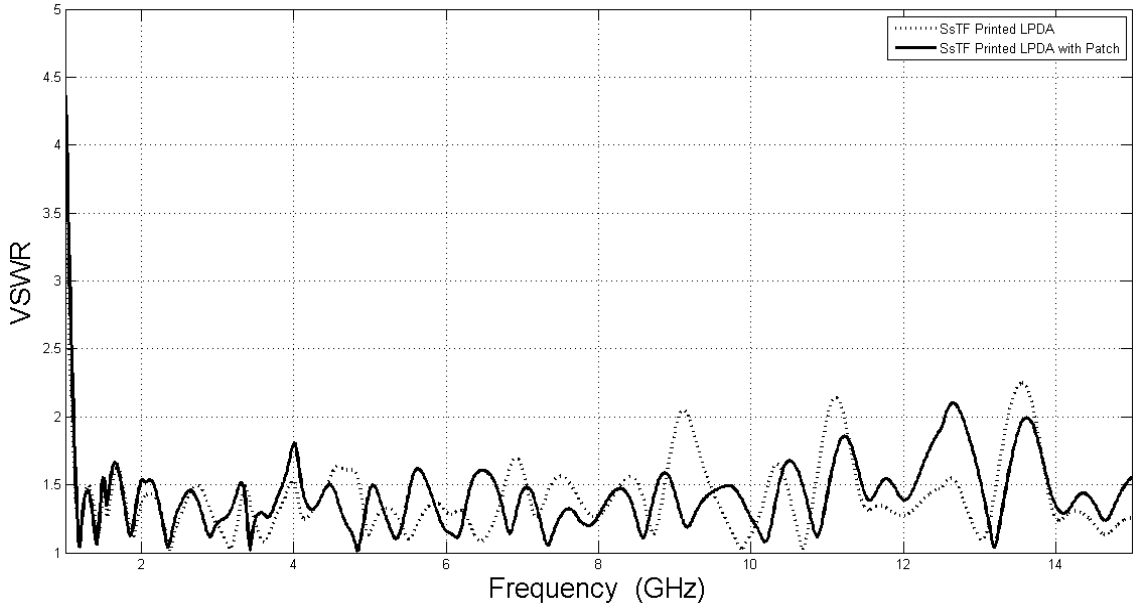

Figure 3.16. Computed VSWR Comparison of SsTF Printed LPDA and SsTF Printed LPDA with Feed Point Patch

The effect of employing a feed point patch can be observed from the Figure 3.15 and Figure 3.16. The upper frequency of the antenna improved from 9 GHz to 12.55 GHz. By the way, the proposed antenna reaches the 11.36:1 bandwidth ratio with having capability of GPS, PCS, IMT-2000, WLAN, WiMAX, UWB and X Band systems.

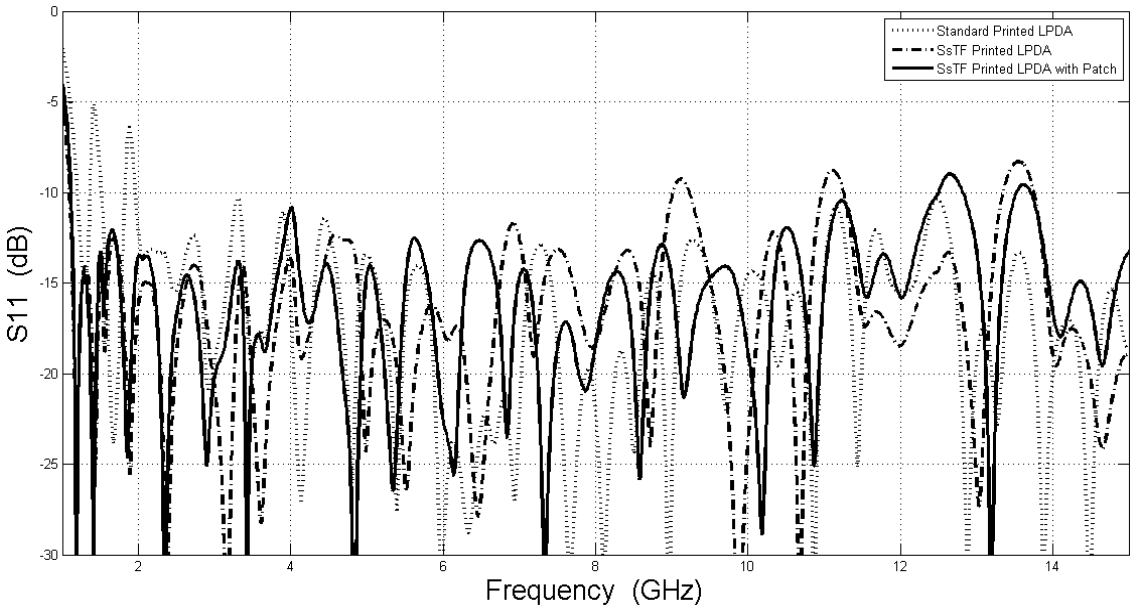

Figure 3.17. Computed S_{11} Comparison of Designed Antennas

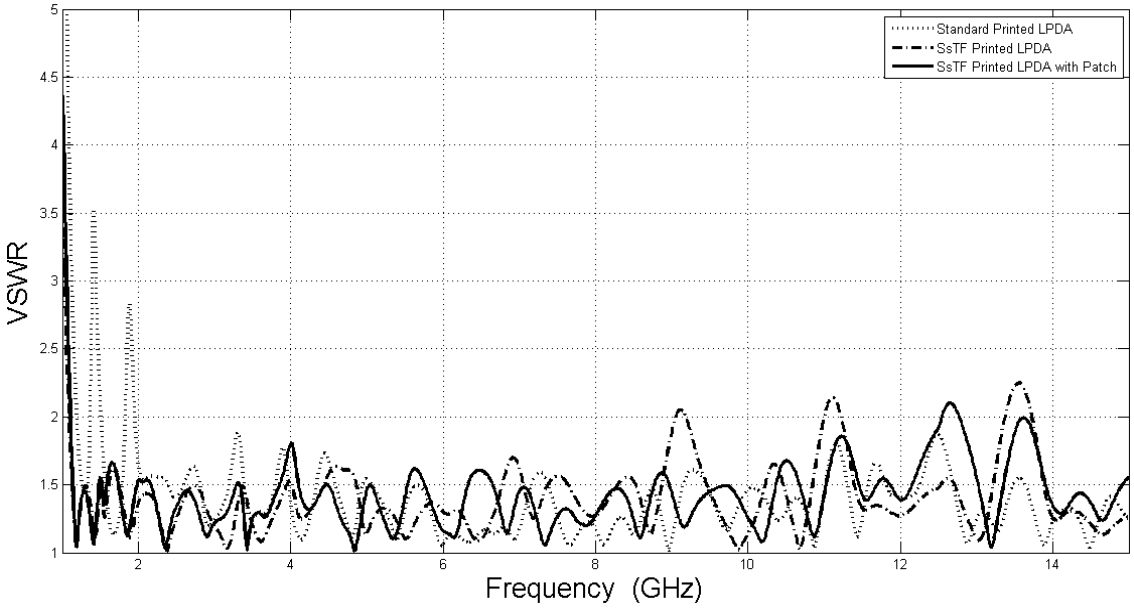

Figure 3.18. Computed VSWR Comparison of Designed Antennas

In Figure 17 and Figure 18, bandwidth performances of the designed antennas are shown. As the results of the simulation comparisons of designed antennas, SsTF Printed LPDA with feed point patch design has a superior bandwidth performance. For this reason, the other antenna parameters such as group delay, radiation pattern and gain will be measured and represented only for this design. Comparisons of measured and simulated results are given in chapter 3.1.5.

3.1.3. Realization Process of Designed Antennas

In printed antennas, particular metallization patterns are realized on the substrate to be able to measure their real performances and use them in real applications. In this study, all of the designed antennas which have very thin slots and lines are realized on a substrate in acceptable limits of accuracy. This process can be categorized in four parts: CAD layout, masking, etching also called developing and soldering.

For realization of any printed antenna, a proper mask has to be prepared first. The mask is a printed layout of the structure of designed antennas on paper. Without no doubt, using a CAD program for drawing of the structure had better to draw it by hand in order to get a accurate mask. Thus, AutoCAD program which provides very sensitive drawing, ease of usage and cooperation with HFSS is used. Firstly, both sides of the designed antennas are exported from HFSS to AutoCAD. Necessary adjustment such as filling the drawing in dark black, aligning the lines or adding some markers are made on imported layouts. Then, two adjusted layouts are printed out on special papers which allow the propagation of UV light such as acetate sheets or translucent sheets. Used masks for realization of standard printed LPDA antenna is shown in Figure 3.19. Dark areas of masks represent the areas which are going to be metallic part of the antenna because of employing positive photoresist material.

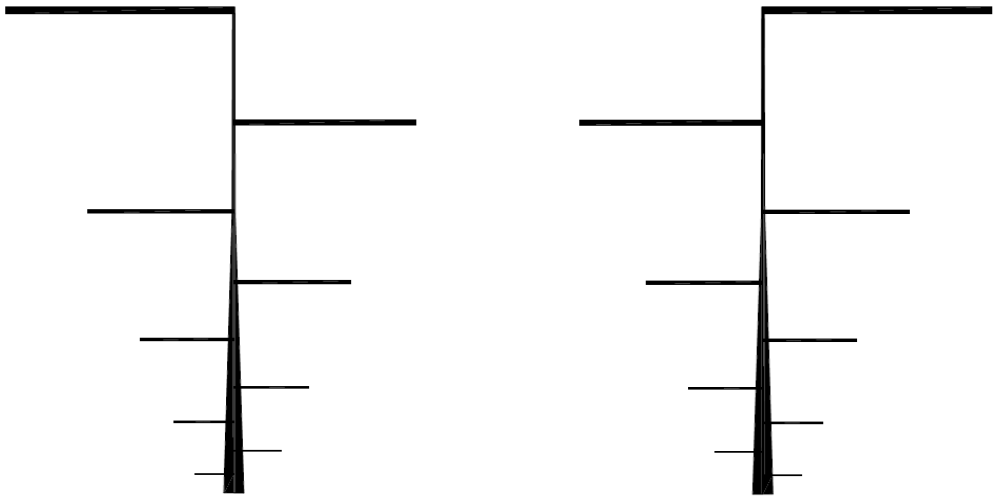

(a) (b)

Figure 3.19. SsTF Printed LPDA Antenna Masks (a) Top Side (b) Bottom Side

Before masking step, the substrates must be prepared to UV exposure process. Bifaced substrates which have two metallic surfaces are employed in this study since designed printed log periodic dipole array antennas and printed monopole antennas whose design considerations will be given in next chapters are bifaced. Two different substrates are used. One of them is Bungard FR-4 and the other one is Rogers 4003C. FR-4 substrates have their own photoresist layers on metallic surfaces but the other type of materials have not. Hence, 4003C substrates have to be covered with photoresist before using them for the next processes. Cramolin Positive Resist spray is used for covering them. The substrate is made grease free by cleaning and it is dried completely to avoid bad effect of humidity on the adhesive strength of photoresist. Then, photoresist is sprayed on the substrate through a nozzle in a very dim light room. Since the difficulty of obtaining constant photoresist thickness, plate is placed horizontally and spray is applied approximately for 10 seconds from a distance of 20 cm. Also, spraying continuously with serpentine lines helps to get uniform coverage. Applying too much photoresist causes undesired thickness differences and increases the thickness of photoresist layer. While longer UV exposure time is required because of thicker photoresist layer, etching performance and quality of metallization decrease because of non-uniformity of photoresist layer. Sprayed substrate is dried in dim light room to reach good characteristics of reproduction and adhesion. Drying process is done by hot-air blower in duration of approximately 6 - 7 minutes. Lastly, same process is applied to

another side of substrates and then substrate becomes ready for next steps of the realization process.

Printed masks properly attached to surfaces of substrates having photoresist layer and they are put into to UV exposure device. In this study, Isel vacuum UV exposure device including 4 florescent tubes and having 135 watt power consumption is used. Duration of exposure varies from application to application but thickness of photoresist plays a dominant role. In this realization work, 3 minutes and 12 minutes are optimized respectively for each side of FR-4 and 4003C substrates. This duration difference caused from thickness uncertainty of handmade photoresist covering of 4003C substrates. Over exposure duration can give better results when thin lines and slots are considered. Otherwise, it means waste of time.

Afterwards, exposed substrates are washed with a sodium hydroxide (NaOH) solution in a few minutes. The solution is prepared with 5gr/l concentration at approximately 40^{o} C. When the solution temperature is increased, the speed of chemical reaction between photoresist and the solution increase, too. Although washing time decrease in this condition, reactions usually highly affect to the masked area and damage the desired metallic pattern. The substrate is taken off from the solution when irrelevant photoresist area is totally removed and only masked area is shown. Then, the substrate is washed with water and put into etching solution which is prepared with sodium peroxidisulfate ($N_2S_2O_8$). This etching solution has 300 gr/l concentrations at approximately 100^{o} C. It removes undesired or unmasked metallic areas on the substrate. High temperature is used as catalyzer in this type of acid-metal reactions and considerable amount of time can be saved increasing or keeping constant of the solution temperature. When unmasked metallic area completely removed approximately 15 - 30 minutes later only desired metallic pattern of antenna with photoresist mask is appeared and the substrate is taken off from the etching solution. Only desired metallic pattern of antenna with photoresist mask is appeared. Finally, printed antenna is got by removing photoresist mask by acetone or alcohol. Etching steps are shown step by step in Figure 3.20.

Printed antennas are going to be ready for measurements after soldering of SMA connectors. They are connected to the produced antennas with using minimum solder. It is an important point because of avoiding unexpected scatterings and measurement errors.

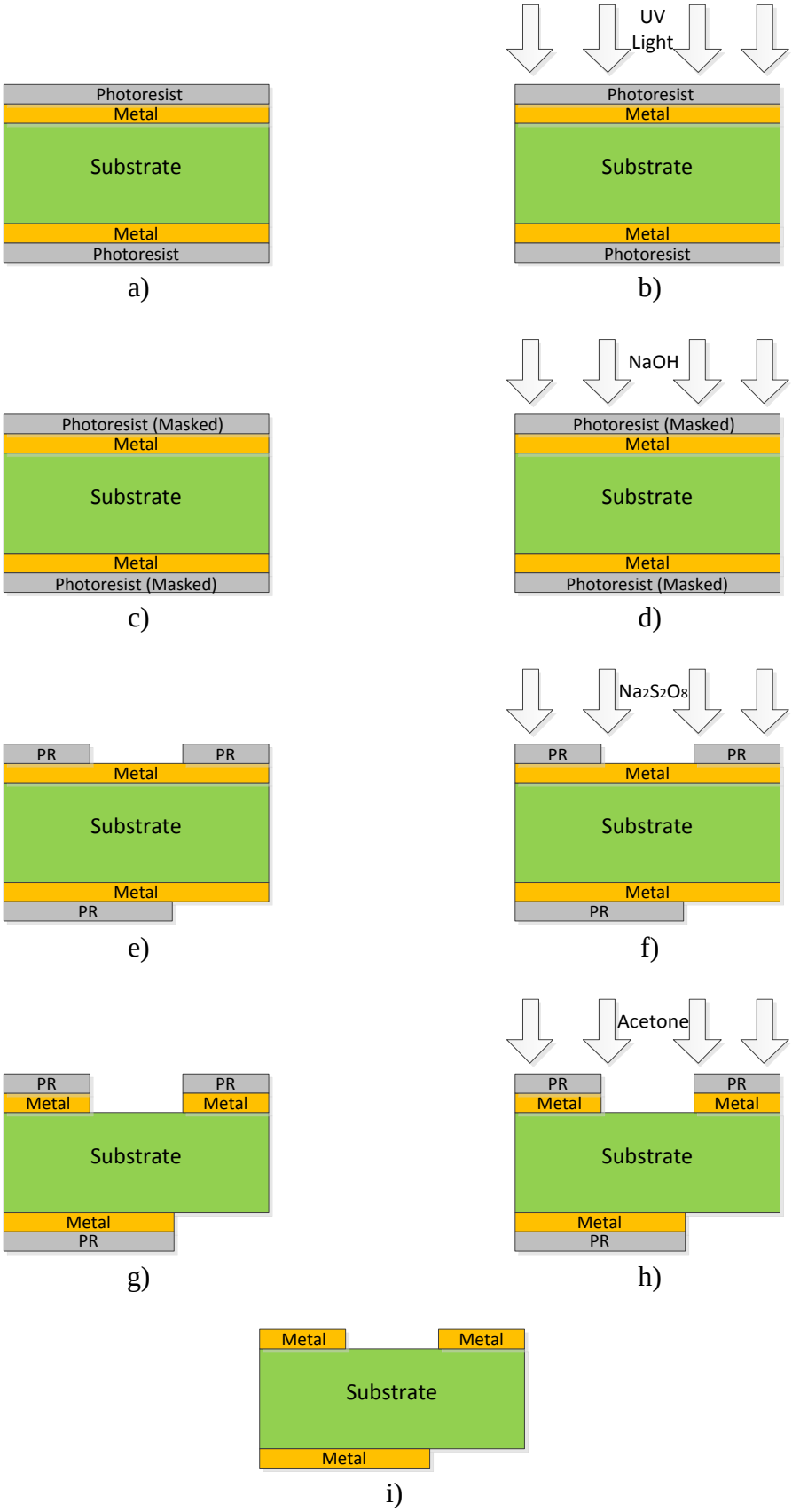

Figure 3.20. Step by Step Etching Process

3.1.4. Measurement Process of Realized Antennas

Determination of an antenna performance accurately is as important as design of the antenna because measurement is the only way to ensure specifications and characteristics of the any antenna. The necessary antenna performance criteria vary according to the applications, employed wireless systems and local or worldwide regulations. In antenna measurement literature, there are many parameters using for determination of antenna performances. However, as it have been mentioned performances of designed antennas are investigated in terms of S_{11}, voltage standing wave ratio, group delay, radiation pattern and gain in this study.

Antenna metrology requires not only solely theoretical background in antenna theory but also sophisticated equipment and measurement environment which are capable of providing the necessary accuracy and purity of the measured data. Commercial equipment specifically designed for antenna measurement become available in the 1960s due to the requirements of the aerospace and defense industries. Roughly, antenna measurement equipment includes: antenna measurement sites such as anechoic chambers, antenna positioners, vector network analyzers (VNAs), spectrum analyzers, RF signal generators, surely sophisticated computer systems providing automated control of devices, performing calculations and processing collected data.

In this study, two computer based measurement systems are used to more accurately measure the performance of realized antennas. Radiation patterns and gain measurements are done in the anechoic chamber of IzTech Wireless Center. The other measurements are done by a VNA in IzTech Microwave and Antenna Research Laboratory.

3.1.4.1. Network Analyzer Measurements

Return loss, voltage standing wave ratio and group delay parameters are measured by Agilent 8720D VNA. Since the VNAs have the potential to provide exceptional accuracy, they are unique devices among the RF instrumentation. Few RF instruments can match the measurement performance of better than ± 0.1 dB that most VNAs offer. One of the reasons of this exceptional performance is calibration which is performed by user before making a measurement. Additionally, VNAs have two key

traits providing such a high performance. First of them is making proportional measurements such as S parameters. The other one is the built-in device architecture where the local oscillator, signal generators and receivers share the same physical platform. Hence, any changes in measurement environment such as temperature variations, electromagnetic interference (EMI) effects equally the parts of the device.

It is obvious that VNAs have no inherent accuracy. Without proper calibration both in amplitude and phase, taking full advantage of VNA measurement accuracy is almost impossible. Further, the quality of the calibration has direct impact on the quality of the measurements because calibration usually addresses systematic errors. To avoid them and reduce measurement uncertainty, calibration must be performed carefully by using proper torque, high quality cables and good connectors must be employed. On the other hand, any change in instrument settings between calibration and measurements invalidates the calibration. After calibration but before starting measurements, calibration is checked by generally measuring S parameters of short, open and load.

After performing and checking of the calibration, measurements are made by an automated computer program to reduce errors, improve quality and get necessary data easily. The program has been developed in LabView and its' connection is provided by USB-GPIB cable. In Figure 3.21, user interface of the program is shown.

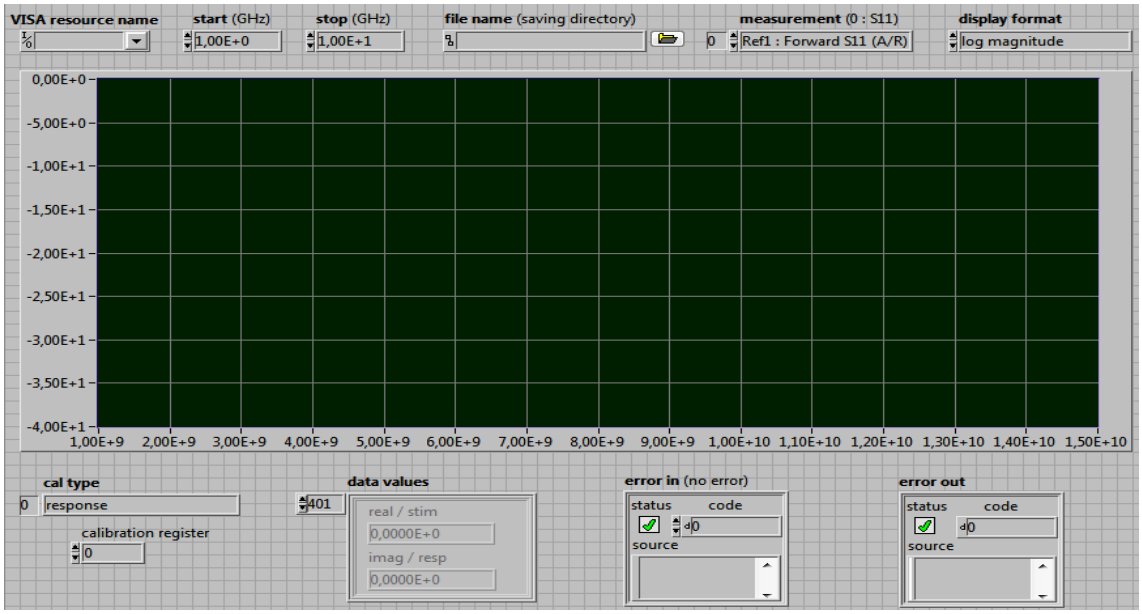

Figure 3.21. User Interface of Network Analyzer Measurements Program

3.1.4.2. Anechoic Chamber Measurements

Radiation pattern and gain measurements of realized antennas are performed in an anechoic chamber which provides convenience and controlled electromagnetic environment. Anechoic chambers are very popular isolated antenna measurement sites. Their outer wall surfaces are covered by steel sheets and their inside surfaces have special lining with RF absorbing material such as ferrite and pyramidal Styrofoam. By the way, both reflections occurred in the chambers are minimized, as well as ideal security against outer electromagnetic noise and interface is provided. Anechoic chamber conditions are highly close to conditions dealing with in numerical calculations and simulations.

To obtain a three dimensional or complete radiation pattern require the measurement of all ϕ and θ angles. It is a very complicated process and needs extra laboratory equipment. On the other hand, the radiation pattern is practically measured in principal planes: XY and XZ planes which can be also called horizontal and vertical planes.

A specific instrumentation set up is prepared for the measurement. This set up can be divided into four main parts: Transmitting, Positioning, Receiving and Display. All of these parts are instrumented and combined via a developed computer program in LabView environment. Transmitting part includes a RF source and a transmitting antenna. HP 83620B Swept Signal Generator is used as RF source and A.H. Systems SAS-571 horn antenna is used as transmitter. In positioning part, a turntable with the controller is employed and antenna under test (AUT) is mounted on the turntable. The necessary positioning, speed and direction data is sent to turntable and got the responses from turntable via the controller. In this set up, Innco DS-1200 turntable and Innco CO 1000 controller are used. AUT and Spectrum Analyzer are the elements of receiving part. AUT is connected to Spectrum Analyzer and received signal is measured. Received signals are recorded and desired representation is plotted in display part. In Figure 3.22, hardware representation and user interface of the software are shown.

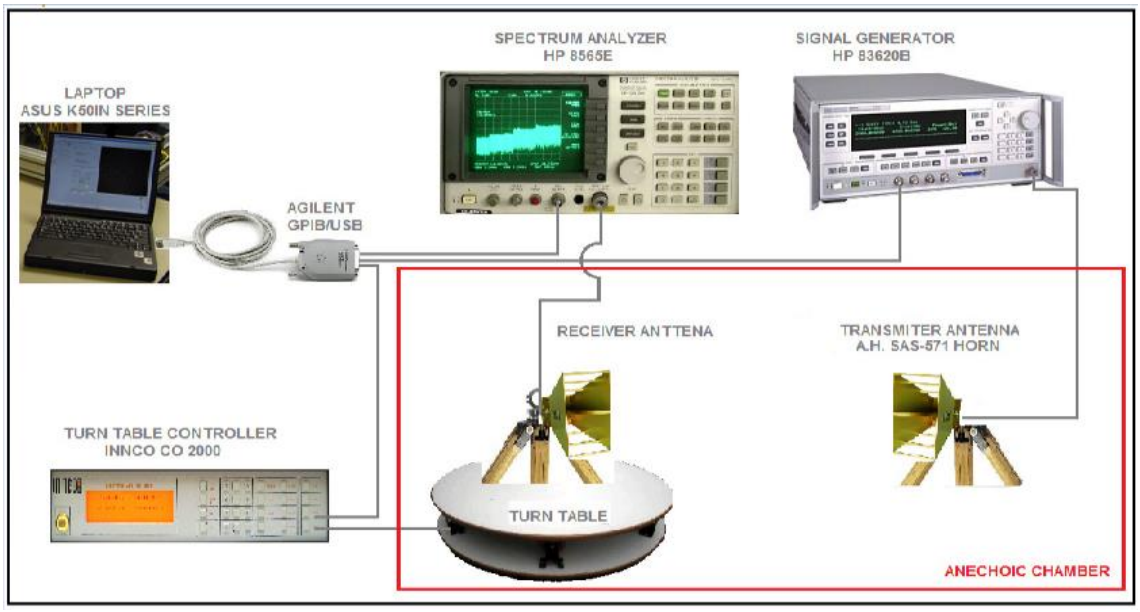

(a)

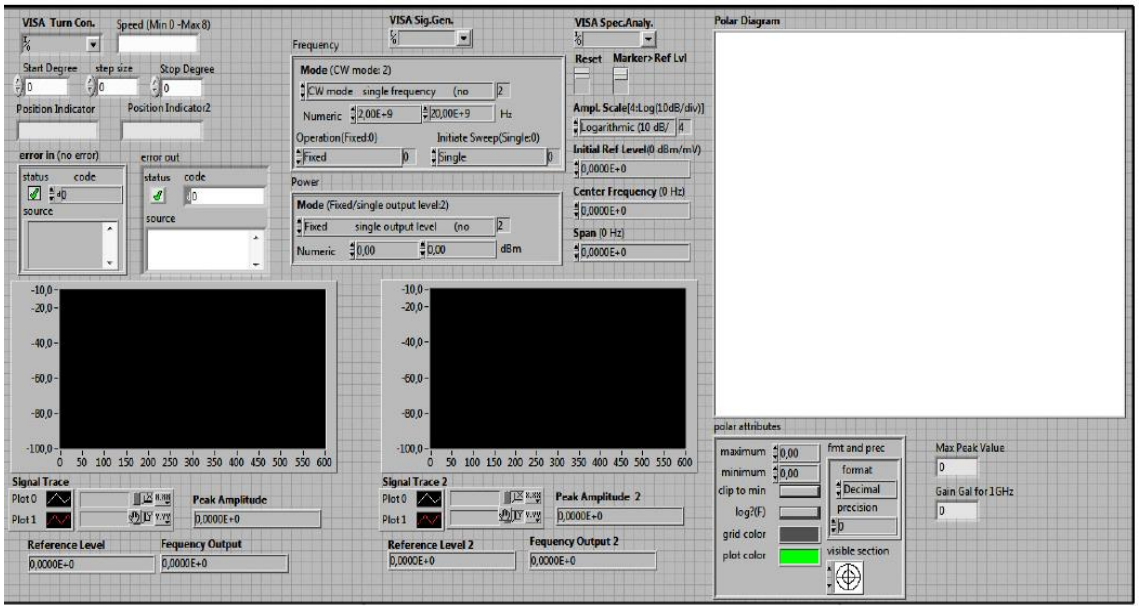

(b)

Figure 3.22. Radiation Pattern Measurement System (a) Hardware and (b) User Interface of Radiation Pattern Measurement System

The gain comparison method is used for antenna gain measurement. In addition to AUT and transmitting antenna, a reference antenna whose gain is exactly known is required in this method. Then, two sets of measurements are performed. In the first measurement, AUT is used in receiving mode and its received power P_{AUT} is measured. In the second measurement, reference antenna is used in receiving mode and received power P_{REF} is measured in the exactly the same arrangements such as keeping the transmitted power P_0 and distance between antennas constant. These two measurements

lead to the equations 3.14 and 3.15. G_{AUT} is the gain of the AUT, G_{REF} is the gain of reference and G_0 is gain of the transmitting antenna in the given equations (Balanis, 2005).

$$G_{AUT\ dB} + G_{0\ dB} = 20log_{10}\left(\frac{4\pi R}{\lambda}\right) + 10log_{10}\left(\frac{P_{AUT}}{P_0}\right) \quad (3.14)$$

$$G_{REF\ dB} + G_{0\ dB} = 20log_{10}\left(\frac{4\pi R}{\lambda}\right) + 10log_{10}\left(\frac{P_{REF}}{P_0}\right) \quad (3.15)$$

From 3.14 and 3.15, the expression is derived for G_{AUT};

$$G_{AUT\ dB} = G_{REF\ dB} + 10log_{10}\left(\frac{P_{AUT}}{P_{REF}}\right) \quad (3.16)$$

3.1.5. Simulation and Measurement Results for LPDAs

According to simulation results in chapter 3.1.2.1, Sub-Sectional Tapered Fed Printed LPDA with a Feed Point Patch Antenna design has a superior performance than Sub-Sectional Tapered Fed Printed LPDA and Standard Printed LPDA. To verify these simulation results, all of the designed antennas are realized and measured bandwidth performances are compared. Then group delay, radiation pattern and gain parameters of SsTF Printed LPDA with Feed Point Patch antenna are measured and compared with the simulated results. Fabricated printed LPDA Antennas are shown in Figure 3.23.

Measured S_{11} and VSWR comparisons are given for three designed printed LPDA antennas in Figure 3.24 and Figure 3.25. It can be obviously seen from Figure 3.24 and Figure 3.25 that SsTF Printed LPDA with a feed point patch design has superior bandwidth performance both lower and higher frequencies. Thus, it will be considered for the next measurement comparisons. Simulation and measurement comparisons of the antenna are given in Figure 3.26 and Figure 3.27 for S_{11} and VSWR.

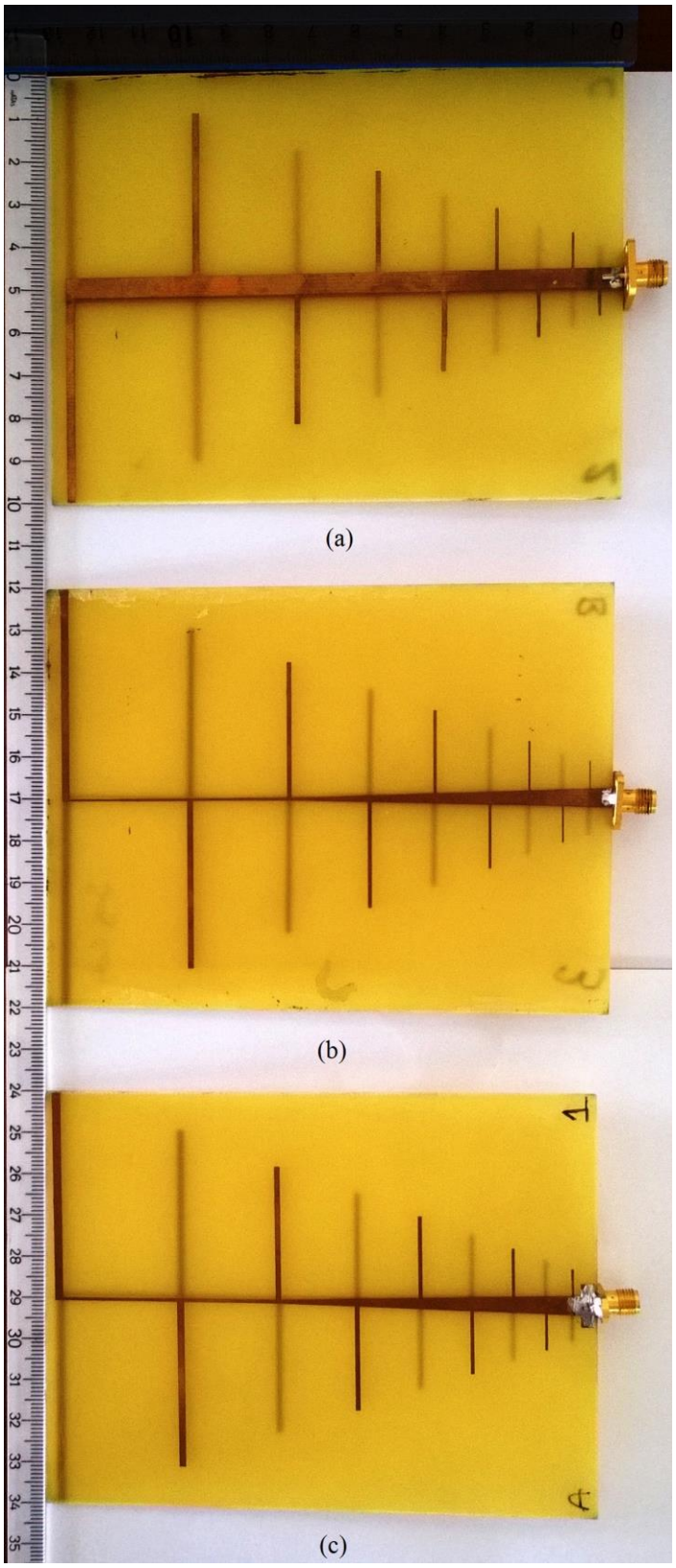

Figure 3.23. Fabricated LPDA Antennas (a) Standard Printed LPDA (b) SsTF Printed LPDA (c) SsTF Printed LPDA with Feed Point Patch

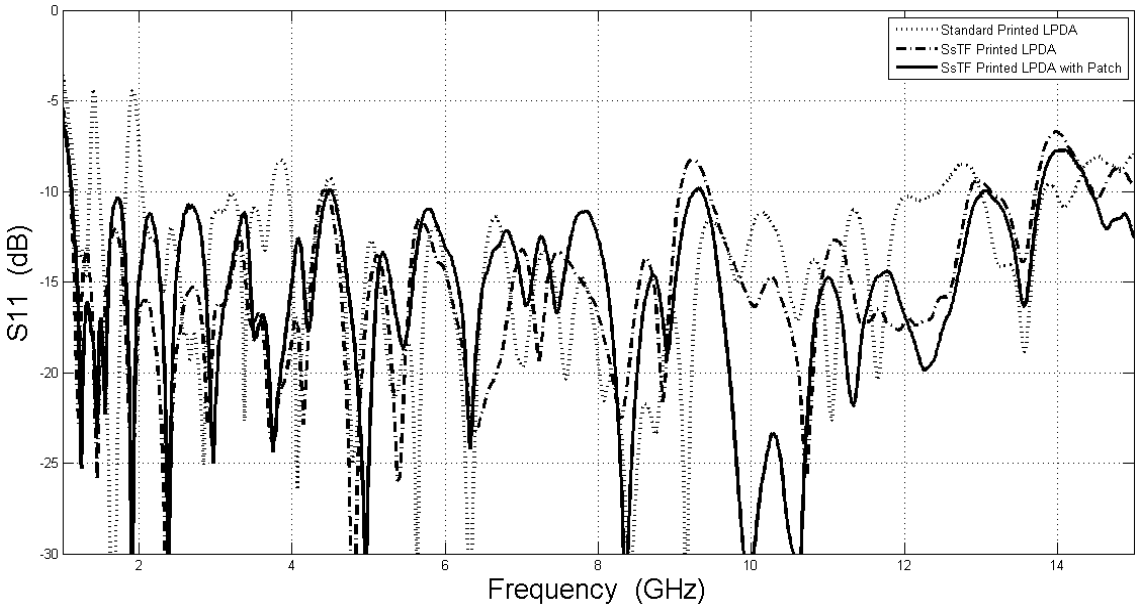

Figure 3.24. Measurement S11 Comparisons of Designed Printed LPDAs

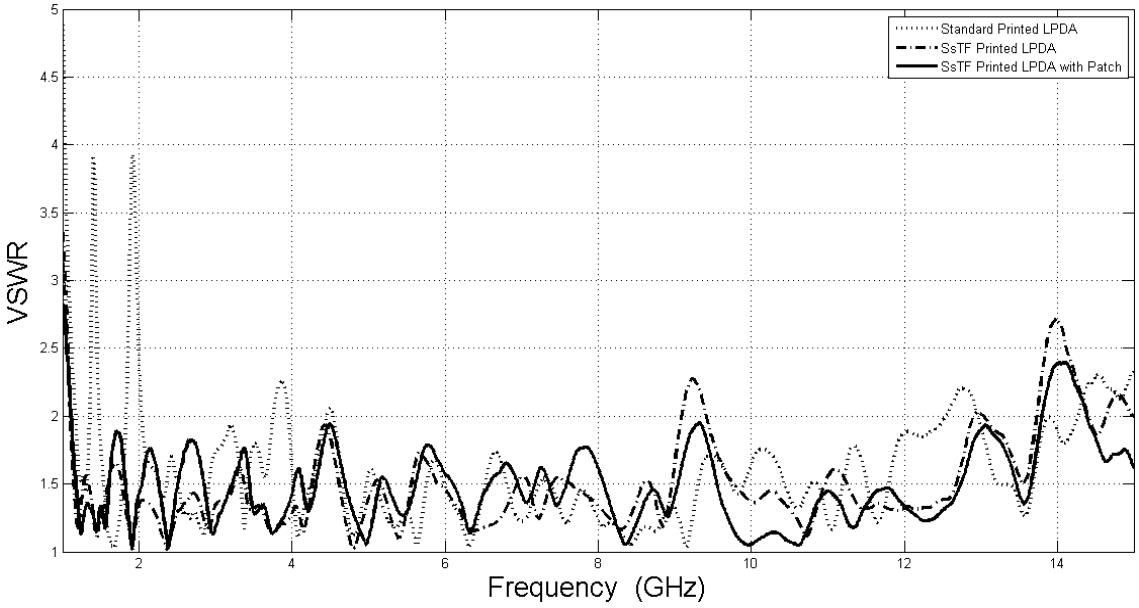

Figure 3.25. Measurement VSWR Comparisons of Designed Printed LPDAs

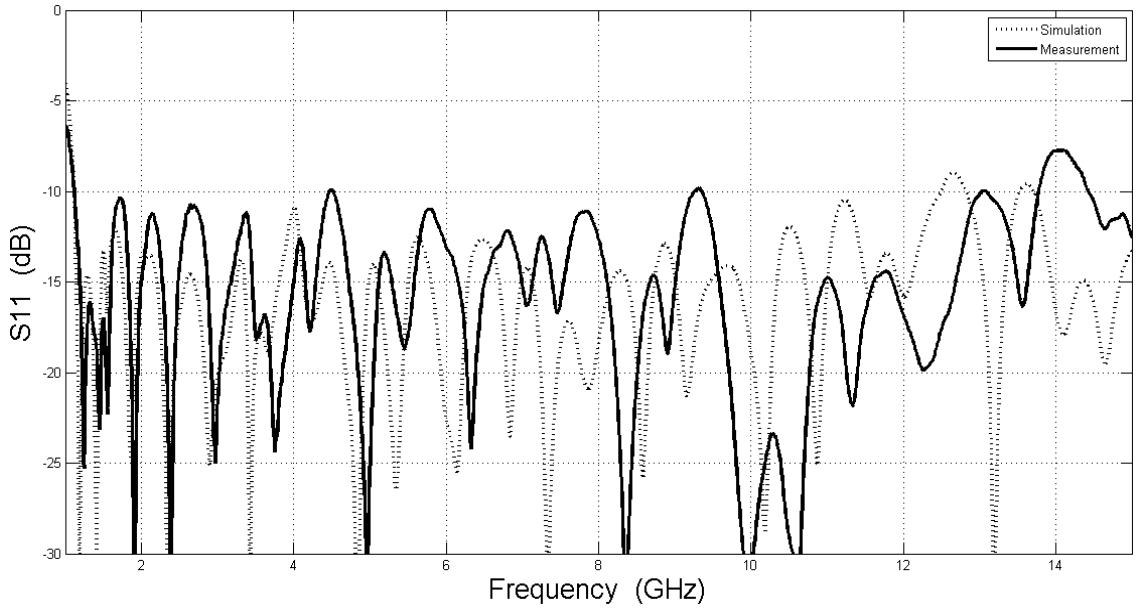

Figure 3.26. Simulated and Measured S_{11} of SsTF Printed LPDA with A Feed Point Patch

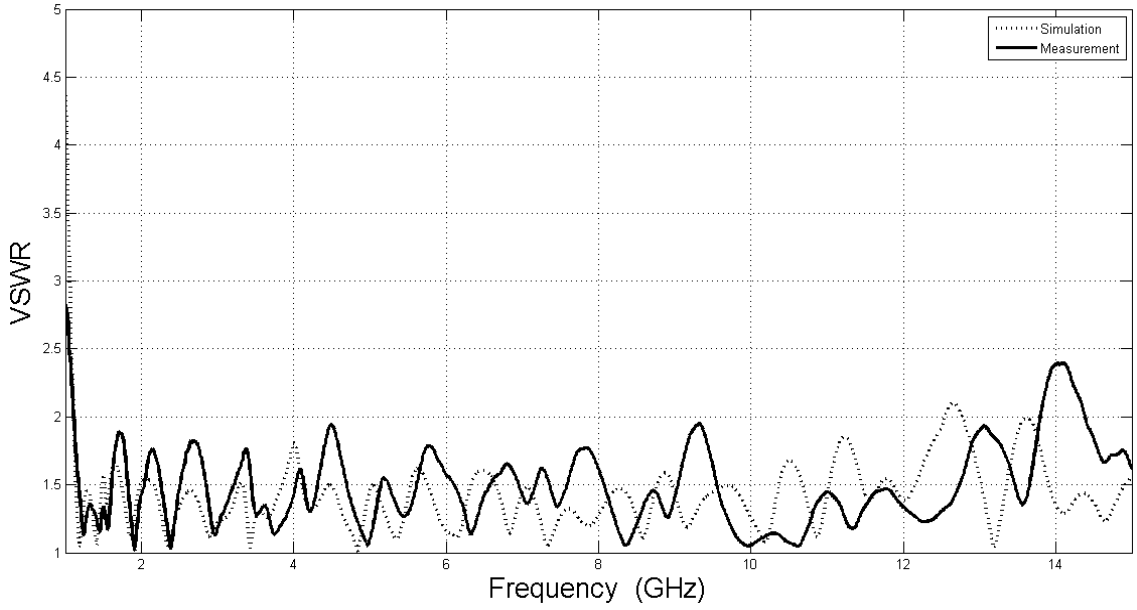

Figure 3.27. Simulated and Measured VSWR of SsTF Printed LPDA with A Feed Point Patch

According to measurement results, the proposed antenna has a 12.55:1 bandwidth ratio and operates between 1.1 GHz and 13.8 GHz. Simulated and measured values of return loss and voltage standing wave ratio have an excellent agreement at lower frequency band. However, a frequency shift occurs towards to higher frequencies

after 5 GHz band and it shifts the simulated upper cut-off frequency from 12.5 GHz to 13.8 GHz. This shifting caused from the unknown dielectric properties of used FR4 in higher frequencies. It can be observed from the measurements that dielectric constant of the used FR4 decreases at higher frequencies.

Measured group delay performance of the antenna is given in Figure 3.28. Since the impulse based communication systems are used in UWB, group delay performance is given between 3 GHz and 11 GHz. As it seen from the Figure 3.28, group delay performance of the antenna is acceptable. It has a good performance because its' deviation is approximately 1 ns and it covers the whole interested frequency band.

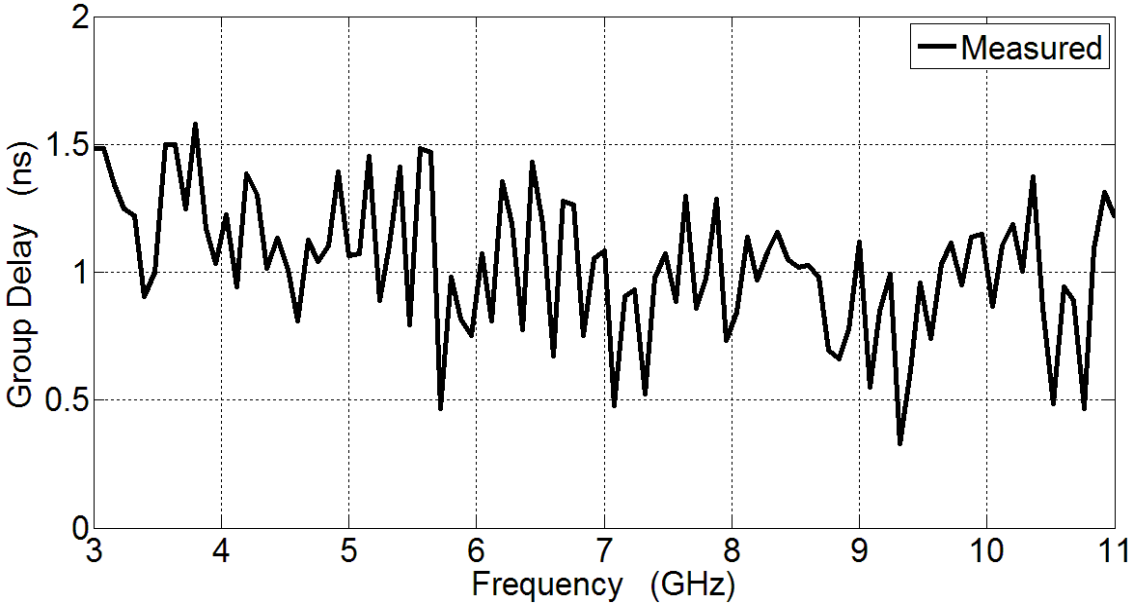

Figure 3.28. Measured Group Delay of SsTF Printed LPDA with a Feed Point Patch

The comparisons of simulated and measured radiation patterns for the frequencies of 1 GHz, 1.227 GHz, 1.575 GHz, 1.8 GHz, 2.1 GHz, 2.45 GHz, 3.1 GHz, 5.8 GHz, 8 GHz and 10.6 GHz are given in Figure 3.29 for XZ Plane and in Figure 3.30 for XY plane. Radiation pattern and gain measurements cannot be performed properly at 12 GHz because of cable loss. R316/U coaxial cable is used as receiver cable and its' insertion loss too high at that frequency. Hence, only noise could be observed.

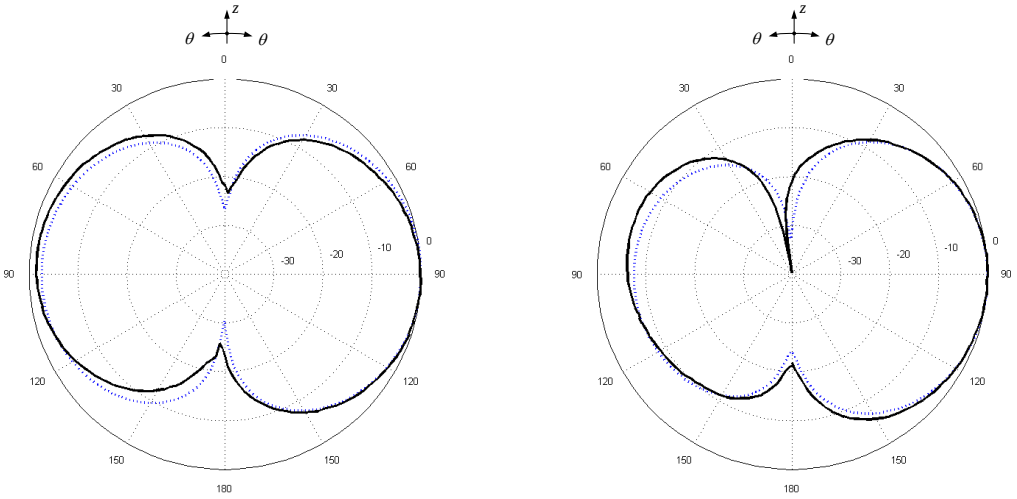

1 GHz

1.227 GHz

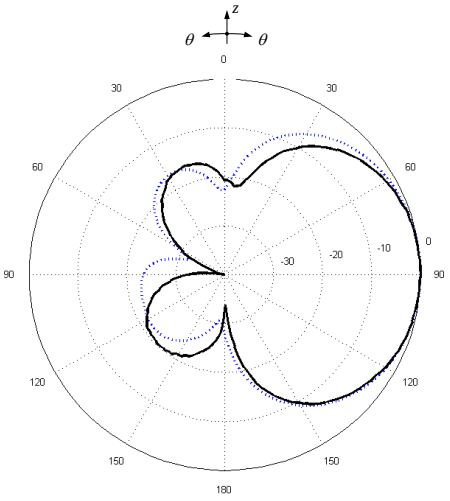

1.575 GHz

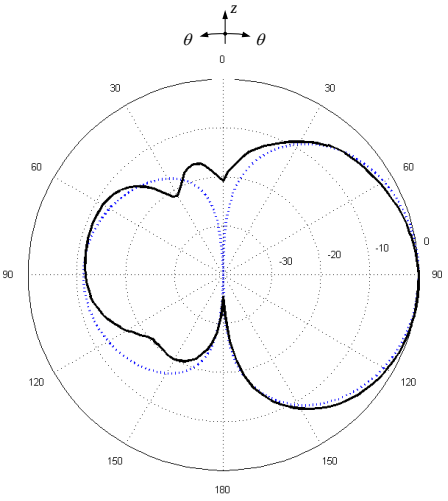

1.8 GHz

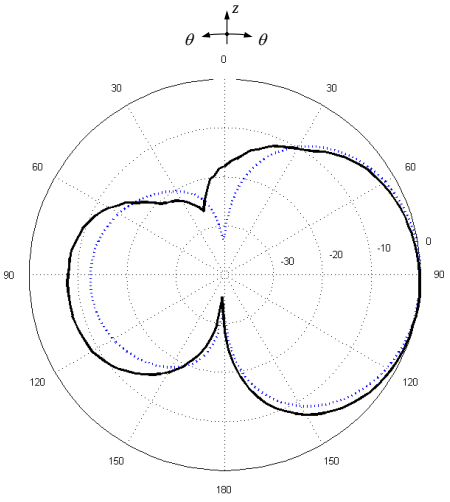

2.1 GHz

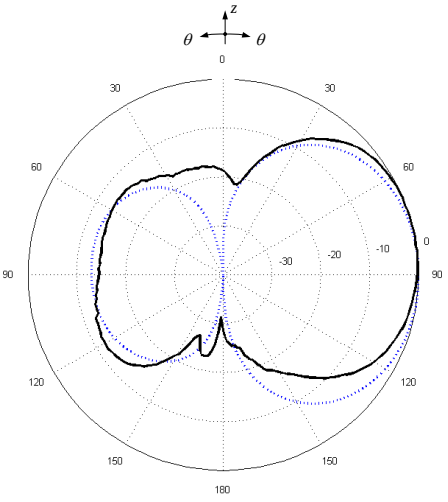

2.45 GHz

Figure 3.29. Measured and Simulated XZ Plane of SsTF Printed LPDA with a Feed Point Patch (···· Simulation — Measurement)

(cont. on next page)

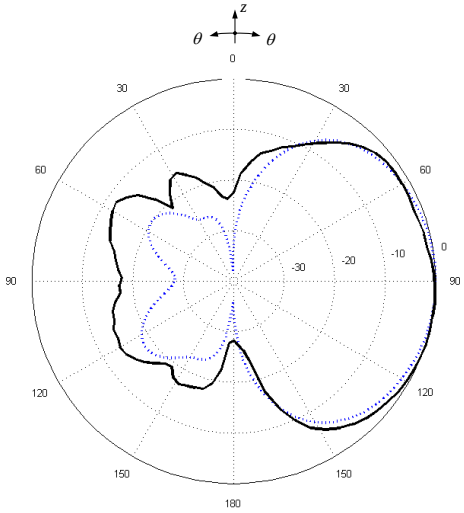

3.1 GHz

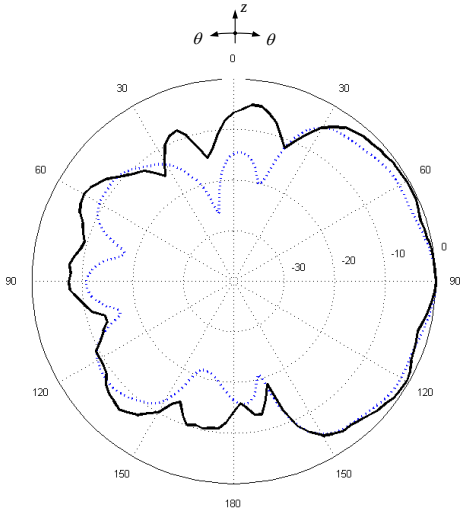

5.8 GHz

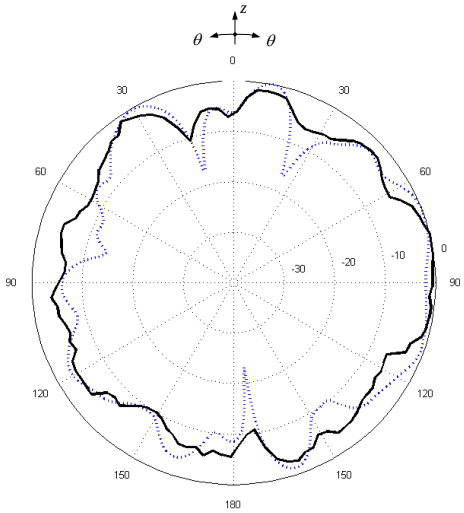

8 GHz

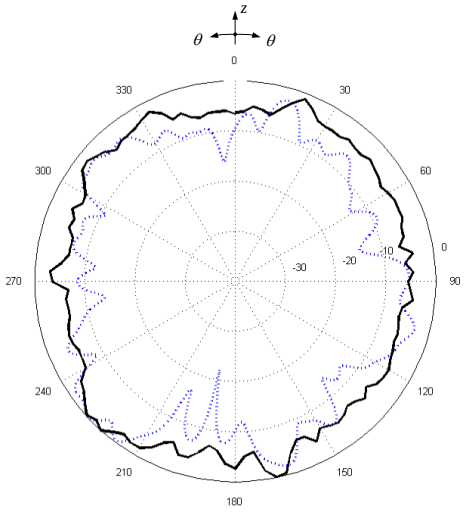

10.6 GHz

Figure 3.29. (cont.)

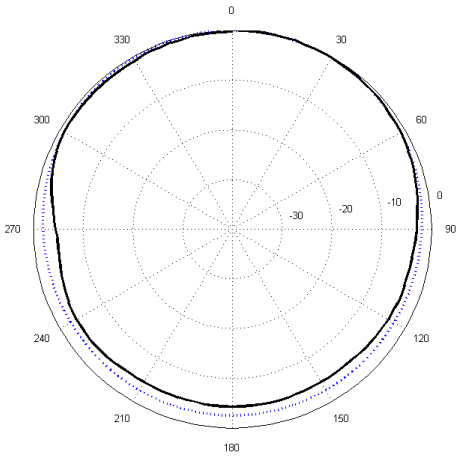

1 GHz

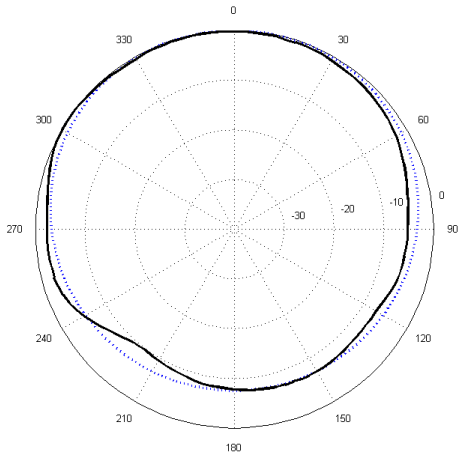

1.227 GHz

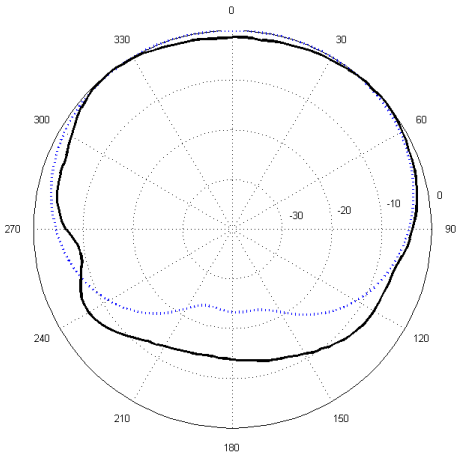

1.575 GHz

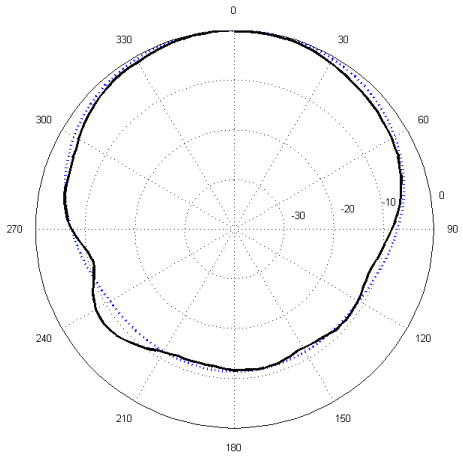

1.8 GHz

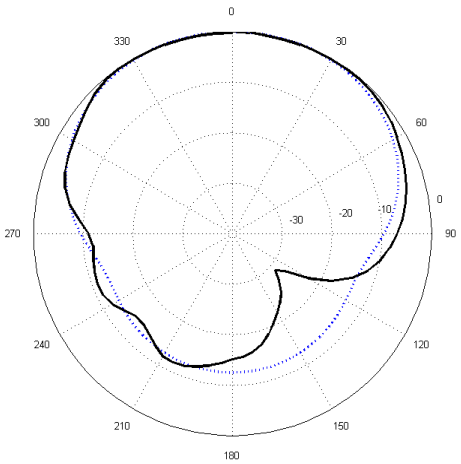

2.1 GHz

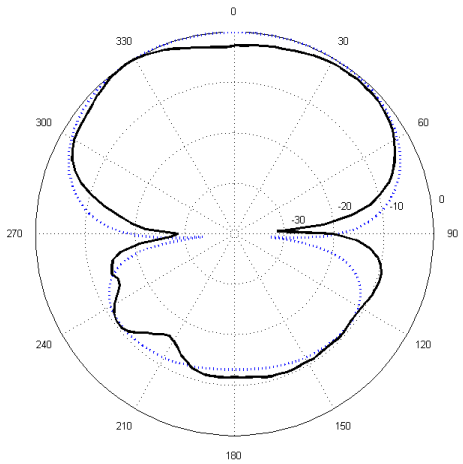

2.45 GHz

Figure 3.30. Measured and Simulated XY Plane of SsTF Printed LPDA with a Feed Point Patch (···· Simulation — Measurement)

(cont. on next page)

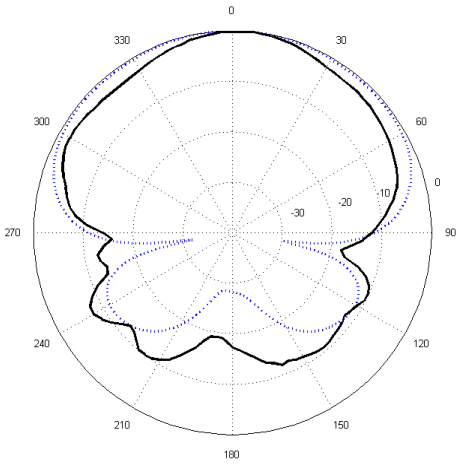

3.1 GHz

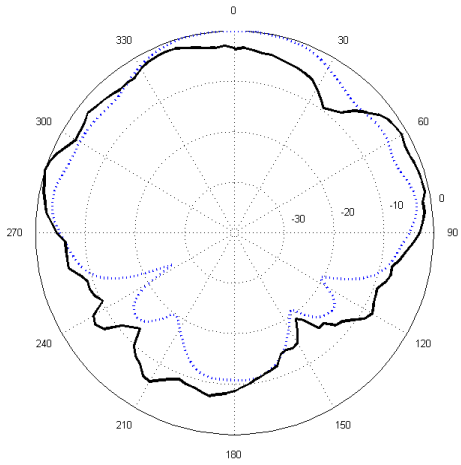

5.8 GHz

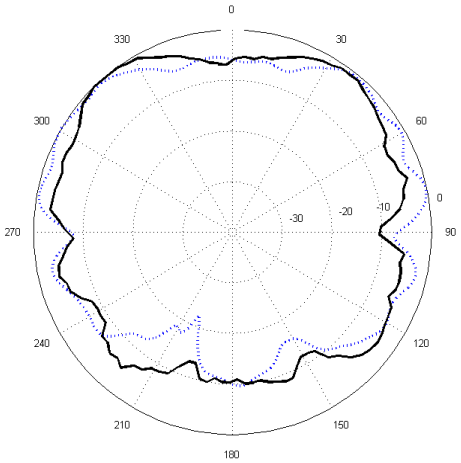

8 GHz

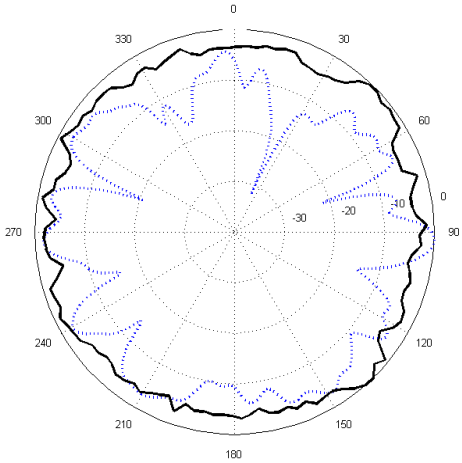

10.6 GHz

Figure 3.29. (cont.)

Figure 3.31 gives the simulated and measured maximum system gains ($\theta = 90^o$, φ= Sweep) at interested frequencies. Computed and measured system gains are in good agreement. However, maximum 2 dB deviations are observed between 4 GHz and 10 GHz. They can be caused from measurement errors such as misalignment of transmitter and receiver antennas or a unexpected computational problem while collecting the data from the measurement program.

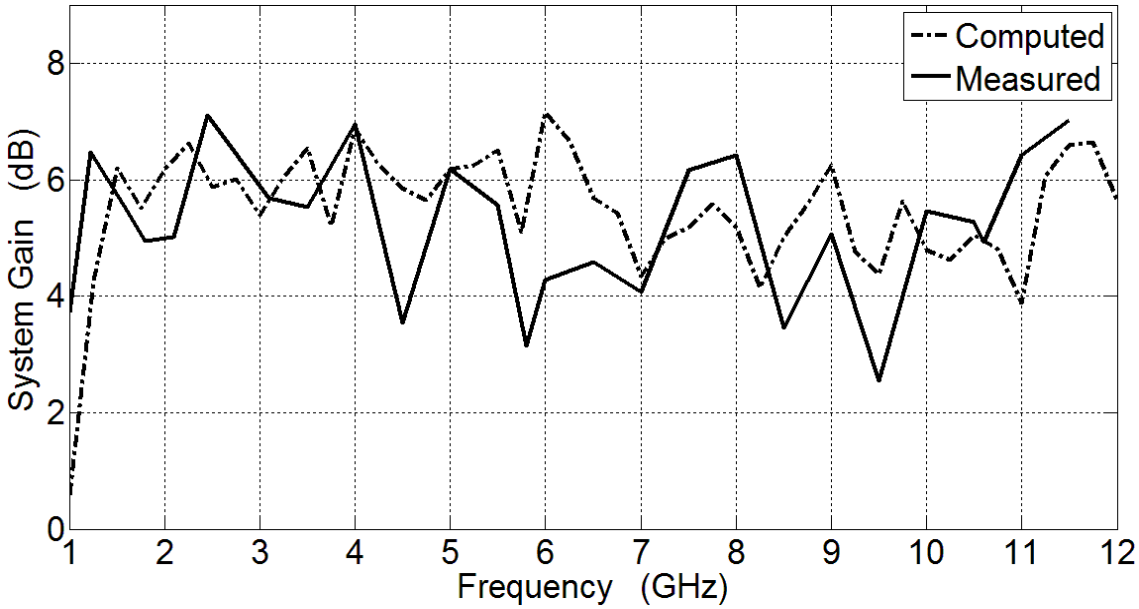

Figure 3.31. Measured and Computed Gains of SsTF LPDA Antenna with Feed Point Patch

3.2. Compact Printed Monopole Antennas

Various wideband antennas have been interesting subjects in antenna designs and have found important applications in military and civil systems. For examples, a wideband antenna is a key component of electric counterwork equipment in the information warfare, impulse radar and communication systems. With the development of high speed integrated circuits and the requirement of the miniaturization and integration, the research and application of wideband printed antennas have been grooving rapidly.

The proposed SsTF Printed LPDA with Feed Point Patch antenna has wide frequency bandwidth with 5.5 dB average gain. However, it is not well enough for small size portable devices and handsets where volume constraint is a significant factor. Moreover, it is not a good choice for devices using pulse based communication systems because of relatively high and fluctuated group delay performance. Having as possible as constant group delay provides preserving the shape of the transmitted and received signals.

Planar monopole antennas are one of the investigated antenna types because of their broad bandwidths, small sizes and constant group delays. The simplest member of

planar monopoles is generated by replacing the quarter wave monopole which is located above the perfect ground plane with a planar element. Brown-Woodward bowtie antenna which is a simple and planar version of a conical antenna can be accepted as the earliest planar monopole antenna. They are first described in a textbook as a variant of cylindrical and conical monopole by Meinke and Gundlach in 1968 (Meinke and Gundlach, 1968). Their wide impedance characteristics are described in detail by Dubost and Zisler in 1976 (Dubost and Zisler, 1976). And in 1990s, various geometries of planar monopoles such as disc shaped, circular, elliptical, trapezoidal and bowtie were proposed (Honda et. al., 1992; Hammoud et. al., 1993; Agrawall et. al, 1998; Chen, 2000). In Figure 3.32, an illustration of square planar monopole antenna is shown.

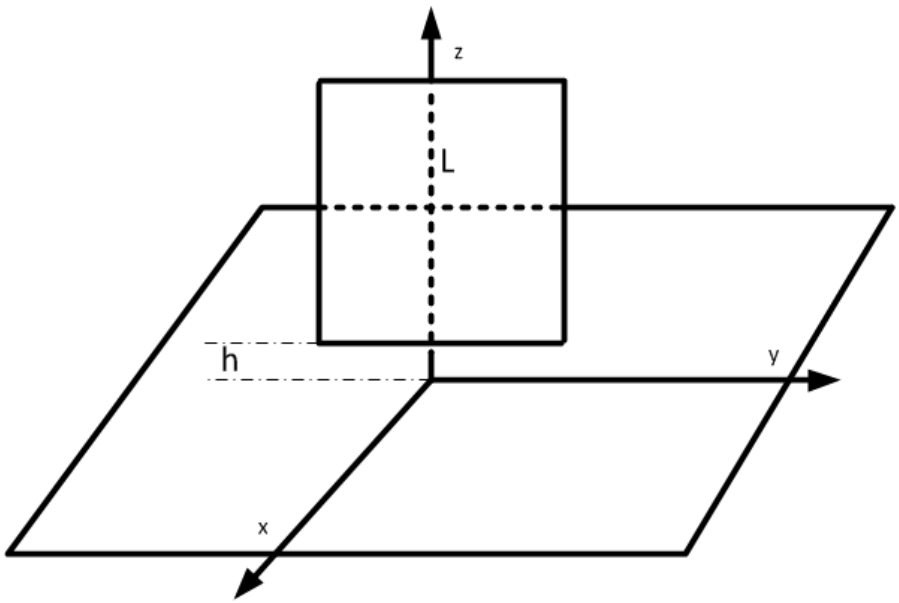

Figure 3.32. Illustration of Square Planar Monopole Antenna

The lower cut-off frequency of a standard monopole antenna typically is inversely proportional with the overall length of the element. Overall length includes the lengths of the resonator and feed gap. Generally, the length of the square planar monopole antenna corresponds to about 0.20 – 0.25 of a free space wavelength at the lower cut-off frequency. Experimental and numerical work has shown that the impedance bandwidth is heavily dependent on the feed gap. This gap must be optimized for maximum bandwidth. The lower cut-off frequency can be determined fairly

independent of the feed gap. However, upper cut-off frequency heavily depends on this gap (Ammann and Chen, 2003). Moreover, impedance bandwidth can be increased by trimming the square edge near the ground plane (Ammann, 2001). These elements were formed by beveling the square on one or both sides of the feed probe. Varying the trim angle shown in Figure 3.33 provides a fine control on the impedance bandwidth.

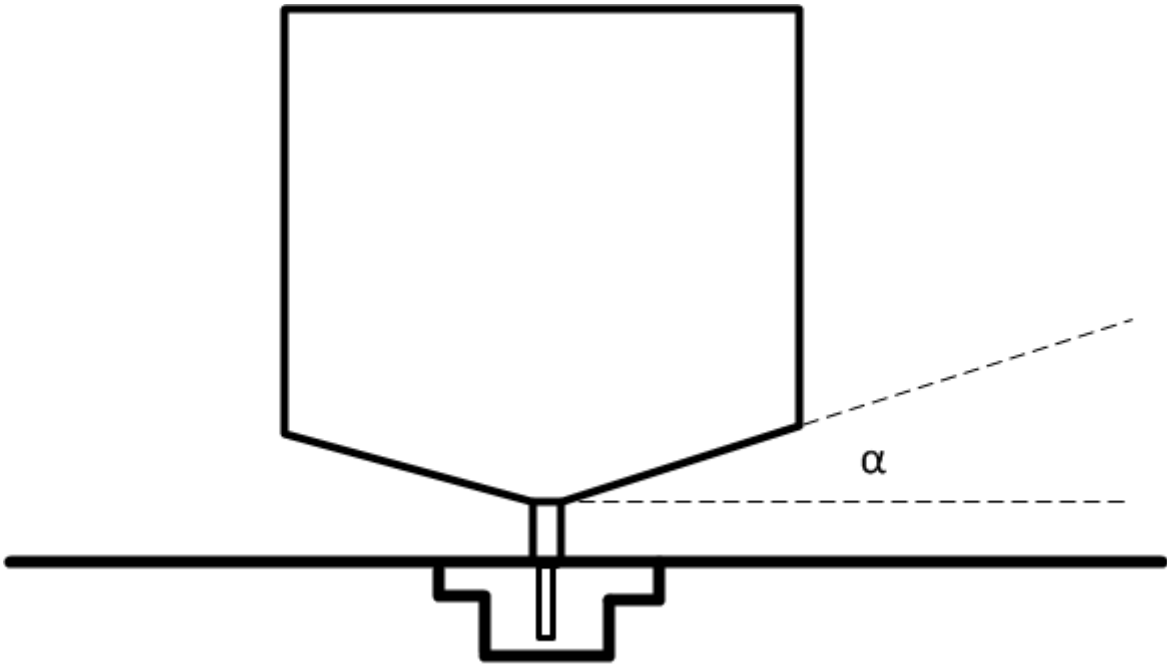

Figure 3.33. Square Planar Monopole with Symmetrical Beveling

Additionally, a shorting pin which is located one of the corner of planar radiator can be employed to reduce the lower cut-off frequency so it provides smaller antenna structure. Slot loading technique is another method using for improving the performance of planar monopole antennas. They reduce wind loading especially having large size antennas and provide lower cut-off frequencies with little effect on radiation performance and impedance bandwidth.

To sum up, planar monopole antennas have a numerous advantages and their performances can be improved according to the desired specifications. However, planar monopoles include metallic sheets such as ground plane and radiator sheet. They increase the size and weight and it makes them unsuitable for todays' electronic devices. One of the methods for taking the advantages of them in todays' electronic

devices is evolving their highly metallic structures to light-weight, low-cost printed structures.

The basic geometry of a printed planar monopole antenna shown in Figure 3.34 has three parts: ground plane, feeding line and radiating patch. Combination of proper design of these parts provides to achieve the performance of metallic planar monopole antennas. Also, employed substrate which has own dielectric constant, tangent loss and thickness has a significant role both determination of antenna size and the radiation performance of the antenna.

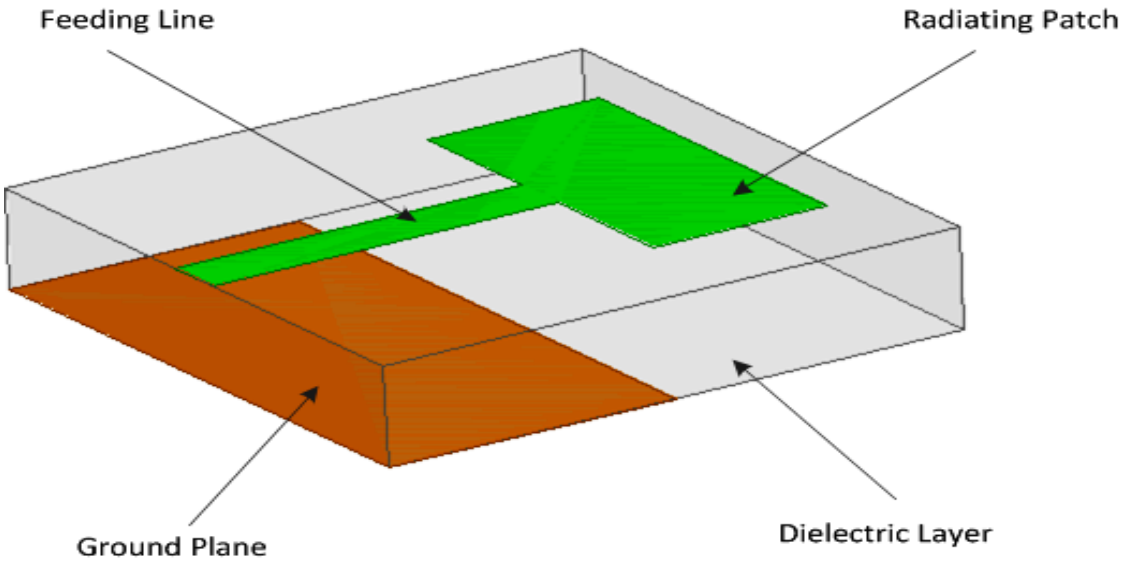

Figure 3.34. Basic Geometry of Printed Planar Monopole Antenna

Structure of printed planar monopole antennas has similarity with standard rectangular or square microstrip antennas but one can easily observe that printed monopoles have larger impedance bandwidths than the other type microstrip antennas. On the other hand, design of a planar monopole antenna is a highly complex process when it is compared with standard microstrip antennas. Because there is no exact formulation or mathematical expressions for printed monopole antennas while there are many mathematical expressions associate the design parameters of standard microstrip antennas with the antenna characteristics. In this condition, design process of a planar monopole basically depends on the optimization of the design parameters such as shape of radiating patch, width and length of ground plane etc. according to results of several

parametric studies that are a good way to understand roughly the role of the investigated parameter on the performance of the antenna. One more important point increasing the design complexity is that unexpected effects of the any optimized design parameter on the other design parameters and different antenna performance criteria. To overcome this design complexity, trial and error method is frequently used in printed monopole antenna analysis to get optimum antenna performance with optimum antenna size.

In this chapter of the study, three compact printed monopole antennas for different frequencies have been designed, realized and measured. In addition to UWB and X Band, which are basically aimed for all three designed antennas, WLAN, WiMAX, PCS or GPS bands are also added to their operating frequencies. In these three designs, microstrip feed line is employed. However, there are many different feeding types such as coaxial, coplanar waveguide or dual feeding are employed in literature, (Zehforoosh and Sedghi, 2014; Li et. al., 2013; Tsai, 2011). Microstrip feeding provides design simplicity beside production and implementation ease.

3.2.1. Compact Printed Monopole Design 1

In this design, a printed monopole antenna operating between 2 GHz and 12 GHz is aimed. In addition to microstrip feeding line, many additional design parameters are needed to be determined. When the simple geometry shown in Figure 3.33 is considered, size of radiator patch, feeding line and ground plane are the main design parameters. Moreover, the length between the upper line of ground plane and the lower line of radiator patch is another critical parameter to be optimized. It corresponds to feeding gap between ground plane and radiator sheet of metallic planar monopole antennas.

Printed monopoles are not as directive as log periodic antennas and also their resonance frequencies are not as explicit as log periodic antennas. For these reasons, the importance of the stability of dielectric constant and lowness of tangent loss becomes more important for design of them. Rogers 4003C substrate, whose dielectric constant is 3.55, thickness is 1.524 mm and tangent loss is 0.0014, is used for realization of the whole designed printed monopoles. It has relatively more stable dielectric constant and highly lower tangent loss than FR4 in the investigated frequency band. Also, its' tangent loss is highly lower than FR4. The realizations and measurements are performed

according to sections 3.1.3 and 3.1.4 which the processes has been extensively mentioned.

While designing the antennas, the width of the radiator patch and ground plane is set to equal each other and the other parameters are substantially determined by bottom-to-up strategy. Although, the length of ground plane is basically related with the minimum operating frequency of the interested antenna, it is fixed for all designed printed monopoles. The width of the antenna structure is set to 35 mm and the length of the ground plane is determined as 20 mm. According to several simulation and realization comparisons which are performed with different printed monopole antenna structures and different substrates, an empirical formula given in 3.17 is proposed for determination the length of ground plane.

$$L \geq \frac{\lambda_{max}}{5.35\sqrt{\varepsilon_r}} \tag{3.17}$$

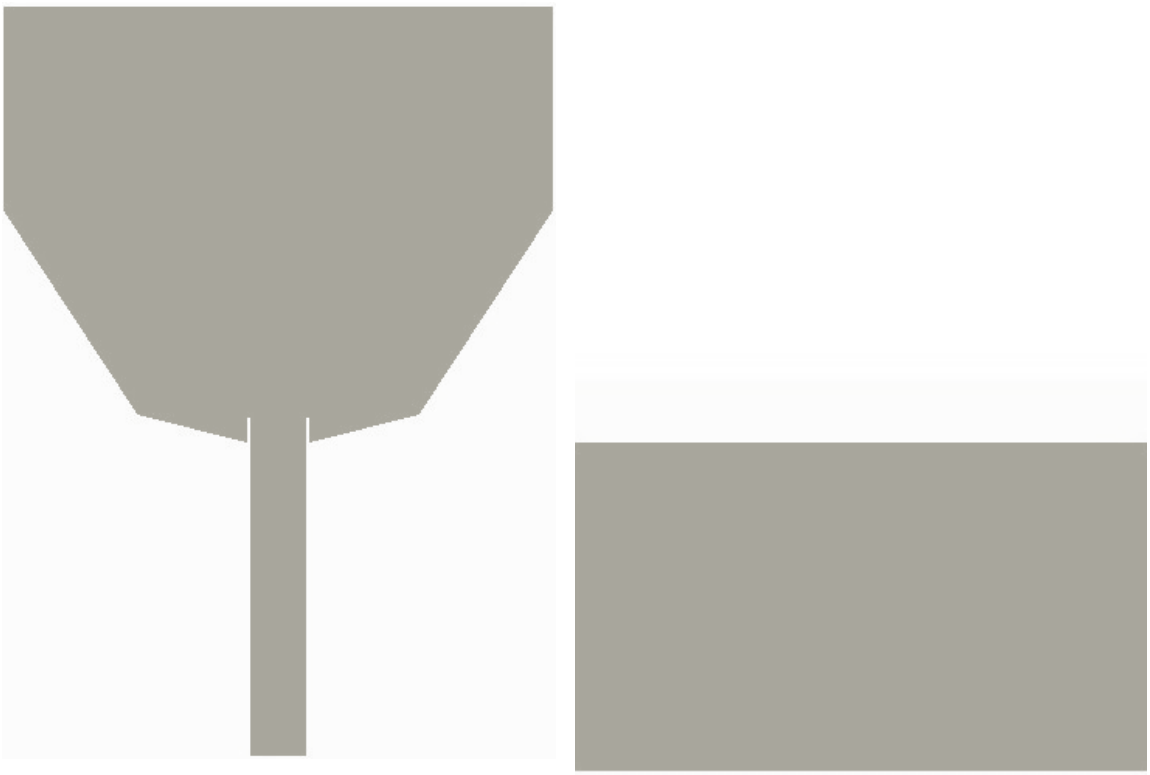

(a) (b)

Figure 3.35. Antenna Geometry of Compact Printed Monopole Design 1 (a) Top Side (b) Bottom Side

Antenna geometry shown in Figure 3.35a divided into three design sections: Feeding line, tapered transition section and radiation section. After determination of ground plane dimensions, design of feeding line is considered in the sense of bottom-to-up strategy. Wideband signal first passes to feeding line before reaching the antenna and it must be designed properly. If the feeding mechanism fails, there will be no wideband radiator. Hence the employed connectors are 50 ohm, characteristic impedance of the feeding line is adjusted to 50 ohm so the width of the feeding line is determined as 3.55 mm. To get better impedance matching, an inset is given to structure. Combination of different width and length of inset helps to match desired frequencies. When inset length is increased, the matching to lower frequencies improves and when the inset length is decreased, the matching to higher frequencies improves. The inset width is fixed to 0.25 mm for both sides and the length is fixed to 0.75 mm. Total length of the feeding line from connector to transition section is determined as 20.85 mm.

Two tapered transition sections are inserted between the feeding line and radiation section to provide smooth transition between them. The current distribution is denser in this section than the others. Thus, the effect of this section on impedance bandwidth is stronger than the other sections.

First tapered transition section is the most sensitive part of the smooth transition. The tapering angle is optimized to get optimum impedance bandwidth. Basically, while the width has much effects on impedance matching, the length has the effects on determining lower and higher cutoff frequencies. The width is determined together with the upper transition section and optimized as 18 mm. The length is optimized as 1.75 mm which allows passing both relatively higher and lower frequencies. The second tapered transition section have similar role with the first tapered transition section. It is used as the fine-tune mechanism for impedance matching. Although its' lower width is common with the first section, their tapering angles are different. The width and the length of this section are optimized as 35 mm and 13 mm.

The shape of the radiation section looks like a rectangular patch. Since the current distribution weaker than the other sections, it has no significant role on impedance bandwidth. However, it is length has an important role on determining the lower cutoff frequency of the antenna. To reach desired frequency range, the length of this section optimized as 13 mm with 35 mm width.

The lower cutoff frequency is determined with the lengths of transition and radiation sections. The feeding gap which locates between the ground plane and

transition section and helps to keep return loss performance of the antenna under -10 dB level is optimized as 0.1 mm. Finally, total length is determined as 47.85 mm and the total width is determined as 35 mm. Fabricated antenna is shown in Figure 3.36.

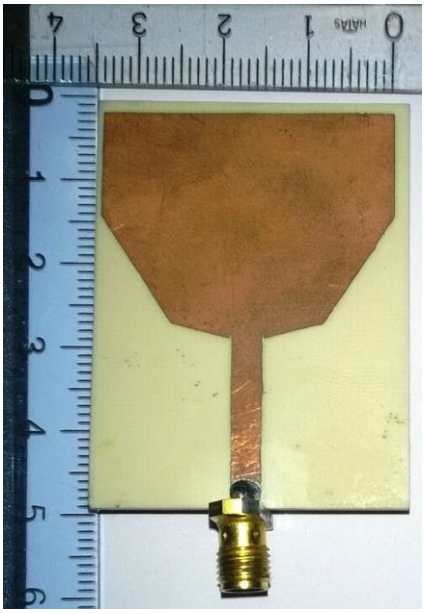

Figure 3.36. Fabricated Printed Planar Monopole Antenna Design 1

The performances of the designed printed monopole antennas are investigated in terms of S_{11}, voltage standing wave ratio, group delay, radiation pattern and gain. The impedance bandwidth performances of the designed antenna are shown in Figure 3.37 and Figure 3.38. In Figure 3.35, S_{11} comparison and in Figure 3.38 voltage standing wave ratio comparisons are given. Although the simulated bandwidth is between 2 GHz and 12.5 GHz, the measured operating bandwidth of the antenna is between 2.37 GHz and 12 GHz. This difference may cause the misalignment of feeding gap. As a result, this operating frequency allows to capability of WLAN, WiMAX, UWB and X Band systems.

Measured group delay performance of the antenna shown in Figure 3.39. According to the figure, maximum group delay is slightly over 1.5 ns and the deviation is approximately 1 ns. It can be said that, group delay performance of the antenna is good for pulse based communication systems.

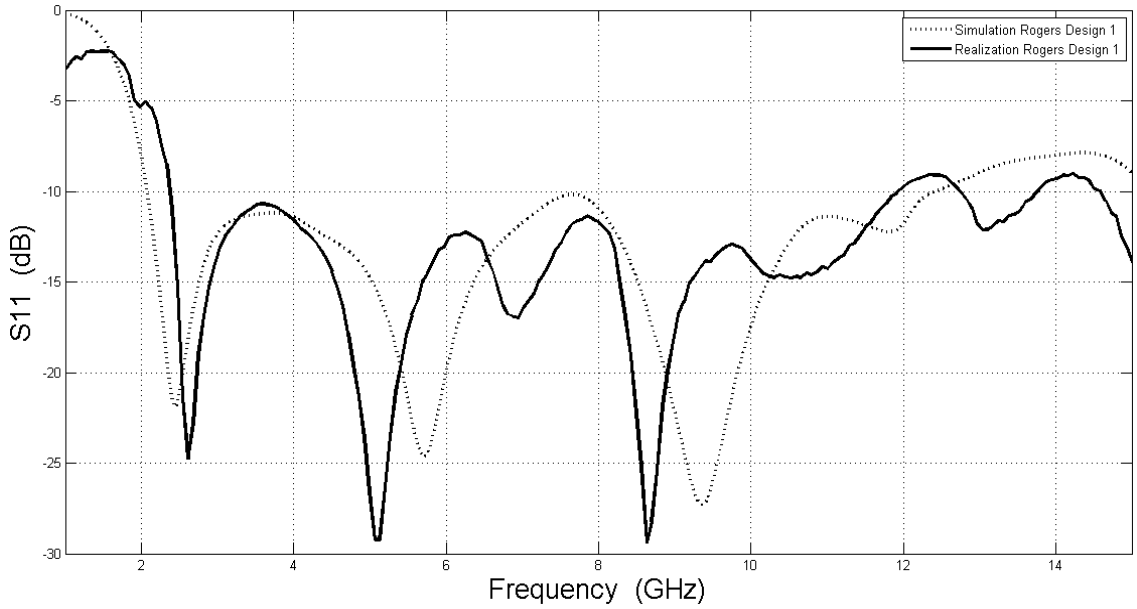

Figure 3.37. Simulated and Measured Return Loss Comparison of Design 1

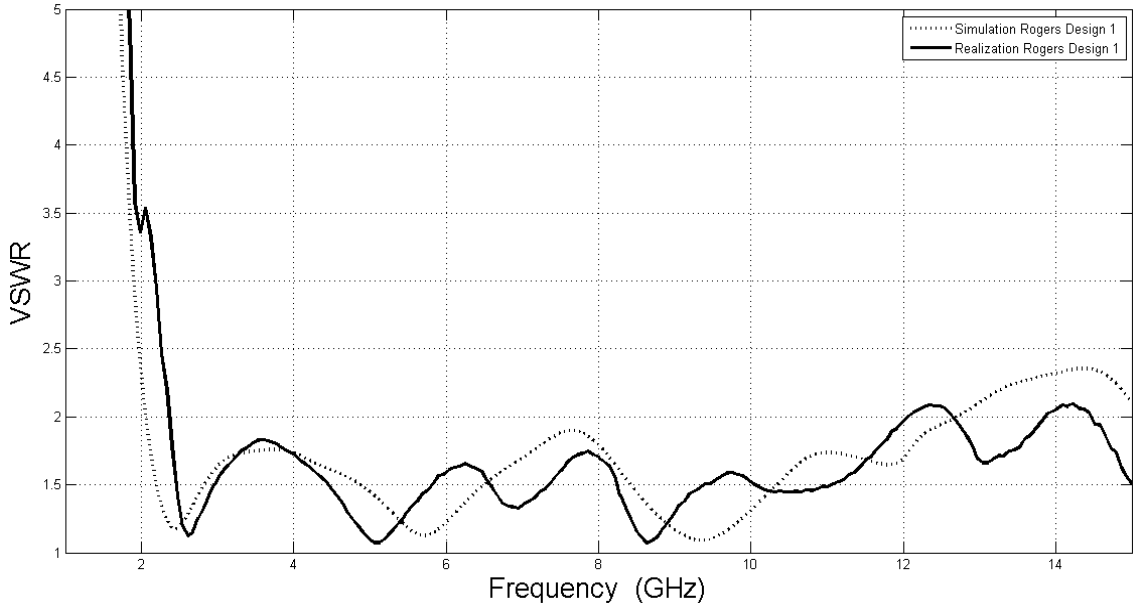

Figure 3.38. Simulated and Measured VSWR Comparison of Design 1

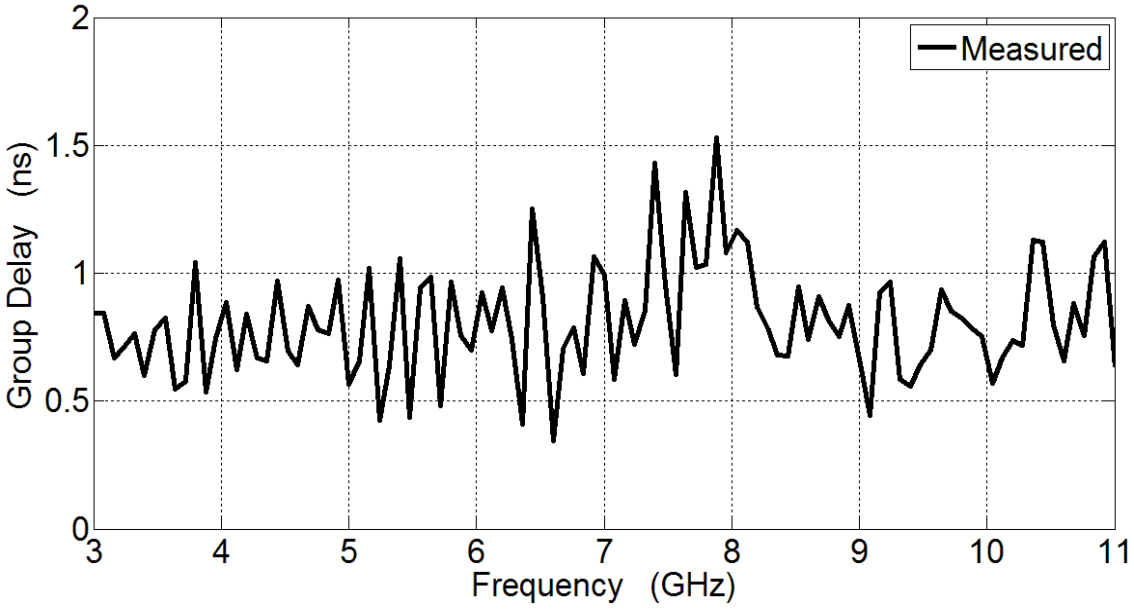

Figure 3.39. Measured Group Delay of Design 1

Simulated and measured radiation pattern comparisons are given in Figure 3.40 and 3.41 for 2.1 GHz, 2.45 GHz, 3.1 GHz, 5.8 GHz, 8 GHz and 10.6 GHz in XZ plane and XY plane. Since the used coaxial cables are not suitable for such high frequency measurements, upper frequency radiation patterns do not show well agreement with computed results. In Figure 3.42, comparative system gains are shown. It can be said that simulated and measured results are in good agreement.

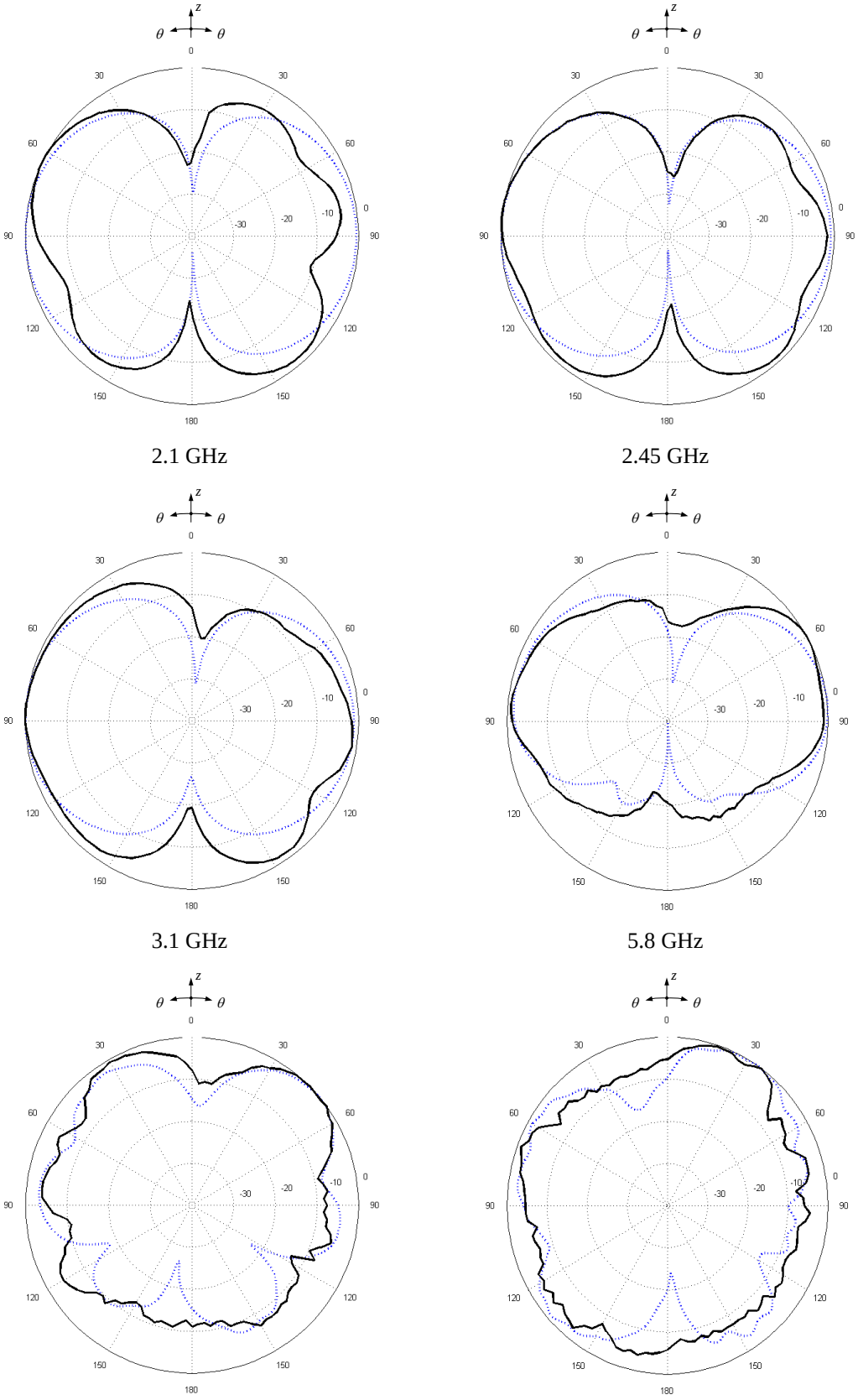

2.1 GHz

2.45 GHz

3.1 GHz

5.8 GHz

8 GHz

10.6 GHz

Figure 3.40. Measured and Simulated XZ Plane of Compact Printed Monopole Design 1 (⋯ Simulation — Measurement)

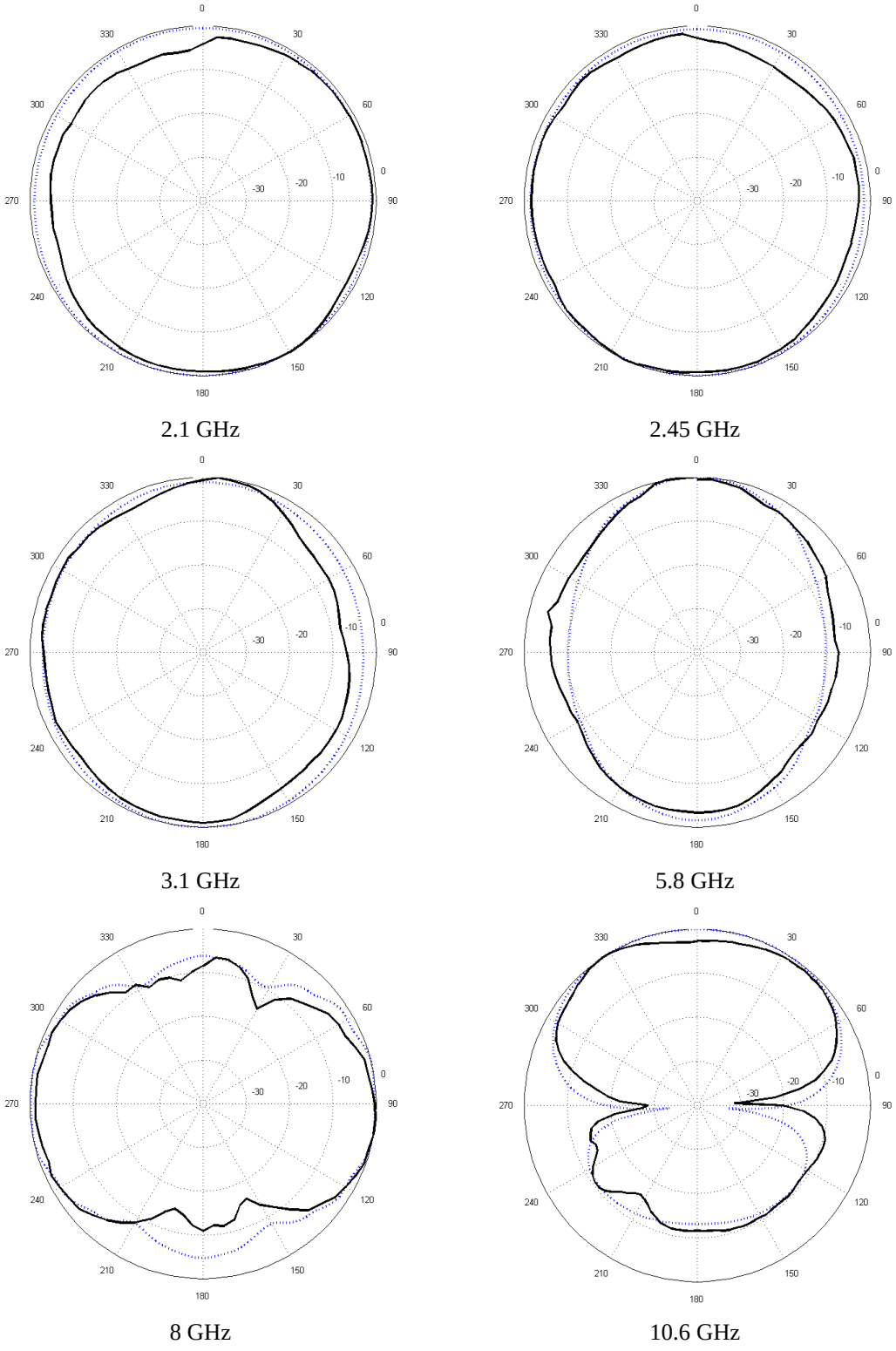

Figure 3.41. Measured and Simulated XY Plane of Compact Printed Monopole Design 1 (···· Simulation — Measurement)

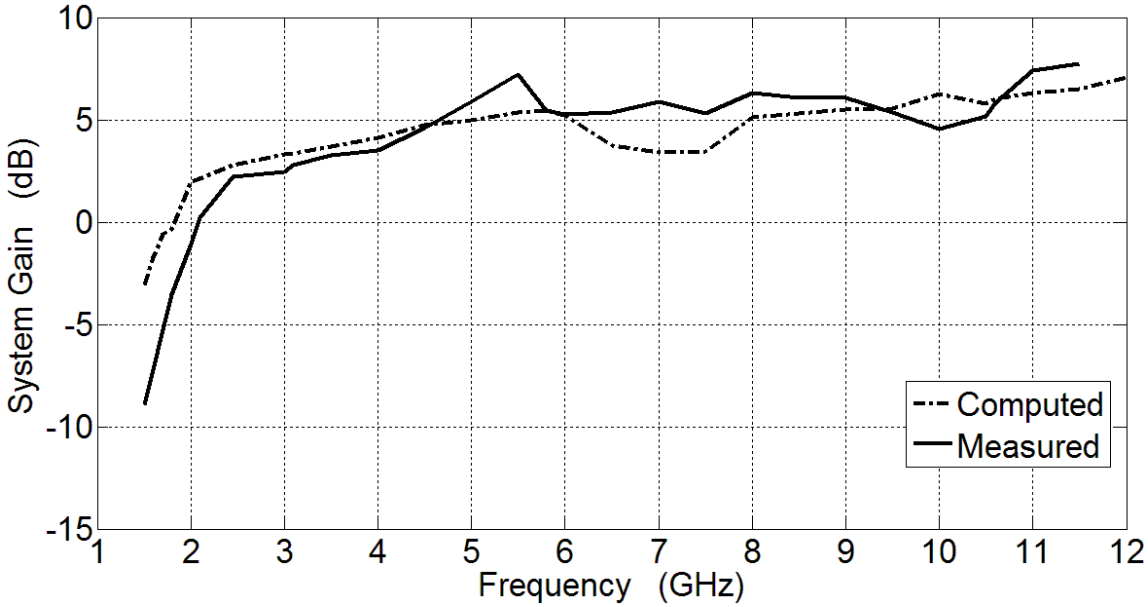

Figure 3.42. Computed and Measured System Gain of Compact Printed Monopole Design 1

3.2.2. Compact Printed Monopole Design 2

In this design, a compact printed monopole antenna which is capable with PCS band in addition to UWB and X Band is aimed. For this reason, slot loading method is employed on the Design 1. Slot loading method is getting more and more popular because it can be implemented easily on the almost all antenna structures. Moreover, they can be used for many different ambitions such as excitation of extra resonant frequencies, gain enhancements, dual polarization, band stopping and broadening the impedance bandwidth by choosing proper slot structures and locations on the target antenna (Shokri et. al., 2013; Qjauridi and Qjauridi, 2013; Bod et. al., 2012; Taheri et. al., 2011; Kumar et. al., 2011; Low et.al., 2005; Wang, 2002).

A novel slot structure is implemented on the previous design to get extra resonance at PCS band with almost 170 MHz bandwidth. While determining the slot location and type the considered point is current flows on the antenna. Since the current denser is higher in transition section and the current flows the edge of the antenna structure, slot loads must be employed on the edge of transition section. Additionally, a wide slot must be used to satisfy bandwidth requirement. Under the light of these key ideas, upper slot shown in Figure 3.43a is implemented. However, desired resonant

frequency cannot be reached. This problem is overcome by increasing 1.15 mm the length of the radiator section and desired frequency resonation with required bandwidth is achieved. On the other hand, this extra resonation affects the frequency bandwidth and compresses WLAN band. Moreover, wideband return loss behavior of the antenna changes and many fluctuations occur in the higher frequency band. To solve this problem, length of the inset feeding is increased to 1.5 mm and compensation slots are employed. For compensation of these fluctuations on S_{11}, lower slots shown in Figure 3.43a are implemented on the antenna structure. As it known from chapter 3.2.1, first transition section has stronger effect on impedance bandwidth so compensation slots are located near this section and since the occurred unexpected fluctuations are in higher frequencies, slot widths and lengths are relatively short. Also, they are located symmetrical to each other due to symmetrical antenna geometry.

Upper slot employing for extra resonation is located 36.85 mm and lower slots employing for compensation are located 27.35 mm away from the feeding connector. The length and the width of the lower slots are 1 mm and 9 mm. Dimensions of the upper slot are given in Figure 3.44. Lastly, the total length and the width of the antenna are determined as 50 mm and 35 mm. Fabricated antenna is shown in Figure 3.45.

(a) (b)

Figure 3.43. Antenna Geometry of Compact Printed Monopole Design 2 (a) Top Side (b) Bottom Side

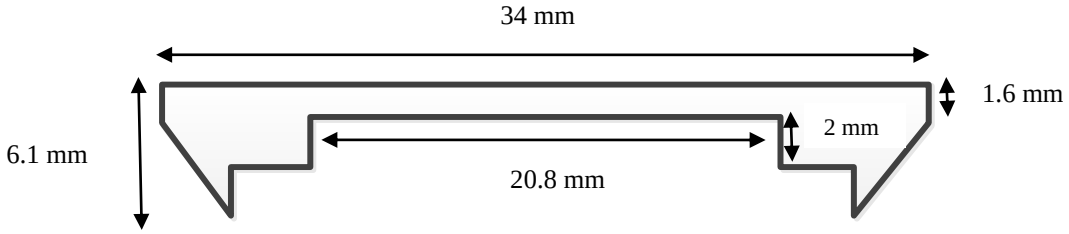

Figure 3.44. Upper Slot Dimensions of Compact Printed Monopole Design 2

Figure 3.45. Fabricated Printed Planar Monopole Antenna Design 2

The impedance bandwidth performance of the second designed printed monopole antenna is shown in Figure 3.46 and Figure 3.47. S_{11} comparison is given in Figure 3.46 and voltage standing wave ratio comparison is given in Figure 3.44. Simulation and measurement results have a good agreement from 1 GHz to 11 GHz. However, a very little fluctuation occurs between 11 GHz and 14 GHz. While the effect of this fluctuation is observed clearly in S_{11} graph, its' effect can be ignored according to VSWR graph. The antenna is designed for PCS, UWB and X Band. The simulated operating frequency of the antenna covers 1.66 – 1.89 GHz band in addition to 2.88 – 12 GHz band. The measured operating frequency bands are 1.67 – 1.91 GHz and 2.99 – 15 GHz which provide the whole simulated frequency bands with extra frequencies. To sum up, this antenna is capable of PCS, UWB and X Band systems.

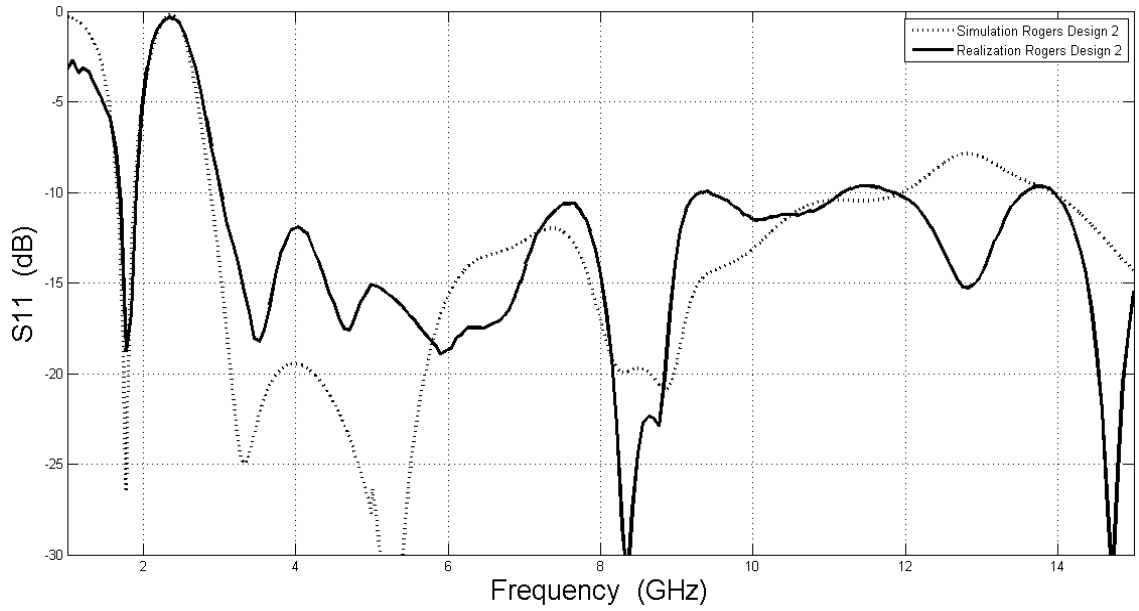

Figure 3.46. Simulated and Measured Return Loss Comparison of Design 2

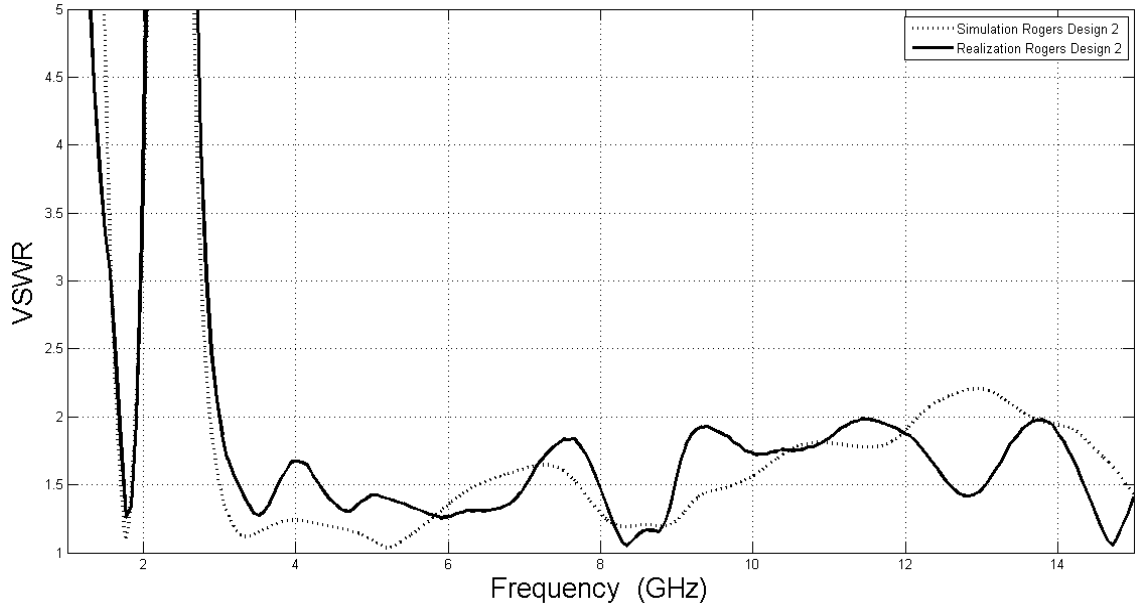

Figure 3.47. Simulated and Measured VSWR Comparison of Design 2

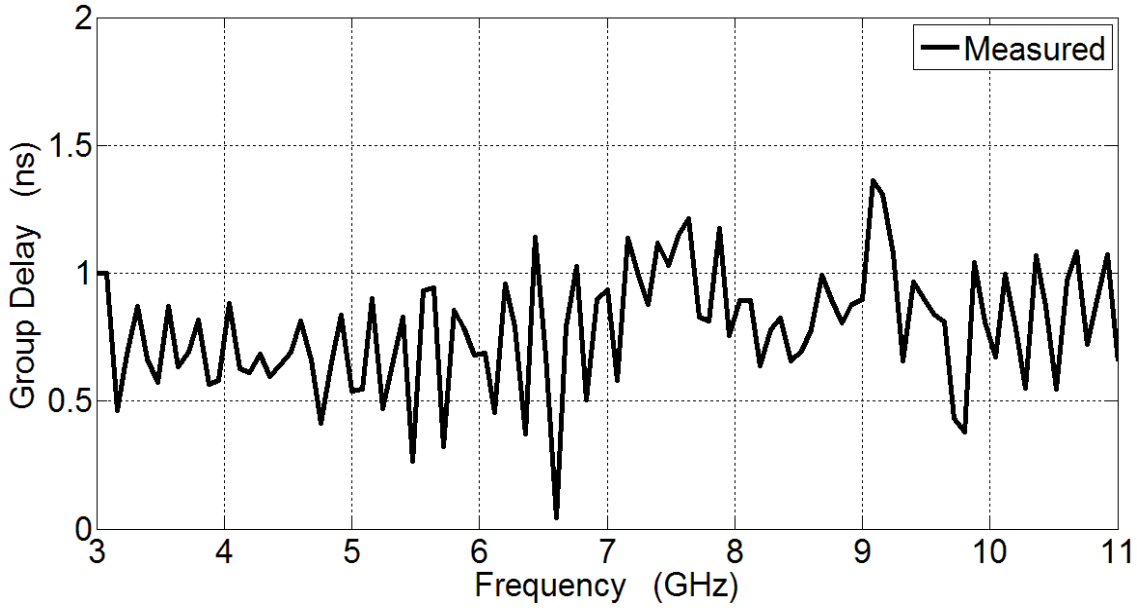

Figure 3.48. Measured Group Delay of Design 2

Measured group delay performance of the antenna is shown in Figure 3.48. One can easily observe that, group delay is lower than 1.5 ns and maximum deviation is approximately 1.25 ns. Hence, the antenna is a good candidate for UWB systems using pulse based communication. Simulated and measured radiation pattern comparisons are given in Figure 3.49 and 3.50 for 1.8 GHz, 3.1 GHz, 5.8 GHz, 8 GHz and 10.6 GHz in XZ plane and XY plane. Simulated maximum peak gains are given in Figure 3.51.

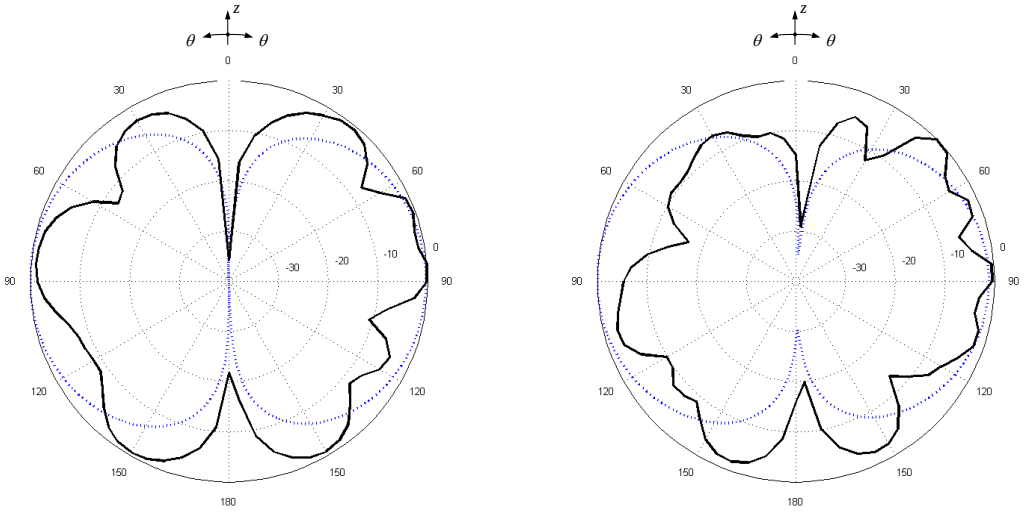

1.8 GHz

3.1 GHz

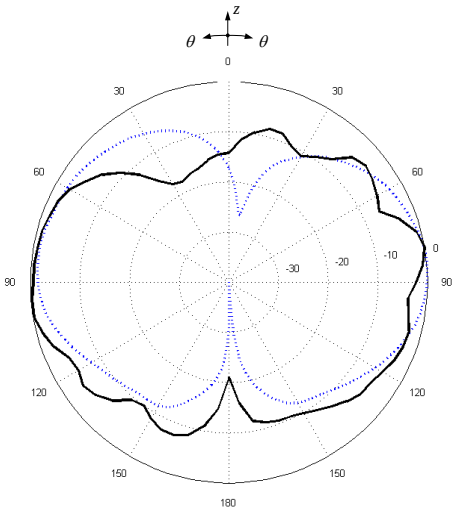

5.8 GHz

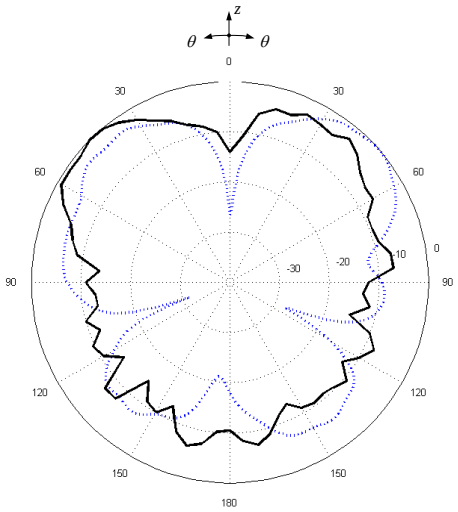

8 GHz

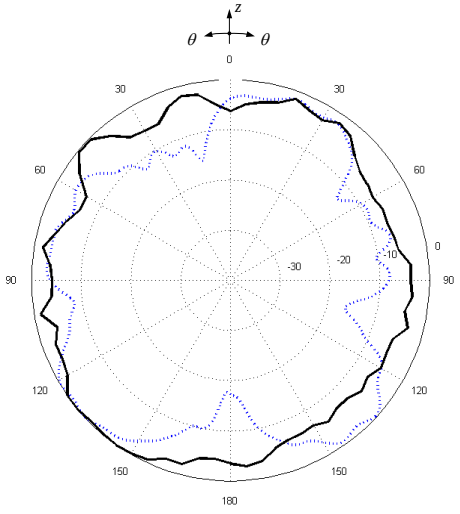

10.6 GHz

Figure 3.49. Measured and Simulated XZ Plane of Compact Printed Monopole Design 2 (···· Simulation — Measurement)

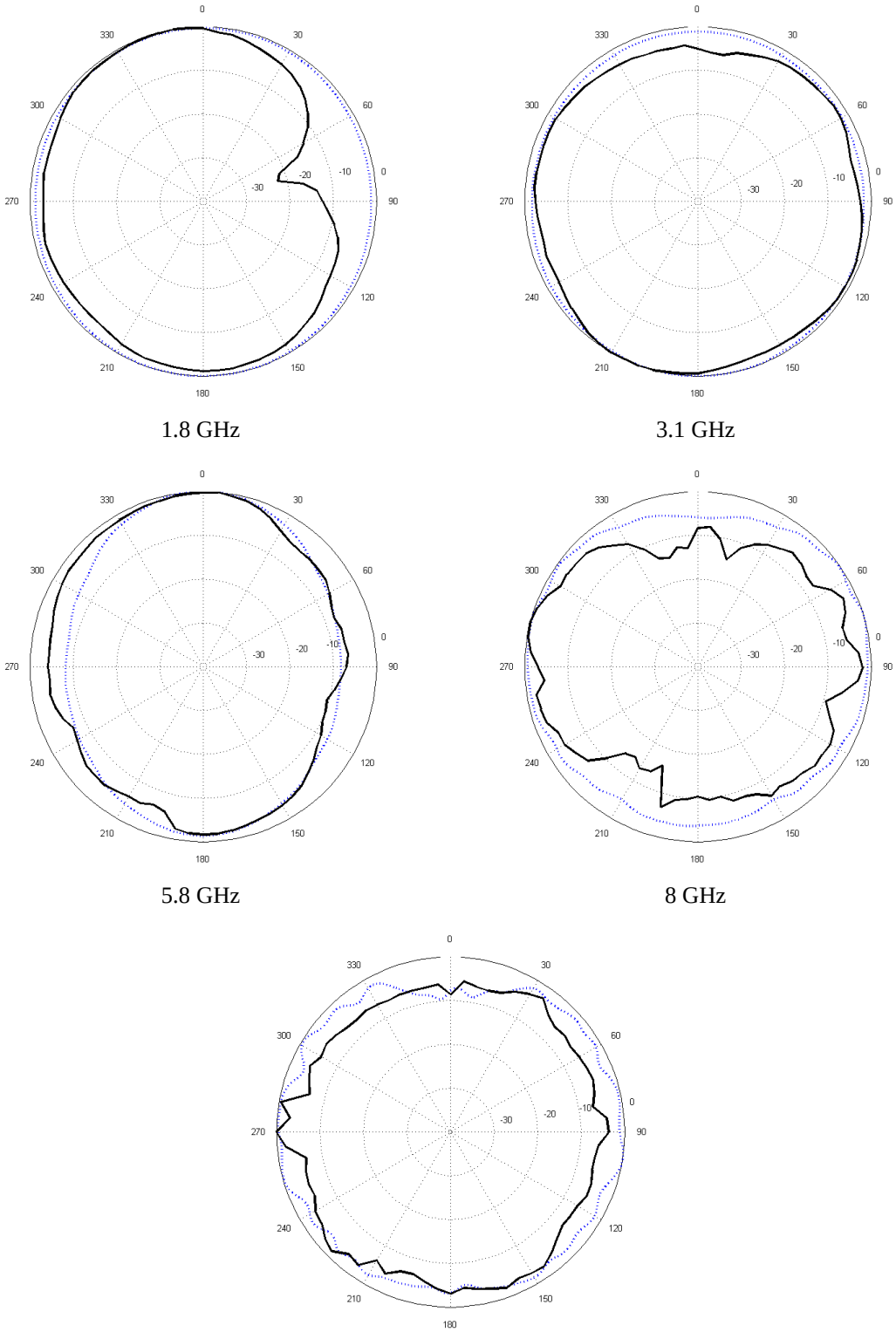

Figure 3.50. Measured and Simulated XY Plane of Compact Printed Monopole Design 2 (···· Simulation — Measurement)

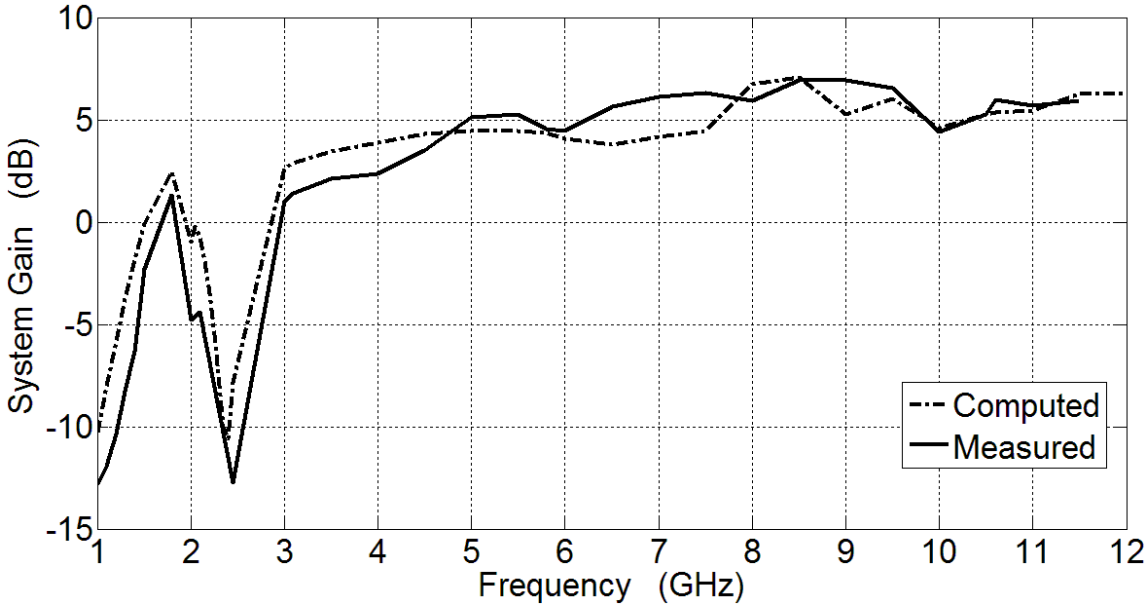

Figure 3.51. Computed and Measured System Gain of Compact Printed Monopole Design 2

3.2.3. Compact Printed Monopole Antenna Design 3

In this design, a compact printed monopole antenna which is capable with GPS and WLAN bands in addition to UWB and X Band is aimed. For this reason, slot loading method is employed on the Design 1. Although the employed slot has different geometry than the used in Design 2, it is designed in the sense of same idea. GPS band does not require wide bandwidth as PCS band. Hence, the width of the employed slot does not require being thicker. On the other hand, its' operating frequency band is relatively lower than PCS band. Thus, electrical length of the employed slot must be larger than the slot used for PCS band to get this lower extra resonance. In this point, the new larger slot is determined to locate between second transition section and radiation section. Because the other sections have more significant effect on impedance bandwidth and such a larger slot affects too much impedance bandwidth if it is located on these sections.

A novel slot for GPS band resonance is implemented on the structure of Design 1 and the length of the radiation section is increased 1.15 mm. Then, desired resonance frequency with required bandwidth is achieved. Even though avoiding the undesired effects of the extra resonance on impedance bandwidth, some fluctuations are occurred same as in Design 2. To solve this problem, again the same techniques are used. Inset

feeding is increased to 1.5 mm and compensation slots are employed. The antenna geometry is shown in Figure 3.51.

Upper slot using for extra resonance is located at 35.85 mm and lower slots using for impedance bandwidth compensation is located at 30.85 mm away from the feeding connector. The length and the width of the lower slots are 2 mm and 10 mm. Dimensions of the upper slot are given in Figure 3.53. Finally, the total length and the width of the antenna are determined as 50 mm and 35 mm. Fabricated antenna is shown in Figure 3.54.

(a) (b)

Figure 3.52. Antenna Geometry of Compact Printed Monopole Design 3 (a) Top Side (b) Bottom Side

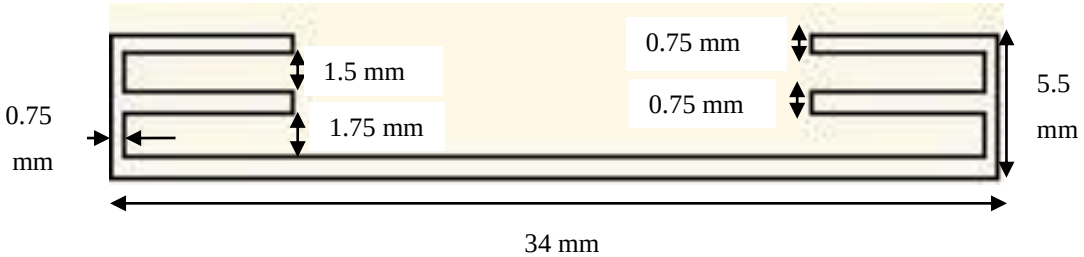

Figure 3.53. Upper Slot Dimensions of Compact Printed Monopole Design 3

Figure 3.54. Fabricated Printed Planar Monopole Antenna Design 3

The impedance bandwidth performance of the third designed printed monopole antenna is shown in Figure 3.55 and Figure 3.56. S_{11} comparison is given in Figure 3.55 and voltage standing wave ratio comparison is given in Figure 3.56. Simulation and measurement results have a good agreement at the whole interested frequency bands. This printed monopole antenna is designed for GPS, WLAN, WiMAX, UWB and X Band applications. The simulated operating frequency of the antenna covers 1.52 – 1.61 GHz band in addition to 2.35 – 12.43 GHz band. The measured operating frequency provides broader bandwidth both for upper and lower frequencies. At lower frequency, antenna bandwidth is between 1.38 GHz and 1.60 GHz. At the upper frequency band, antenna operates from 2.33 GHz to 13.74 GHz. Consequently, designed antenna can be used in the applications of GPS, WLAN, WiMAX, UWB and X Band.

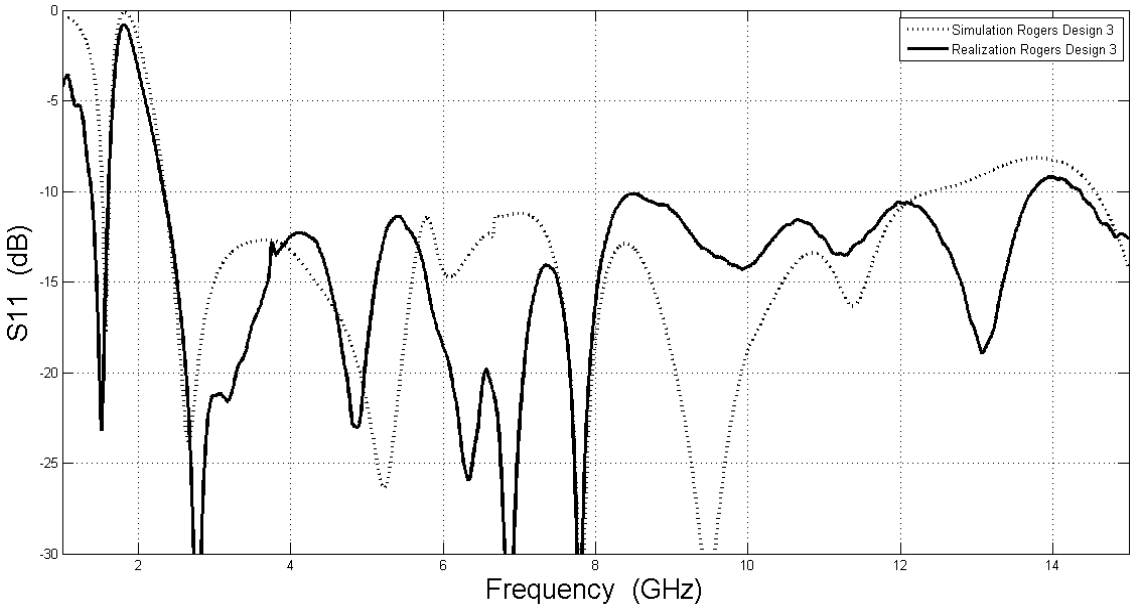

Figure 3.55. Simulated and Measured Return Loss Comparison of Design 3

Measured group delay performance of the antenna is shown in Figure 3.57. The same group delay behavior with the other printed monopole designs is observed. It can be observed from the graph that, group delay is lower than 1.5 ns and maximum deviation is approximately 1.4 ns in the whole UWB frequencies.. Hence, the antenna is a good candidate for pulse based communication.

Simulated and measured radiation pattern comparisons are given in Figure 3.58 and 3.59 for 1.575 GHz, 2.45 GHz, 3.1 GHz, 5.8 GHz, 8 GHz and 10.6 GHz in XZ plane and XY plane. The results are in better agreement at lower frequencies than higher frequencies because of cable losses. Simulated and measured system gains are given in Figure 3.60 and the results are in good agreement.

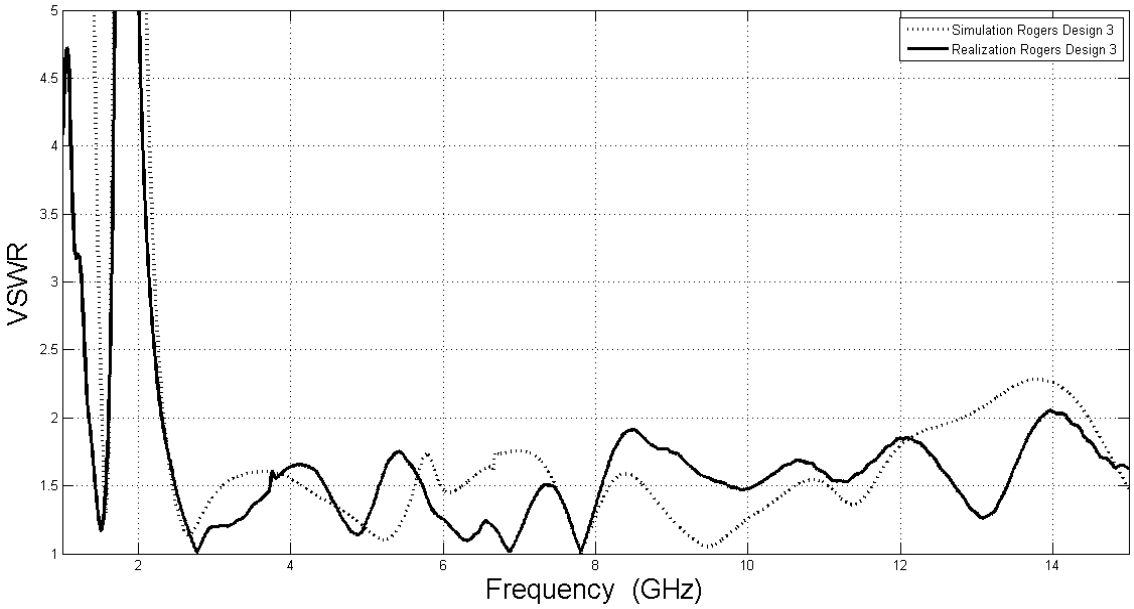

Figure 3.56. Simulated and Measured VSWR Comparison of Design 3

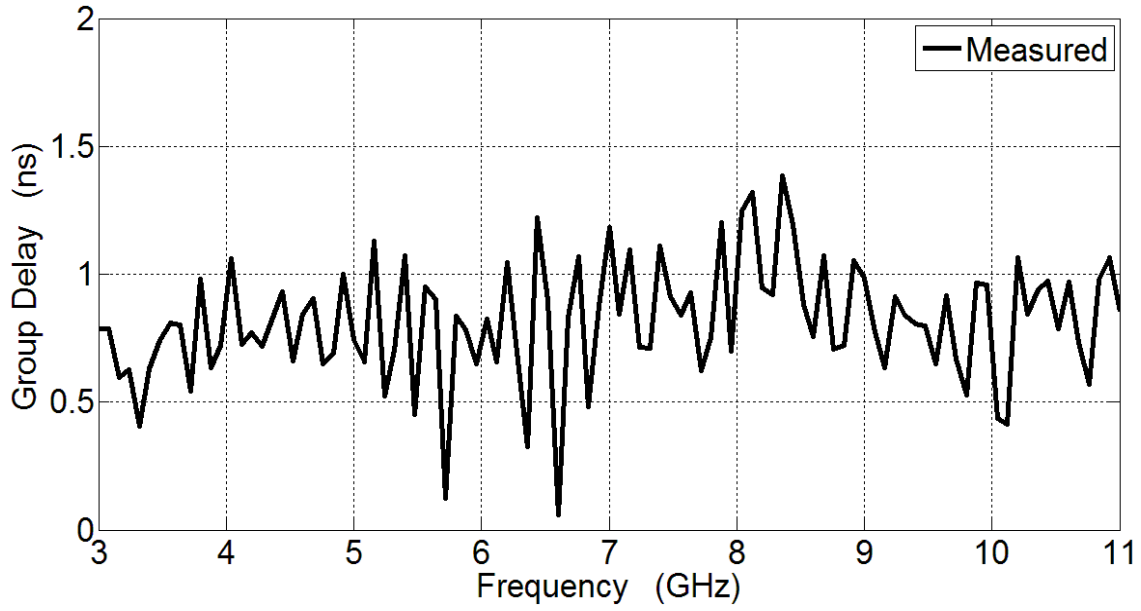

Figure 3.57. Measured Group Delay of Design 3

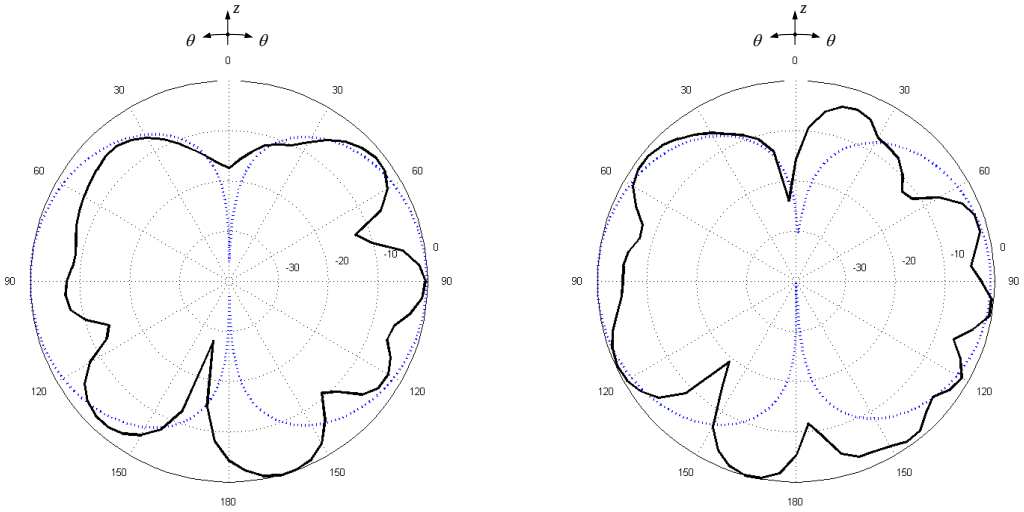

1.575 GHz

2.45 GHz

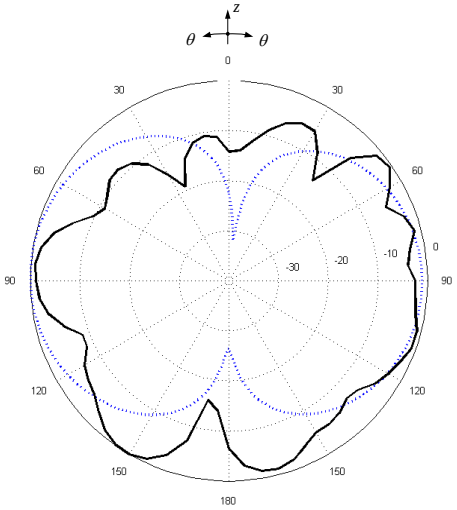

3.1 GHz

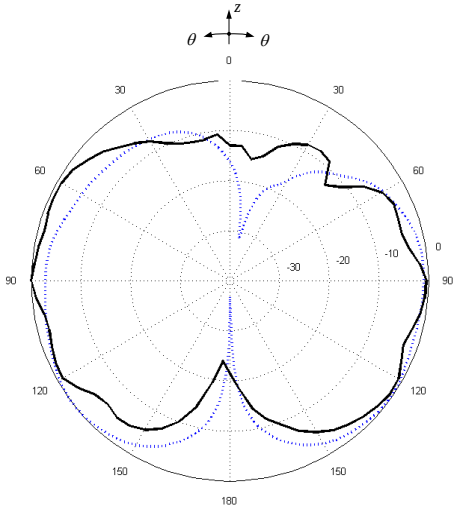

5.8 GHz

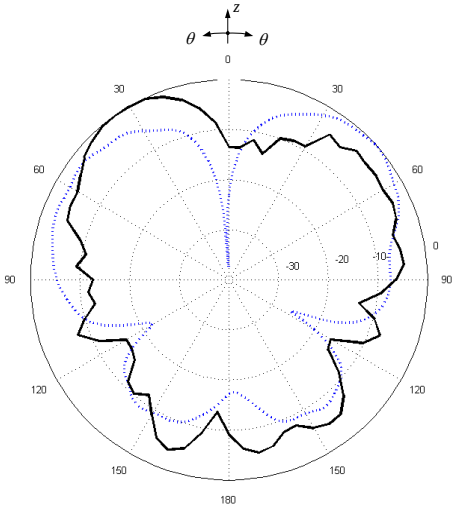

8 GHz

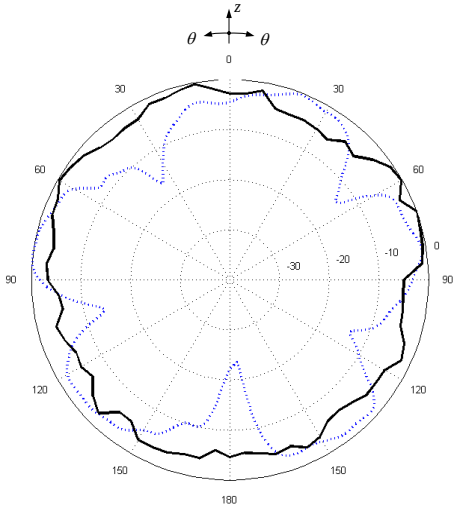

10.6 GHz

Figure 3.58. Measured and Simulated XZ Plane of Compact Printed Monopole Design 3 (···· Simulation — Measurement)

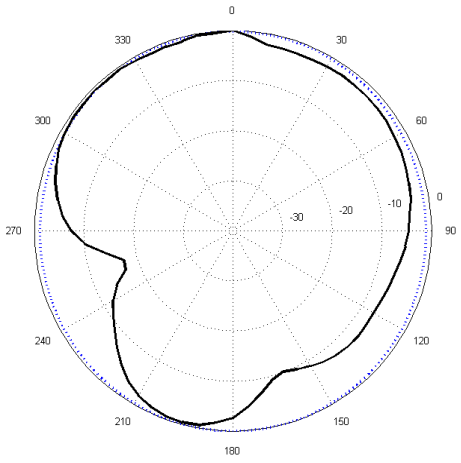

1.575 GHz

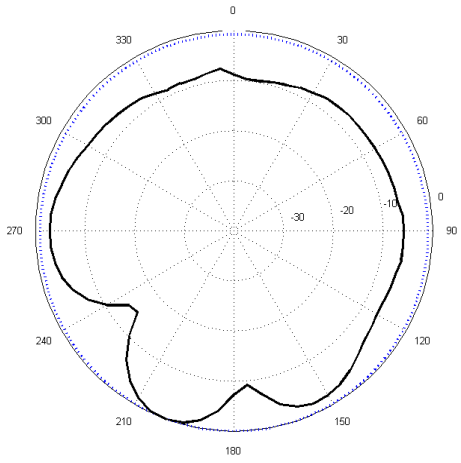

2.45 GHz

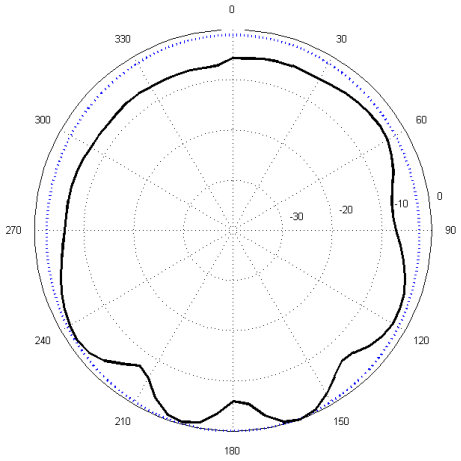

3.1 GHz

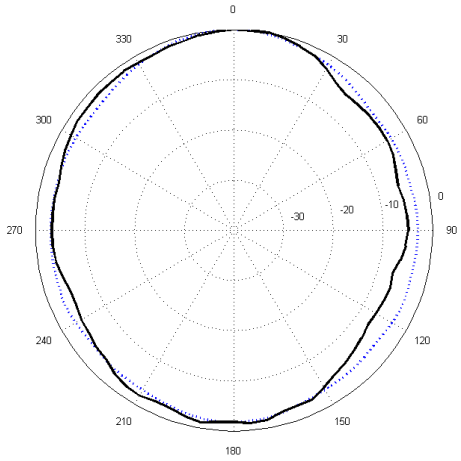

5.8 GHz

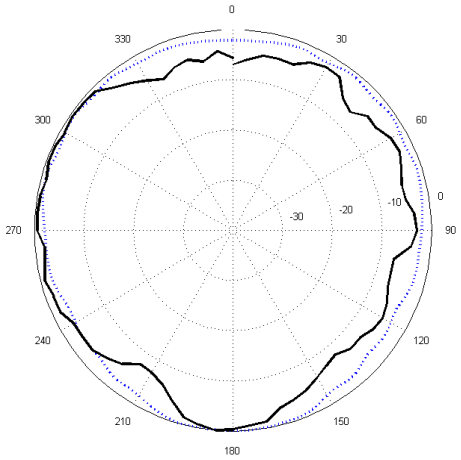

8 GHz

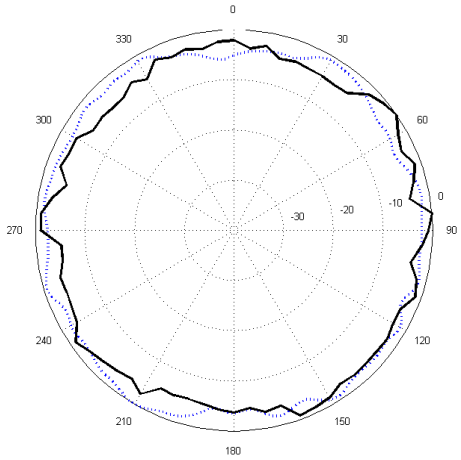

10.6 GHz

Figure 3.59. Measured and Simulated XY Plane of Compact Printed Monopole Design 3 (···· Simulation — Measurement)

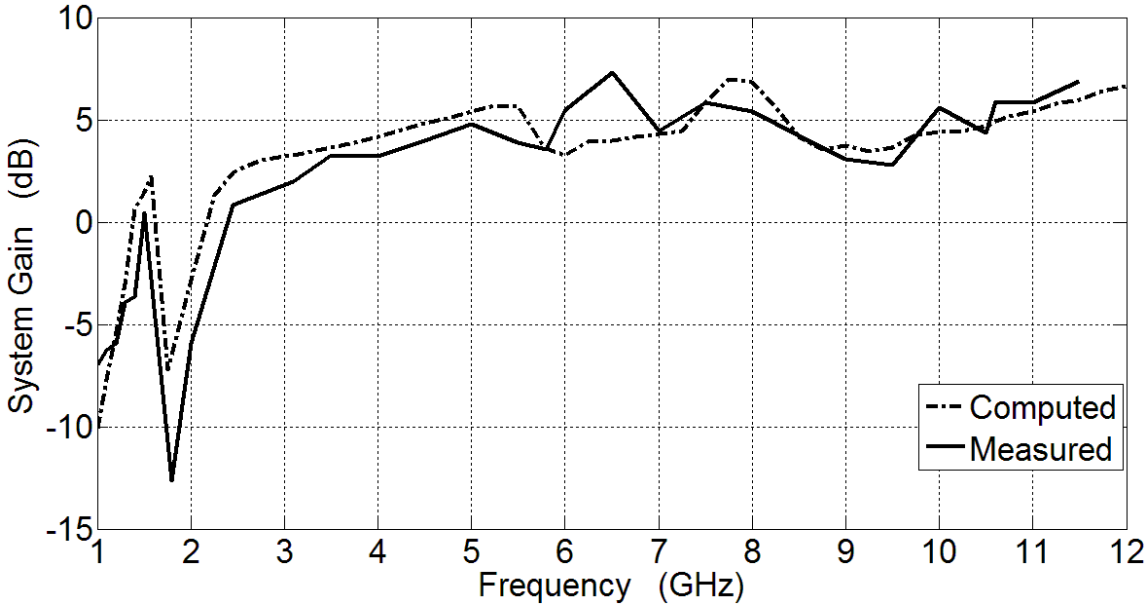

Figure 3.60. Computed and Measured System Gain of Compact Printed Monopole Design 3

CHAPTER 4

CONCLUSIONS

In this study, four novel antennas in two different types are designed, analyzed, realized and measured. For numerical analysis of the antennas a Finite Element Method based package software program High Frequency Structure Simulator program is used. The performances of the simulated antennas are compared with the measurements in terms of S_{11}, voltage standing wave ratio, group delay, radiation pattern and gains. These comparisons generally have a good agreement between simulated and measured values.

One of the investigated antenna types is LPDA antenna. First of all, its' standard design procedure is revised for producing a standard printed LPDA antenna. Then, multiband behavior of standard printed log periodic dipole array antenna is converted to wideband by making simple but effective modifications on the structure of the antenna. During this study, the size of the antenna is determined as 130 x 100 mm^2 and the total number of elements is fixed to 9. The basic modification is employing a novel sub-sectional tapered feeding line instead of standard straight line feeding line. It provides almost 8.27:1 impedance bandwidth ratio. The other modification is adding a 3 x 10 mm^2 rectangular patch at feeding point and only one side. Then, 12.55:1 impedance bandwidth ratio is reached. It operates between 1.1 GHz and 13.8 GHz under -10 dB S_{11} level. Hence, the proposed novel printed LPDA antenna is capable of GPS (L1 and L2), IMT-2000, PCS, WLAN, WiMAX, UWB and X Band. Measured gains vary between 3.5 dB and 7 dB in the interested frequency bands and group delay is lower than 1.5 ns with maximum 1 ns deviation at the whole UWB frequencies. Thus, it can be also preferred for pulse based communication systems. Finally, it can be said that it has a superior bandwidth performance, simpler structure and smaller size than the other printed LPDA antennas in literature.

The other investigated antenna type is printed planar monopole antennas. Since the log periodic dipole array antennas have larger dimensions and higher group delay, they are not good candidates for todays' mobile or handset electronic devices. However, printed planar monopole antennas can provide both smaller antenna sizes and lower group delay performances. Three different printed monopole antennas are designed,

realized and measured. Mainly, UWB and X Band frequencies are aimed in these designs. Additionally, one or more conventional frequency bands of GPS, PCS, WLAN and WiMAX are added to operating frequency band of the antennas.

Firstly, a printed monopole antenna is designed for roughly 2 – 12 GHz band. In this design, a novel microstrip inset feeding is employed. Antenna structure divided into three design sections and each of them optimized individually to get desired bandwidth. Finally, total width and length of the antenna determined as 47.85 mm and 35 mm. According to measurement results, antenna operates between 2.37 GHz and 12 GHz and it has approximately maximum 1 ns group delay deviation in UWB. Hence, the antenna is capable of WLAN, WiMAX, UWB and X Band applications.

A printed monopole antenna operating at the whole PCS band in addition to UWB and X Band is aimed in this design. For this reason, a novel slot geometry is implemented on the structure of the first printed monopole antenna design. Moreover, the length of the first design is increased from 47.85 mm to 50 mm. As a result of these modifications on antenna structure, PCS band is reached. However, some unexpected fluctuations are occurred on the impedance bandwidth. Then, inset feeding is readjusted and extra two symmetrical compensation slots are employed to overcome the problem. Finally, designed slot loaded novel antenna is realized and measured. According to measurement results, it operates between 1.66-1.89 GHz and 2.88-12 GHz bands. It has maximum 1.5 ns group delay with 1.25 ns deviation in UWB. It can be said that measurement and simulation results are in good agreement and the antenna is capable of PCS, UWB and X Band.

In the third printed monopole design, the ambition is to get GPS, WLAN and WiMAX bands in addition to UWB and X Band. To get GPS band, the length of the first printed monopole antenna design is increased from 47.85 mm to 50 mm and a novel slot geometry is implemented on it. Then, desired GPS resonance is reached but with fluctuations on impedance bandwidth. Resizing inset feeding and employing extra compensation slots provide to keep S_{11} under -10 dB level. Since the lowest frequencies in second and third designs are close to each other, design steps are also close to each other. However, required bandwidths are different so implemented slot geometries are highly different each other. According to measurement results, it operates at 1.38-1.60 GHz and 2.33-13.67 GHz bands. In the whole UWB, maximum group delay is 1.5 ns with approximately 1.4 ns deviation. Lastly, the proposed antenna is capable of GPS, WLAN, WiMAX, UWB and X Band.

Consequently, todays' multifunctional, mobile and handset devices need wideband antennas. In the near future, it is assumed that this need will be increased and become more crucial. In this study, four different novel antennas are proposed to satisfy this need by considering both frequently used conventional bands and very promising frequency bands.

REFERENCES

Acedo de L. E., "SKALA: A Log Periodic Antenna for SKA," *International Conference on Electromagnetics in Advanced Applications, pp. 353-356, 2012.*

Agrawall N. P., Kumar G. and Ray K. P., "Wideband Planar Monopole Antennas", *IEEE Transactions on Antennas and Propagation, Vol. 46, Iss. 2, pp. 294-295, February 1998.*

Ammann M. J. and Chen Z. N., "Wideband Monopole Antennas for Multiband Wireless Systems", *IEEE Antennas and Propagation Magazine, Vol. 45, No:2, pp. 146-150, April 2003.*

Ammann M. J., "Control of the Impedance Bandwidth of Wideband Planar Monopole Antennas Using a Beveling Technique", *Microwave and Optical Technology Letters, Vol. 30, No:4, pp. 229-232, August 2001.*

Azim R., Islam M. T., 2013. *Printed Wide Slot Ultra-Wideband Antenna, Advancement in Microstrip Antennas with Recent Applications, Prof. Ahmed Kishk (Ed.),* InTech, DOI: 10.5772/51961.

Bahl I. J. and Garg R., "Simple and Accurate Formulas for a Microstrip with Finite Strip Thickness", *IEEE Proceedings, Vol. 65, Iss. 11, pp. 1611-1612, November 1977.*

Balanis C. A., 2005. *Antenna Theory Analysis and Design*, United States: Jhon Wiley & Sons.

Banerji S. and Chowdhury R. S., 2013, "Wi-Fi & WiMAX : A Comparative Study ", *Indian Journal of Engineering, Vol. 2, Issue:5, 2013.*

Bernardi P., Cicchetti R., Pisa S., Pittella E., Piuzzi E. and Testa O., "Desgin, Realization and Test of a UWB Radar Sensor for Breath Activity Monitoring", *IEEE Sensors Journal, Vol. 14, No:2, February 2014.*

Bod M., Hassani H. R. and Taheri S. M. M., "Compact UWB Printed Slot Antenna With Extra Bluetooth, GSM and GPS Bands", *IEEE Antennas and Wireless Propagation Letters, Vol. 11, No:2, pp. 531-534, 2012.*

Cakır G., 2004. *Gezgin İletişim Sistemleri İçin Hüzme Yönlendirmeli Mikroşerit Anten Tasarımı: Analitik Hesaplama, Bilgisayar Benzetimleri ve Ölçümleri*, PhD. Thesis, Kocaeli University, Turkey.

Campbell C. K., Traboulay I., Suthers M. S., Kneve H., "Design of Stripline Log Periodic Dipole Antenna ", *IEEE Transactions on Antennas and Propagation, Proceedings, Vol. AP-25, pp. 718-721, September 1977.*

Carrel R., *"The Design of Log-Periodic Dipole Antenna", IRE International Convention Record, Vol. 9, Part 1, pp. 61-75, 1961.*

Casula G. A., Maxia P. and Mazzarella G., "A Printed LPDA with UWB Capability", *International Workshop on Antenna Technology, pp. 1-4, 2010.*

Casula G. A., Maxia P. and Montisci G., "Design of a Printed Wide Band Log-Periodic Antenna Dipole Array with a New Feeding Technique", *6th European Conference on Antennas and Propagation, pp. 1882-1884, 2011.*

Casula G. A., Maxia P., Mazzarella G. and Montisci G., "Design of a Printed Log-Periodic Dipole Array for Ultra-Wideband Applications", *Progress in Electromagnetics Research C, Vol. 38, pp. 15-26, 2013.*

Chatterjee J. S. and Roy M. N., "Helical Log Periodic Array", *IEEE Transactions on Antennas and Propagation, Vol. 16, Iss. 5, pp. 582-583, September 1968.*

Chen Z. N., "Impedance Characteristics of Planar Bow-Tie Like Monopole Antennas", *Electronics Letters, Vol. 36, Iss. 13, pp. 1100-1101, June 2000.*

Dadel M. and Srivastva S., "Arrays of Patch Antenna Using Log Periodic Property", *IEEE International RF and Microwave Conference, pp. 363-367, December 2011.*

Desai S. C. and Abel J. F., 1971. *Introduction to The Finite Element Method A Numerical Method for Engineering Analysis,* United States: Van Nostrand Reinhold Company.

Dubost G. and Zisler S., 1976. *Antennas a Large Bande,* United States: New York.

DuHumel R. H. and Isbell D., "Broadband Logarithmically Periodic Antenna Structures"*, IRE International Convention Record, Vol. 5, pp.119-128, March 1957.*

Elbert B. R., 2004. *Introduction to Satellite Communication,* United States: Artech House.

Elsheakh D. and Abdallah E., "Compact Printed Log-Periodic Dipole Antenna for Terrestrial Digital Video Broadcast Application", *Microwave and Optical Technology Letters, Vol. 56, No. 4, April 2014.*

Ergin E., Ciftcioglu B., Ozcan M. and Tekin I., 2007, "High Resolution Ultrawideband Wall Penetrating Radar", *Microwave and Optical Technology Letters, Vol. 49, No:2, February 2007.*

FCC, 2002. *02-48: First Report and Order.*

Filho V. A. A., Silva P. H. F. and D'Assuncao A. G.,"A Comparative Study of Three Ultra Wideband Log-Periodic Microstrip Antenna Arrays", *International Workshop on Antenna Technology, pp. 1-4, 2010.*

Garg R., Bhartia P., Bahl I. and Ittipiboon A., 2001. *Microstrip Antenna Design Handbook,* United States: Artech House.

Ghavami M., Michael L. B., Kohno R., 2005. *Ultra Wideband Signals and Systems in Communication Engineering,* Great Britain: Jhon Wiley & Sons.

Guha D. and Anter Y. M. M., 2011. *Microstrip and Printed Antennas New Trends, Techniques and Applications,* United Kingdom: Jhon Wiley & Sons.

Guinvarc'h R. and Ribiere-Tharaud N., "A Wideband Antenna for P Band Airborne SAR Applications", *IEEE Antennas and Propagation Society International Symposium, pp.1-4, July 2008.*

Hagiwara K., Arai H., Izumi S. and Tanaka T., "A Beam Switched Log-Periodic Antenna for EMI Measurements", *IEEE International Symposium on Antennas and Propagation, 2012*.

Harrison R. W. S. and Jessup M., "A novel Log Periodic Implementation of a 700 MHz–6 GHz Slant Polarized Fixed-Beam Antenna Array for Direction Finding Applications", *Proceedings of the 9th European Radar Conference, pp. 401-404 , 2012.*

Hommoud M., Poey P. and Colombel F., "Matching the Input Impedance of a Broadband Disc Monopole", *Electronics Letters, Vol. 29, Iss. 4, pp. 406-407, February 1993.*

Honda S., Ito M., Seli H. and Jinbo Y., "A Disk Monopole Antenna with 1:8 Impedance Bandwidth and Omnidirectional Radiation Pattern", *Proceedings of the International Symposium on Antennas and Propagation, Vol. 4, pp. 1145-1148, 1992.*

IEEE, 2002. *IEEE Std 802.11-2002 Part 11: Wireless LAN Medium Access Control (MAC) and Physical Layer (PHY) Specifications.*

ITU, 2003. *ITU-R M.1036-2: Frequency Arrangements for ımplementation of the Terrestrial Component of International Mobile Telecommunications-2000 (IMT-2000) in the bands 806-960 MHz, 1710-2025 MHz, 2110-2200 MHz and 2500-2690 MHz.*

James J. R. and Hall P. S., 1989. *Handbook of Microstrip Antennas*, United Kingdom: IEE Electromagnetic Waves Series.

Javahashvili O., 2009, *UWB Antennas for Wall Penetrating Radar Systems*, MSc. Thesis, University of Gavle, Sweden.

Jin J., 2002. *The Finite Element Method in Electromagnetics*, United States: John Wiley & Sons.

Kim D., Chen Q. and Sawaya K., *"Microstrip Log-Periodic Dipole Array Antenna", IEEE Proceedings, Vol. 35, Part H, No:2, pp. 61-75, April 1988.*

Korowajczuk L., 2011. *LTE, WiMAX and WLAN Network Design, Optimization and Performance Analysis*, United States: John Wiley & Sons.

Kumar G. and Ray K. P., 2003. *Broadband Microstrip Antennas*, United States: Artech House.

Lee K. F., Chen W., 1997. *Advances in Microstrip and Printed Antennas*, United States: Jhon Wiley & Sons.

Li L., Cheung S. W. and Yuk T. I., "Compact MIMO Antenna for Portable Devices in UWB Applications", *IEEE Transactions on Antennas and Propagation, Vol. 61, No:8, pp. 4257-4264, August 2013.*

Lin S., Luan S., Wang Y. D., Luo X., Han X., Zhang X. Q., Tian Y. and Zhang X. Y., "A Printed Log-Periodic Tree-Dipole Antenna (PLPTDA)", *Progress In Electromagnetics Research M, Vol. 21, pp. 19-32, 2011.*

Low Z. N., Cheong J. H. and Law C. L., "Low Cost PCB Antenna for UWB Applications", *IEEE Antennas and Wireless Propagation Letters, Vol. 4, pp. 237-239, 2005.*

Matin M. A., 2010. *Ultra Wideband edited by Boris Lembrikov* , India: Sciyo.

McEvoy P., John M., Curto S. and Ammann M. J., "Group Delay Performance of Ultra Wideband Monopole Antennas for Communication Applications", *Loughborough Antennas and Propagation Conference, pp. 377-380, 2008.*

Meinke H. and Gundlach F. W.., "Taschenbuch der hochfre-quenztechnik", *Springer-Verlag, pp. 531-535, 1968.*

Mishra S. K., Gupta R. K., Vaidya A and Mukherjee J., "A Compact Dual Band Fork Shaped Monopole Antenna for Bluetooth and UWB Applications", *IEEE Antennas and Wireless Propagation Letters, Vol. 10, pp. 627-630, 2011.*

Neelgar B. I. and Raju G. S. N., "Impedance Characteristics of Log Periodic Antenna", *International Journal of Computer Applications, Vol. 21, No: 1, pp. 12-19, 2011.*

Parallax Motion Detector. "X-Band Motion Detector". (accessed September 10, 2013) http://www.parallax.com/product/32213

Peixeiro C., "Design of Log-Periodic Dipole Antennas", *IEE Proceedings, Vol. 35, Part H, No:2, pp. 61-75, April 1988.*

Pozar D. M., 1998. *Microwave Engineering,* United States: John Wiley & Sons.

Pozar D. M., 1983. "Considerations of Milimiter Wave Printed Antennas ", *IEEE Transactions on Antennas and Propagation, Vol. AP-31, No.5, September 1983.*

Proakis J. G., 2004. *Digital Communications,* United States: John Wiley & Sons.

Qjaroudi M and Qjaroudi N., "Ultrawideband Slot Antenna with Frequency Band-Stop Operation", *Microwave and Optical Technology Letters, Vol. 55, No:9, pp. 2020-2023, September 2013.*

Radar Development Kit. "Novelda NVA6100". (accessed September 10, 2013) http://novelda.no

Raltson T. S., Charvat G. L. and Peabody J. E., 2010, "Real Time Through-wall Imaging Using an Ultrawideband Multiple-Input Multiple-output Phased Array Radar System", *IEEE International Symposium on Phased Array Systems and Technology , 2010.*

Rappaport T. S., 2002. *Wireless Communications Principles Practice*. Prentice Hall International.

Rumsey V. H., "Frequency Independent Antennas", *IRE National Convention Record, pt.1, pp. 114-118, 1957.*

Sadiku M. N. O., 2000. *Numerical Techniques in Electromagnetics,* United States: CRC Press.

Sea Based Radar. “Sea Based X-Band Radar”. (accessed September 10, 2013) http://www.mda.mil/global/documents/pdf/sbx.pdf

Shokri M., Ghobadi C., Nourina J., Shirzad H., Amiri Z and Asiaban S., “Compact Circularly Polarized Printed Slot Antenna with a Wrench Shaped Patch for UWB Application”, *International Journal of Natural and Engineering Sciences, Vol. 7, pp. 57-60, 2013.*

Skolnik M. I., 2008. *Radar Handbook*, United States: McGraw-Hill Companies.

Smith H. K. and Meyes E., “Log-Periodic Array of Dual-Feed Microstrip Patch Antennas”, *IEEE Transactions on Antennas and Propagation, Vol. 39, No:12, pp. 1659-164, December 1991.*

Snow Depth Sensor. “SDS-X2 Snow Depth Sensor”. (accessed September 10, 2013) http://flatearthinc.com/products/sds-x2-snow-depth-sensor/

Stutzman W. L., 1981. *Antenna Theory and Design*, United States: John Wiley & Sons.

Taheri M. M. S., Hassani H. R. and Nezhad S. M. A., “UWB Printed Slot Antenna with Bluetooth and Dual Notch Bands”, *IEEE Antennas and Wireless Propagation Letters, Vol. 10, pp. 255-258, 2011.*

Tanyer F. M., 2005. *Design of Log-Periodic Dipole Array Feed and Wide Band Reflector Antenna System,* MSc. Thesis, Middle East Technical University, Turkey.

Tanyer-Tiğrek M. F., 2009. *Printed Antenna Elements with Attested Ultra Wide Band Array Applicability,* PhD. Thesis, Delft University of Technology, The Netherlands.

Telephonics X-Band Radar. “Telephonics RDR 1600”. (accessed September 10, 2013) http://www.telephonics.com/pdf/RDR-1600.pdf

Thompson G. T. and Butson P. C., “A note on the Calculation of Gain of Log Periodic Dipole Antennas”, *IEEE Transactions of Antennas and Propagation, Vol. 24, Iss. 1, pp. 105–106, January 1976.*

Tsai C. L. and Deng S. M., “A Dual Port Antenna For GPS and UWB Operations” *Journal of Electromagnetic Waves and Applications, Vol. 25, pp. 365-377, 2011.*

User’s Guide HFSS, 2005. United States: Ansoft Cooparation.

Vaddagiri K., 2012, *Ultra Wideband Leaky-Wave for Medical Imaging*, MSc. Thesis, Delft University of Technology, The Netherlands.

Wakabayashi R., Shimada K., Kawakami H. and Sato G., "Circularly Polarized Log-Periodic Dipole antenna for EMI Measurements", *IEEE Transactions on Electromagnetic Compatibility, Vol. 41, No. 2, pp. 93-99, May 1999.*

Wang K. L., 2002. *Compact and Broadband Microstrip Antennas,* United States: John Wiley & Sons.

Wang Y., Abbosh A. M., Henin B. and Nguyen P. T., 2014, "Synthetic Bandwitdh Radar for Ultrawideband Microwave Imaging System", *IEEE Transactions on Antennas and Propagation, Vol. 62, No:2, February 2014.*

Waterhouse R. and Novak D., 2007. *Printed Antennas for Wireless Communications edited by Rod Waterhouse*, England: Jhon Wiley & Sons.

Wavestorm Satcom Antenna. "EMS Wavestrom GS-X". (accessed September 10, 2013) http://www.militaryaerospace.com/articles/print/volume-22/issue-7/product-applications/antennas-ems-defense-space-to-supply-satcom-antenna-for-army-rc-12.html

Yang J., "Periodicity of the Input Impedance of Log-Periodic Array Antennas", *IET Microwave, Antennas & Propagation, Vol. 6, Iss. 10, pp. 1117-1122, 2012.*

Yeo J. and Lee J., "Miniaturized LPDA Antenna for Portable Direction Finding Applications," *ETRI Journal, Vol. 34, No. 1, pp. 118-121, February 2012.*

Zehforoosh Y. and Sedghi, "A CPW-Fed Printed Antenna with Band Notched Function Using An M Shaped Slot", *Microwave and Optical Technology Letters, Vol. 56, No:5, pp. 1018-1092, May 2014.*

Zhang Y., Wang J. and Yang J., "Design of Log-Periodic Dipole Antennas", *Journal of Electromagnetic Waves and Applications, Vol. 21, Iss.12, pp. 1621-1633, 2007.*